Spring 2014

Bridge deck condition assessment using destructive and nondestructive methods

Brandon Tyler Goodwin

Department:

BRIDGE DECK CONDITION ASSESSMENT USING DESTRUCTIVE AND NONDESTRUCTIVE METHODS

by

BRANDON TYLER GOODWIN

A THESIS

Presented to the Faculty of the Graduate School of the

MISSOURI UNIVERSITY OF SCIENCE AND TECHNOLOGY

In Partial Fulfillment of the Requirements for the Degree

MASTER OF SCIENCE IN CIVIL ENGINEERING

2014

Approved by

Lesley H. Sneed, Advisor
Neil L. Anderson
John Myers

ABSTRACT

This study investigates two bridge decks in the state of Missouri using both nondestructive and destructive testing methods. The Missouri Department of Transportation (MoDOT) is responsible for the monitoring and maintenance of over 10,000 bridges. Currently monitoring of these bridges includes a comprehensive visual inspection. In this study, ground-coupled ground penetrating radar (GPR) is used to estimate deterioration, along with other traditional methods, including visual inspection, and core evaluation. Extracted core samples were carefully examined, and the volume of permeable pore space was determined for each core. After the initial investigation, the two bridges underwent rehabilitation using hydrodemolition as a method to remove loose or deteriorated concrete. Depths and locations of material removal were determined using light detection and ranging (lidar). Data sets were compared to determine the accuracy of GPR to predict deterioration for condition monitoring and rehabilitation planning of bridge decks. As shown by the lidar survey of the material removed during rehabilitation, the GPR top reinforcement reflection amplitude accurately predicted regions of deterioration within the bridge decks. In general, regions with lower reflection amplitudes, indicating more evidence of deterioration, corresponded to regions with greater depths of material removal during the rehabilitation. Also, the GPR top reinforcement reflection amplitude indicated deterioration in areas where visual deterioration was noticed from the top surface of the deck. The majority of cores with delaminations were extracted from sections where the GPR top reinforcement reflection amplitude indicated greater evidence of deterioration based on lower amplitude values.

ACKNOWLEDGMENTS

First off, I would like to thank my advisor Dr. Lesley Sneed. She has guided my studies both as an undergraduate and graduate advisor during my time at Missouri S&T. She has constantly encouraged me to strive for excellence. I greatly appreciate all of the professional development opportunities she has given me, including the opportunity to give several presentations on my research. I greatly appreciate all of the advice and guidance she has given me throughout my college journey.

Next, I would like to thank the Missouri Department of Transportation (MoDOT) and the National University Transportation Center (NUTC) at Missouri S&T for funding this research. Special thanks to Andrew Hanks and Jennifer Harper and all of the MoDOT team who spent numerous hours providing information, traffic control, coring, and chloride ion analysis to support this study. I would like to also thank Jeremy Bexten with APAC, Missouri who allowed us onto his construction site during the rehabilitation of the two bridges to collect data.

In addition, I would like to thank my committee members, Dr. Neil Anderson and Dr. John Myers, for their guidance and instruction throughout this study. I would also like to thank all of the members of the research team who participated in the field and laboratory work, and for their assistance and support, along with allowing the use of their data sets in my thesis. Members of the research team include: Dr. Evgeniy Torgashov, Aleksey Khamzin, Aleksandra Varnavina, Mengxing Li, Stanley Nwokebuihe, Faraj Eljabri, Abdallah Dera, Adel Elkry, Abdulrahman Alotaibi, Jeremiah Obi, and Payman Hajiani. Also many thanks go out to Dr. Norbert Maerz and Ken Boyko of Missouri S&T, for their acquisition of lidar data.

Finally, I would like to give special thanks to my parents, Kevin and Sherry Goodwin, my brother Nathan Goodwin, my future wife Krishawn Ridenhour, and all the rest of my friends and family who have inspired me throughout my journey.

TABLE OF CONTENTS

LIST OF ILLUSTRATIONS

LIST OF TABLES

1. INTRODUCTION

Bridge decks are typically the first component of a bridge to require major repair after construction. Harsh conditions such as deicing salts and heavy traffic applied to the deck can lead to deterioration of the concrete and corrosion of the steel reinforcing bars in the deck. The Missouri Department of Transportation (MoDOT) has 10,405 bridges in its inventory that have to be monitored and maintained [1].

Various techniques have been used in the past to evaluate concrete bridge decks, including coring, visual inspection, and sounding using chains or hammers. In this study, traditional techniques were used as well as Ground Penetrating Radar (GPR) to evaluate concrete bridge decks. GPR is a nondestructive evaluation (NDE) tool that can be used to detect steel reinforcing bar corrosion and determine the extent of deterioration of concrete. GPR can be used to scan a typical bridge deck (2 lanes, 300 feet long) in a few hours using a ground coupled antenna. GPR has been used to investigate the deterioration of bridge decks in other research projects worldwide, however some doubt still exists amongst the Civil Engineering field regarding the applicability and accuracy of the technology, which lends cause to the study discussed in this thesis.

Three of the concrete bridge decks in this study underwent rehabilitation using hydrodemolition as the method to remove loose and deteriorated concrete after the bridge decks were evaluated using both traditional methods and GPR. Hydrodemolition is a process that is used to remove deteriorated concrete from bridge decks using high pressure water jets. The hydrodemolition process allowed for measurements of material removal depth. The depth of material removal is function of the concrete strength, and since deterioration leads to decreased strength, the rehabilitation process provided a method of determining correlations between traditional evaluation methods, GPR data, and deterioration in the concrete deck. The goal of this research is to investigate the applicability and accuracy of GPR to locate and estimate the level and amount of deterioration present in bridge decks so that it can be used for estimation purposes for rehabilitation as well as monitoring the deterioration levels.

1.1. PROBLEM DEFINITION

With an average cost of $250,000 to rehabilitate a minor bridge in Missouri, it is important that the bridge owner is able to accurately predict the deterioration to ensure resources are being spent where they are most needed [1]. Bridge decks are commonly the first component of a bridge structure to require major rehabilitation or replacement. Using nondestructive techniques, such as GPR, to monitor the health of bridge decks over time could allow bridge owners to better plan for the funding and construction of bridge rehabilitation. Even though GPR has been in existence since the early 1900s, the applicability and accuracy of the technology is still unknown to some Civil Engineers.

1.2. SCOPE AND OBJECTIVES

The work discussed in this thesis is part of the project entitled, Nondestructive Evaluation of MoDOT Bridge Decks – Pilot Study. The project was a collaborative effort between MoDOT and researchers from the Civil Engineering Department and the Geological Engineering Department at Missouri University of Science and Technology (Missouri S&T).

1.2.1. Project Scope and Objectives. The pilot study included twelve field investigations of eleven different bridges on MoDOT's road network to evaluate bridge deck condition using destructive and nondestructive methods. The bridges that were investigated were selected by MoDOT and researchers from Missouri S&T. The project goal of this research was to demonstrate proof of concept that advanced nondestructive testing/evaluation (NDT/NDE) techniques can be rapidly, effectively, and economically implemented as part of MoDOT bridge deck surveys to improve the overall quality and cost of bridge deck evaluation. Data acquired from each deck included a detailed visual inspection, GPR data, portable seismic property analyzer (PSPA) data, concrete cores, and chloride ion content measurements. During the project timeframe, three of the bridges in the study underwent rehabilitation, which included concrete removal by hydrodemolition of the decks. The project scope was expanded to include determining the amount and locations of concrete removal from the three decks and compare that information to data collected in the field investigations. A different crew from Missouri

S&T obtained light detection and ranging (lidar) data before and after the hydrodemolition so that the amount and locations of concrete removal could be documented and determined. Researchers involved with the original field investigations also returned to the three bridges after hydrodemolition to document the removal using photographs and video footage, and measure concrete removal depths for segments of the bridges.

1.2.2. Thesis Work Scope and Objectives. The focus of this thesis is relating the visual inspection, GPR, and core data to the information collected from the hydrodemolition surveys. The objective of this thesis is to determine the ability of GPR to accurately estimate the deterioration of bridge decks so that it can be used for monitoring and rehabilitation planning. This shall be done by comparing the GPR data to the visual inspection, core data, and the hydrodemolition results from two bridge decks in Missouri. The following research tactics were performed as part of this thesis:

1. A background review was completed (Section 2).
2. Extensive field investigations were performed on two bridge decks using in-depth visual inspection, concrete cores, and GPR to determine the condition of the bridge decks (Section 3).
3. Extensive field investigations were performed during the rehabilitation of the two bridge decks to document the surface of concrete removed (Sections 3.2.2.4 and 3.3.2.4). Results were compared to the visual inspection, cores, and GPR results to validate and improve estimations for future use (Section 4).

2. BACKGROUND

Bridge decks experience harsh conditions that lead to their deterioration. In order to monitor the health of bridge decks, transportation officials commonly use both nondestructive and destructive test methods. Once a bridge deck reaches a certain deterioration level, it will require repair or replacement. This section discusses causes of bridge deck deterioration, along with evaluation and repair methods.

2.1. CAUSES OF BRIDGE DECK DETERIORATION

The causes of bridge deck deterioration are placed into four main categories for this thesis, which are degradation caused by chemicals, poor design and/or construction, thermal changes, and that which is induced by traffic. All of these deterioration mechanisms are unique and should be taken into consideration when evaluating a bridge deck.

2.1.1. Chemical Degradation. According to the Portland Cement Association (PCA), "corrosion of reinforcing steel and other embedded metals is the leading cause of deterioration in concrete" [2]. Chloride ions found in deicing chemicals and some admixtures can accelerate the rate of steel corrosion, resulting in a decreased service life of the bridge deck. Even though careful design and construction practices can limit the intrusion of deicing chemicals and extend the life of a bridge deck, the concrete will eventually crack and allow these chemicals to come in contact with the reinforcement. It is also important to recognize that many bridges constructed during the 1960s-1970s thatare still in service were not built with the design standards that transportation agencies use today. For example, as discussed in Section 3, the two bridges examined in this thesis had a design clear cover of 2 in. or less, which is less than the current clear cover requirement of 2.75 in. Currently, bridges constructed during the 1960s and 1970s era are structures for which DOTs are most interested in obtaining nondestructive data for monitoring and rehabilitation planning. Therefore, it is crucial to understand the main deterioration mechanism that affects bridge decks in Missouri.

According to PCA, common deicing chemicals used on roadways include sodium chloride, calcium chloride, magnesium chloride, and potassium chloride [3]. Although these chemicals greatly aide in keeping the roadways navigable during ice and snow by reducing the freezing point of water, they cause substantial damage to highway infrastructure.

In order for corrosion of steel to occur, there has to be at least two electrically connected metals or two locations of a single metal at different energy levels acting as the anode and cathode, and an electrolyte to connect the two. The anode is the location where the corrosion occurs, or where the loss of cross section is noticed. The cathode is the area where steel is not consumed. Moist concrete acts as the electrolyte. Figure 2.1 below illustrates the corrosion mechanism [2].

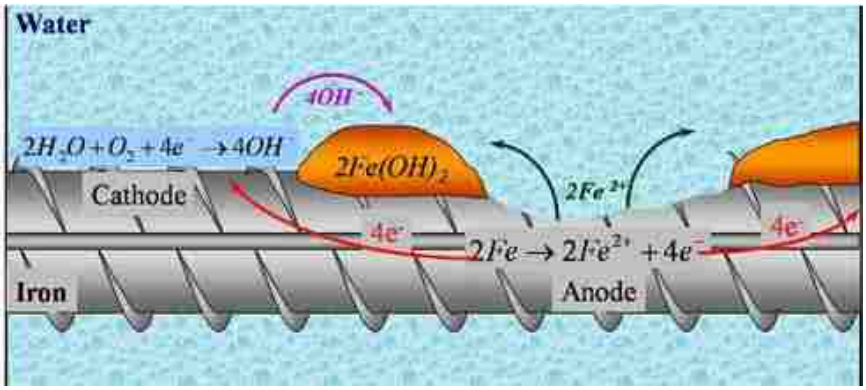

Figure 2.1. Steel Corrosion Mechanism [2]

Concrete naturally protects the steel reinforcement from corroding because of its high alkalinity with a pH between 12 and 13. This high pH allows a thin oxide layer to form on the steel and prevents metal atoms from dissolving. The oxide layer does not stop corrosion, but it does reduce the corrosion rate enough that it is insignificant [2]. Chlorides present in the concrete from deicing chemicals and possibly the concrete mixture can break through this passive layer and initiate higher corrosion rates. According to the Federal Highway Administration (FHWA), it is not fully understood how chloride ions break down the passive layer [4]. Once the passive layer is broken,

oxygen and water can reach the steel allowing corrosion to occur. Corrosion products from the steel occupy a volume between three to six times that of original steel, inducing large tensile stresses in the concrete [4]. If the tensile strength of the concrete is exceeded, a horizontal crack called a delamination will occur. According to the American Concrete Institute (ACI), a delamination is defined as "a horizontal splitting, cracking, or separation within a slab in a plane roughly parallel to, and generally near the upper surface" [5]. Delaminations can cause an increased rate of corrosion as well as visible deterioration on the bridge deck surface such as spalling and potholes. Figure 2.2 below shows a delamination present in a bridge deck cross section [6].

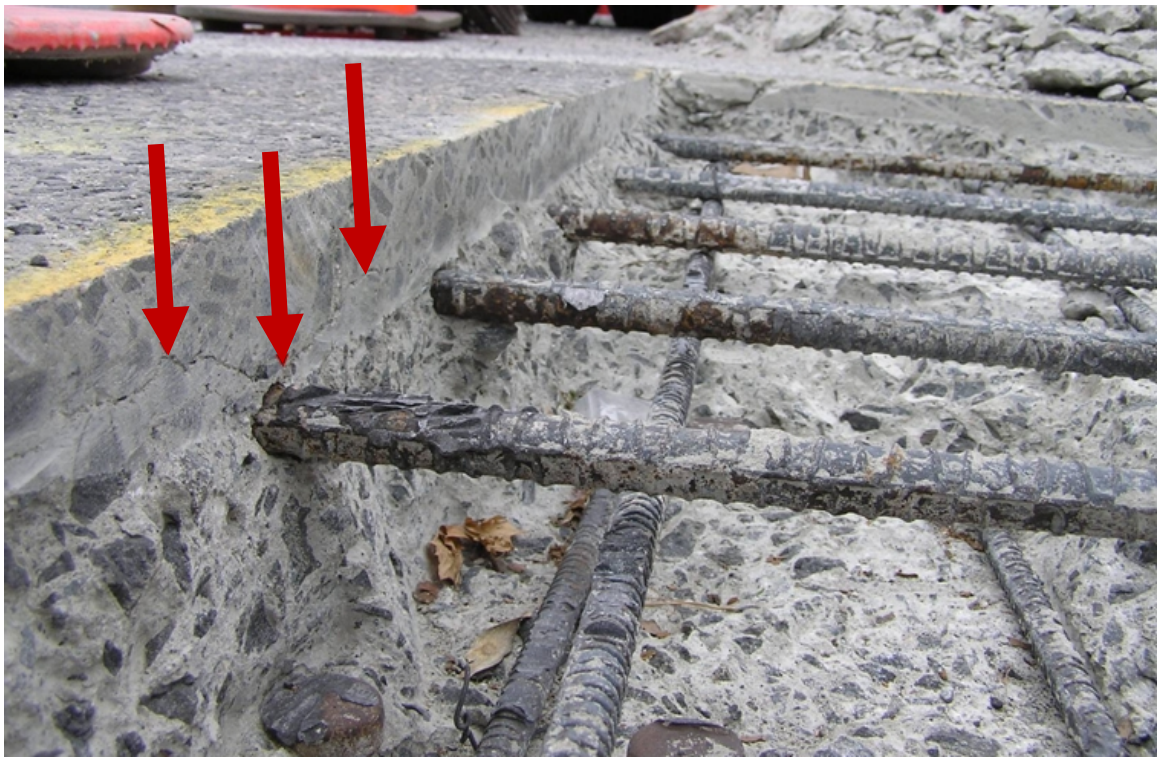

Figure 2.2. Delamination in Bridge Cross Section [6]

2.1.2. Poor Design and/or Construction. Poor bridge deck design and construction can cause accelerated deterioration. One of the most effective ways to decrease the rate of corrosion is to ensure steel reinforcement has adequate concrete cover. MoDOT currently has a minimum top reinforcement clear cover requirement of

2.75 in., with a preferred cover of 3.0 in. [7]. The greater the clear cover, the longer it will take for chlorides to reach the steel and initiate corrosion. Figure 2.3 below illustrates how increased concrete cover on reinforcement can greatly reduce the corrosion rate of the steel reinforcement [8]. The model presented in the figure was generated using a constant humidity and temperature of 75% and 20°C (68°F), respectively.

Figure 2.3. Clear Cover Effect on Corrosion Rate for Various w/c Ratios [8]

Another important consideration in the deterioration rate of steel-reinforced concrete bridge decks is the concrete mixture used. Figure 2.3 above illustrates that mixtures with lower water-to-cement ratios (w/c) have lower corrosion rates than those with higher w/c ratios. The material being used in the concrete mixture is also important to the durability of the bridge deck. For example, alkali-aggregate reactions (AAR) are very important to consider when specifying aggregates for use in concrete. AAR is a chemical reaction in concrete between hydroxyl ions of the alkalies from hydraulic cement and certain constituents of some aggregates [9]. Although uncommon in Missouri, deterioration due to AAR can greatly decrease the life of a bridge deck. AAR cause the concrete to expand and crack, allowing for water and deicing chemicals to

reach the reinforcing steel rapidly. The reaction can eventually cause failure of the concrete. AAR can be prevented by using a combination of aggregate and cement that will not react.

Placement and consolidation of the concrete can have a significant impact on the deterioration rate of the bridge deck. Concrete should be properly consolidated to ensure that there are no large voids present in the deck. If the concrete is not well consolidated, these voids can cause accelerated deterioration as they trap water and deicing chemicals. Studies completed at the Arabian Gulf University showed that the amount of consolidation can significantly affect the rate of chloride intrusion as illustrated in Figure 2.4 below [10].

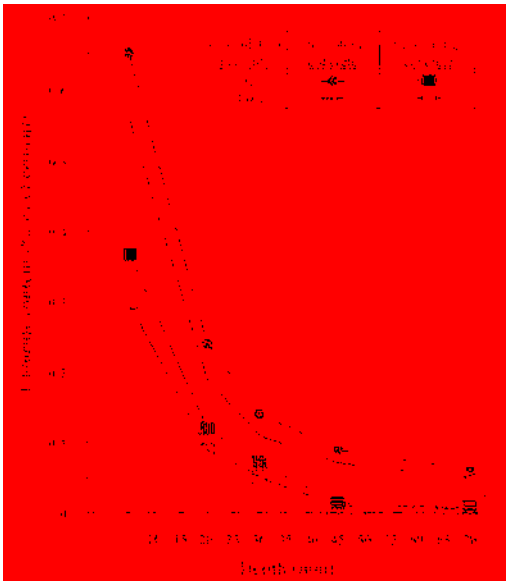

Figure 2.4. Effect of Consolidation on Chloride Ingress as Studied at Arabian Gulf University [10]

After the concrete placement of a bridge deck is complete, it is critical that the deck is cured properly. The quality of curing greatly affects the quality of the top layer of concrete in the bridge deck, which is closely related to the durability and longevity of the deck [11]. Proper curing can greatly reduce initial cracking and permeability of the concrete. Shrinkage cracks caused from improper curing can allow for deicing chemicals

to penetrate to the reinforcing steel at a greater rate than for uncracked concrete. According to PCA, standard recommendations for curing bridge decks consist of moist curing for a minimum of seven days for concrete mixtures containing only portland cement and as long as 14 days when supplementary cementitious materials are used [12].

2.1.3. Temperature Induced Deterioration. Temperature changes can induce deterioration of the bridge deck, mainly through the creation and propagation of cracks. Any type of crack in the concrete can allow aggressive agents such as deicing chemicals to penetrate the deck causing damage to either the concrete itself or the reinforcing steel [13]. Freezing and thawing cycles are one form of temperature change that can cause deterioration of bridge decks. Solutions in the pores of the concrete expand during a freezing event and exert high pore pressures. If the tensile strength of the concrete is exceeded, then cracking will result [14]. There are also other causes of temperature induced deterioration. When deicing agents are placed on the bridge deck, they decrease the freezing point of water and allow ice and snow to melt. This process draws heat from the concrete and chills it, which can act like a cold shock. The pore water on the concrete surface then freezes and can cause cracking if internal stresses exceed the tensile strength of the concrete [15].

Damage from temperature differences can also occur due to layered freezing. Layered freezing is caused due to the deicing agent concentration and temperature gradients within the concrete. The surface layer has a relatively low temperature and a high deicing agent concentration. The interior of the concrete has a relatively low deicing agent content and higher temperature. The layer in between the surface layer and interior freezes at lower temperatures than the other two, which can cause high pressures on the surface layer. If the stresses exceed the tensile strength of the concrete, it will crack [15].

2.1.4. Traffic Induced Deterioration. Traffic loading can have an impact on the deterioration of bridge decks. According to a report by the Iowa Department of Transportation, “various surveys indicate that highway bridges are subjected to vehicular load levels and combinations far in excess of those for which they were designed” [15]. Damage typically caused from overloading includes hair line cracks, bending, splitting or shear cracks [15].

Traffic induced damage was observed on several concrete bridge decks with bituminous overlays. Typical damage included rutting and shoving of the asphalt, especially where traffic is stopping and turning. The asphalt overlay can also debond from the concrete, allowing moisture with and/or without chlorides to be trapped in the debonded region, allowing for further deterioration [16]. Even though the deterioration of the asphalt layer does not necessarily reflect the strength or deterioration of the concrete bridge deck, it is important to note when using nondestructive evaluation techniques that are sensitive to all layers on the bridge decks because asphalt deterioration could influence the interpretation of results.

2.2. NONDESTRUCTIVE METHODS FOR INVESTIGATING BRIDGE DECK DETERIORATION

Nondestructive evaluation (NDE) methods are simply defined as methods of detecting flaws or deterioration without damaging the material. Basic forms of NDE methods used for bridge decks include visual inspection and sounding by chain dragging or hammer sounding. More advanced methods, such as ground penetrating radar (GPR), are becoming more widely used as they become further studied and better understood. It is important to consider the strengths and limitations of each technology, and in many cases the use of a combination of techniques is the best method to accurately determine bridge deck deterioration.

2.2.1. Visual Inspection. The first step in evaluating the condition of a bridge deck is a visual inspection [17]. A careful visual inspection of a bridge deck involves examining the top and bottom sides of the bridge deck. Important characteristics to take note of during an investigation include concrete stains, cracks, localized depressions, spalling, and scaling. Rust stains on the concrete are indicators that the steel reinforcement may be corroding, but sometimes it can be a result of other actions such as ferrous sulfide inclusions in the aggregate or rusting of form ties [17].

Cracks are precursors of deck deterioration and are one of the most important features to document. Cracks can eventually allow deicing agents and water to reach the reinforcing steel, accelerating deterioration of the deck. It is also important to document the orientation of the crack as either longitudinal, traverse, diagonal, or random. This can

help determine the cause of the cracking. Typically, crack widths and depths are not measured on a bridge deck. However, if desired, crack widths can be measured by instruments such as a crack width comparator card [18], or a hand-held crack comparator microscope. Localized depressions can indicate areas where the concrete has deteriorated below the surface. Spalling occurs when the surface of the concrete pops out and leaves the aggregate exposed. Scaling occurs when the surface of the concrete flakes off.

Even though visual inspection is a very common method used to evaluate bridge decks, it is very subjective. A study completed by the Federal Highway Administration (FHWA) shows that inspector's visual ratings of bridge decks can be substantially different. Figure 2.5 below shows the results of a t-test performed on the results of the study. Evaluations from four of the six bridges failed the t-test, indicating significant differences in results. Between 47 and 49 individual assessments were performed on each of the bridge decks [19].

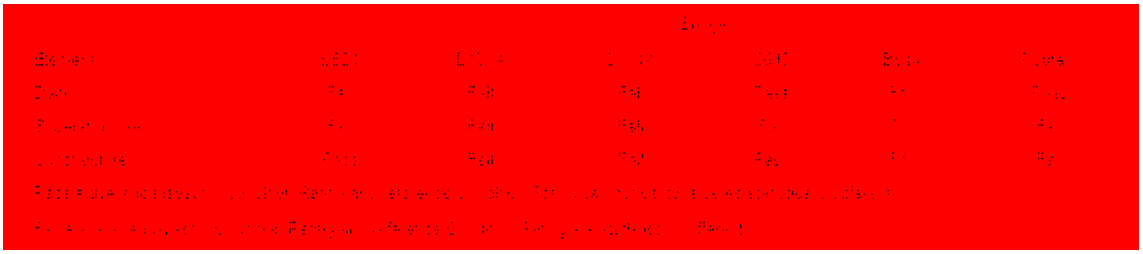

Figure 2.5. T-test Results of FHWA Study on Reliability of Visual Bridge Inspection [19]

2.2.2. MoDOT bridge deck rating criteria. MoDOT follows a bridge deck rating system set by the FHWA. Each bridge deck is rated on a scale from 0 to 9, with 9 being excellent and 0 being failed condition. Table 2.1 below was generated using information directly from MoDOT's Engineering Policy Guide (EPG) [20].

Table 2.1. MoDOT Bridge Deck Rating Categories as Defined in MoDOT's EPG [20]

Rating 9	**Excellent condition.**
	No deficiencies noted.
Rating 8	**Very good condition. Potential exists for minor preventative maintenance.**
	No noteworthy deficiencies that affect the condition of the deck.
	No spalling, scaling, or delamination. Minor transverse or longitudinal cracking.
	No water saturation.
	Minor transverse or longitudinal cracking.
Rating 7	**Good condition. Potential exists for minor maintenance.**
	Deck cracks with or without efflorescence, including transverse cracks in P/C panels (cracks are sealable).
	Reflective cracks over precast panels or L-cracks between Dbl-Tee beams (cracks are sealable).
	Light scaling (1/4" depth or less).
	Visible wear in the wheel lines.
	Minor water saturation. This area would include any repaired areas and/or minor areas in need of repair.
	Minor popouts.
	Minor lifting of non-composite deck off beams due to pack rust.
	Small areas of shallow delamination.
	Minor edge deterioration with no rebar exposed.
Rating 6	**Satisfactory condition. Potential exists for major maintenance.**
	Minor spalling of the deck.
	Medium scaling (1/4" – 1/2" in depth).
	Up to 10% of the deck is water saturated and/or deteriorating. This area would include any repaired areas and/or areas in need of repair.
	Deterioration of deck edges or outlets with spalling and rebar exposed.
	Excessive number of open cracks (excessive being at 5' intervals or less over the majority of a span) with or without efflorescence.
	Extensive lifting of deck off beams (no damage).
	Noteworthy areas of delamination to rebar.
	Pounding of deck with no signs of distress.
	Numerous t-cracks in precast panels, with or without efflorescence.
Rating 5	**Fair condition. Potential exists for minor rehabilitation. Capacity for carrying wheel loads not reduced.**
	Deck has many spalls, some of which may expose rebar.
	Excessive cracking resulting in spalling.
	Heavy scaling (1/2" – 1" in depth).
	10%-40% of the deck is water saturated and/or deteriorating. This area would include any repaired areas and/or areas in need of repair.
	Disintegration of deck edges or outlets that is still outside curb line. Loss of linear deck edge.

Table 2.1. MoDOT Bridge Deck Rating Categories as Defined in MoDOT's EPG [20] (cont.)

	Excessive amount of pack rust lifting non-composite deck off beams with some cracking of the deck.
	Considerable delamination to rebar.
	Deck pounds when loaded and showing signs of distress.
Rating 4	**Poor condition. Potential exists for major rehabilitation. Capacity for carrying wheel loads slightly reduced.**
	Considerable spalling of the deck.
	40%-60% of the deck is water saturated and deteriorating. This area would include any repaired areas and/or areas in need of repair.
	Heavy disintegration of the deck edges that encroaches inside curb line.
	Abutment or concrete pavement pressure causing severe damage, usually requiring the deck ends to be removed and replaced.
	Extensive delamination to rebar.
	Severe pounding of deck when loaded – damage evident.
Rating 3	**Serious condition. Repair or rehabilitation required immediately. Capacity for carrying wheel loads in question.**
	This rating will apply if severe or critical signs of structural distress are visible.
	More than 60% of the deck is water saturated and/or deteriorated and the deck is in need of repair or is showing structural distress. This area would include any repaired areas and/or areas in need of repair. Saturation alone, without structural distress or need for deck repair, should be rated 4.
	Bridge may warrant one-lane traffic or load restriction.
	Heavy rusting of steel decking resulting in extensive section loss and numerous holes through deck. Load transfer of wheel loads to superstructure in question.
Rating 2	**Critical Condition. The need for repair or rehabilitation is urgent. Facility should be closed until the indicated repair is completed.**
	Deck span on verge of collapse or section has failed.
Rating 1	**"Imminent" failure condition – facility is closed. Study should determine the feasibility for repair. Corrective action may put structure back into light service.**
Rating 0	**Failed condition – facility is closed and is beyond repair. Replacement of structure is necessary.**

2.2.3. Chain Dragging and Hammer Sounding. Chain dragging and hammer sounding techniques are commonly used to locate delaminations in bridge decks. ASTM D4580-12 describes the process that should be followed for the sounding of bridge decks [21]. Sounding is not recommended for bridge decks overlaid with bituminous mixtures

but can be used for bridge decks that have been overlaid with portland cement concrete mixtures. The procedure listed in the ASTM standard includes laying out a grid system on the bridge deck, followed by dragging chains over the deck surface. Areas that are delaminated have a dull or hollow sound when the chain is drug across. Areas that are believed to be delaminated are outlined on the deck surface, and a map is prepared indicating the location of the delaminations with respect to the grid lines. A steel rod or hammer can be substituted for chains as long as it produces a clear ringing sound when dragged or tapped over nondelaminated concrete and a dull or hollow sound over delaminated concrete [21]. Figure 2.6 below shows a chain dragging and hammer sounding [22].

Figure 2.6. Chain Dragging (Left), and Hammer Sounding (Right) [22]

Chain dragging is the second most widely used method in the United States to assess the condition of bridge decks because it is relatively simple, economical, and quick to perform [17]. Even though it is widely used, sounding techniques are susceptible to inconsistencies due to subjective interpretations an inspector must make during the survey [23]. Sounding methods can only detect delaminations when they have progressed to the point where major rehabilitation is required [24].

2.2.4. Ground Penetrating Radar. Ground penetrating radar (GPR) is a rapid nondestructive testing method that utilizes electromagnetic (EM) waves that can be used to locate buried objects inside the bridge deck such as steel reinforcement, wire mesh, or other interfaces in the structure [25]. GPR has many applications, such as condition assessment of bridge decks and tunnel linings, pavement profiling, mine detection, archaeological investigations, geophysical investigations, and borehole inspections [16]. According to Maser, "GPR was originally developed for overlaid decks since access to the concrete surface via traditional methods is limited" [26].

A GPR antenna transmits small high-frequency EM pulses into the structure of interest. A portion of the energy is reflected back to the antenna from reflectors such as reinforcing bars or any other change in the material. The remaining energy continues to propagate further into the structure, and some energy is continually reflected until it is diminished. A receiver measures the amplitude and two-way travel time of the reflected signals. Figure 2.7 below illustrates how GPR works.

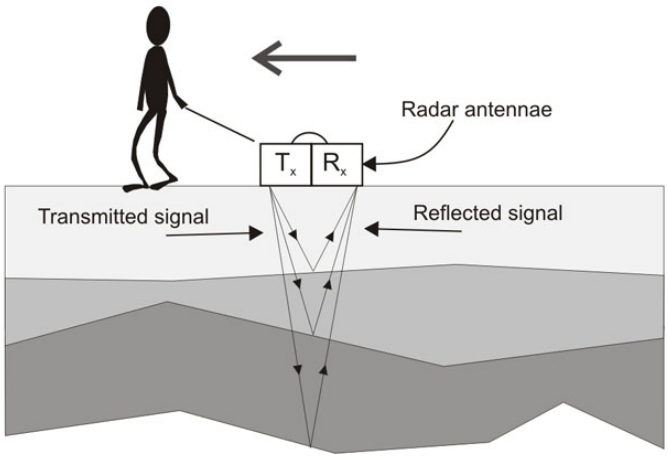

Figure 2.7. GPR Operating Principle [27]

GPR responds to variations in electrical properties of the materials making up various interfaces in a bridge deck. Material interfaces are typically recognizable with the GPR results because the materials on either side of the interface have different

electrical conductivity and dielectric constants. These properties affect the ability of GPR energy to penetrate the material, and the speed at which the GPR waves travel through the material. Table 2.2 below lists the dielectric constants of various materials [28]. Notice that water has a relatively high dielectric constant compared to concrete.

Table 2.2. Dielectric Constants of Various Materials [28]

Air	1	Sand	4-6
Water (fresh)	81	Gravel	4-7
Ice	4	Clay	25-40
Asphalt	4-8	Silt	16-30
Concrete	8-10	Silty sand	7-10
Crushed base	6-8	Insulation board	2-2.5

Due to the large difference in dielectric constant between water and concrete, moist concrete with high free chloride ions (or other conductive materials) attenuates the GPR signal and creates a longer two way travel time than that of dry concrete [28]. Therefore, deteriorated regions that are filled with moisture and conductive materials, such as chloride ions, can be located.

Electromagnetic waves cannot penetrate into metals, therefore steel reinforcing bars are excellent reflectors of EM waves. ASTM D6087 describes the use of GPR for the evaluations of bridge decks with and without asphalt overlays [29]. Two methods of analyzing GPR results are presented in this standard. They include deterioration measurements at the top reinforcing steel using the bottom deck reflection attenuation technique, and deterioration measurements at or above top reinforcing steel using top reinforcing reflection attenuation technique. Even though there are two analysis methods, typical GPR surveys utilize the second method, which uses the reflection amplitude from the top layer of reinforcement to analyze results. Figure 2.8 below shows

sample GPR results from a bridge deck [30]. The hyperbolas in the image represent reflections from the reinforcing bars. The boxed area shows a section of the bridge deck that is predicted to be deteriorated, as indicated by signal attenuation and varying apparent depths of reinforcing bars.

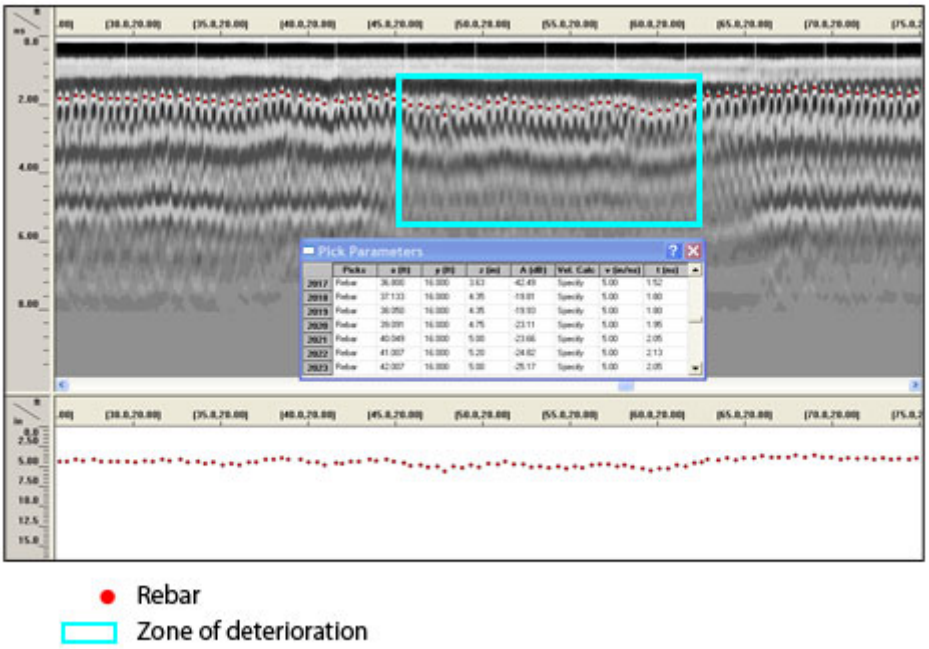

Figure 2.8. GPR Results from a Bridge Deck [30]

There are many references in the literature that study the use of GPR for determining bridge deck deterioration. For one study, a sample of ten bridge decks were scanned with GPR in New York, Virginia, and Vermont, with an average error in GPR predicted top delamination area of ±11.2% as determined by chain drag, core samples, and actual repair quantities [29]. A different study conducted by the FHWA concluded that GPR was able to accurately detect delaminations [16]. Another study by Yehia et al. indicated that GPR was able to accurately identify 77% of the deteriorated areas in two bridge decks, compared to a 23% accuracy of chain dragging [31].

Although GPR does have many advantages when used for the determination of bridge deck deterioration, it does have some limitations. According to the Strategic Highway Research Program (SHRP) [32], some limitations include:

1. GPR can determine the locations of delaminations only if they are filled with water or epoxy-impregnated.
2. Extreme cold weather can negatively influence GPR results. Studies by the FHWA state that frozen water is relatively transparent to EM waves in the frequency range typically used for bridge scans [33].
3. De-icing agents can limit the ability for GPR signal to penetrate the deck.
4. GPR cannot provide any information on mechanical properties of concrete.
5. GPR cannot provide any information about the presence of corrosion, corrosion rates, or reinforcing bar section loss.
6. Other test methods may be more cost-effective than GPR, especially for smaller structures.
7. The design of new GPR systems is limited by FCC restrictions on transmitting power output and the pulse repetition rate.
8. GPR results typically benefit from being correlated or validated by some other NDE methods or limited destructive sampling such as core extraction, or chloride sampling and testing.

Although these limitations exist, GPR is still a beneficial tool that can be used in combination with other evaluation techniques to evaluate bridge deck deterioration.

2.2.5. Other Nondestructive Evaluation Methods. Many other methods exist that can be applied to detecting bridge deck deterioration. Although methods in this section are not discussed in other sections of this thesis, they are still evaluation tools that can be used in bridge deck condition assessments. In this section, several nondestructive testing methods that can be used for bridge deck condition assessments are briefly summarized.

2.2.5.1 Half-cell potential. Half cell potential (HCP) measurements are used to evaluate the active corrosion in steel reinforcement. The potential difference between reinforcement and a standard portable half-cell is measured, which can be used to

determine the probability of active corrosion. Some limitations of the device include difficult interpretation due to numerous material properties that can influence measurements, and required prewetting of the test object to allow galvanic coupling [16].

2.2.5.2 Infrared thermography. Infrared thermography (IR) utilizes temperature variations of the bridge deck surface to predict areas of deterioration. Voids, cracks, delaminations, and concrete disintegration can be located using IR. Sections of the bridge deck that contain concrete with different material properties, such as density, thermal conductivity, and specific heat capacity have different rates of heating and cooling, therefore these differences can be located [16].

2.2.5.3 Seismic methods. Seismic methods can be used to detect bridge deck deterioration. Two methods discussed in this section are impact echo (IE) and ultrasonic surface-wave (USW). Both of these techniques are utilized in the Portable Seismic Property Analyzer (PSPA). The PSPA is shown in Figure 2.9 below.

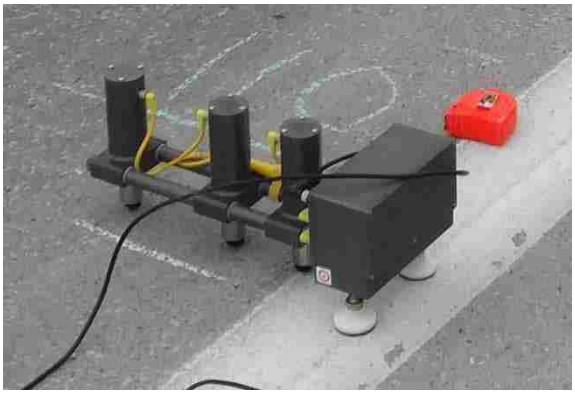

Figure 2.9. Portable Seismic Property Analyzer (PSPA)

The IE method is used to detect and assess delaminations, evaluate vertical cracks, and evaluate materials, such as concrete. According to Gucunski, IE is primarily used to identify the position of wave reflectors in the bridge deck using the return frequency spectrum [15].

During the USW test, the surface material is impacted using a high frequency source. The time domain signals are recorded and then processed to obtain dispersion

curves, which are phase velocity vs. wavelength or frequency. Current USW devices automatically process this data. From the USW test, elastic modulus profiles can be generated [16].

2.2.6. Combined Methods of Nondestructive Evaluation. Each nondestructive test method has its advantages and limitations. In order to increase the accuracy of interpretation and overall condition assessment of the bridge deck, multiple nondestructive methods can be used together. Recent work has focused on the development of tools that integrate various individual NDT tools to optimize the results. As an example, the FHWA has developed the RABIT bridge deck assessment tool as part of the Long-Term Bridge Performance (LTBP) program [34]. This tool, shown in Figure 2.10 below, contains a panoramic camera, high-definition imaging, electrical resistivity, impact echo and ultrasonic surface waves, GPR, and GPS.

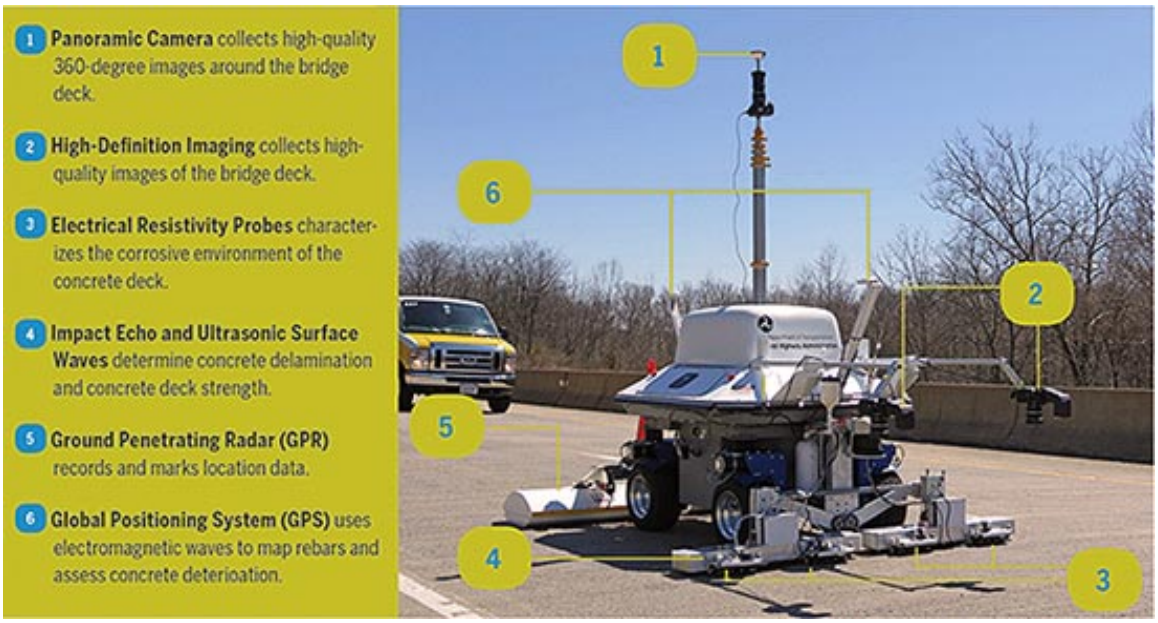

Figure 2.10. RABIT Bridge Deck Assessment Tool [34]

Ultimately, the RABIT is designed to allow engineers to detect current and future areas of concern on a bridge deck. This tool enables a faster and more comprehensive deck evaluation than acquiring individual data sets. The LTBP program states that

"improved understanding of concrete deck performance will promote the safety, mobility, longevity, and reliability of the Nation's highway transportation assets [34]."

2.3. DESTRUCTIVE EVALUATION METHODS FOR INVESTIGATING BRIDGE DECK DETERIORATION

Destructive evaluation techniques are commonly used by transportation officials to monitor bridge decks and plan for repairs and rehabilitations. Two methods discussed in this section include coring and chloride ion concentration testing. Both methods provide localized information about the condition of bridge decks, but they can also be used to validate the results of NDE methods which typically cover more area of the bridge deck.

2.3.1. Coring. Extracting concrete cores from bridge decks is an accurate method to assess localized areas of a bridge deck. ASTM C 42 describes a procedure that can be followed to extract cores from concrete [35]. Core specimens are extracted perpendicular to the concrete surface in the area of interest. Cores are typically taken from areas where distress is noticed to determine the cause of the deterioration. Typically a simple visual inspection is performed on the cores after extraction. ASTM C 856 can be followed if a petrographic analysis is desired [36].

Although coring does provide accurate data, and there are many tests that can be performed on the extracted cores, there are some limitations. Coring provides data for a very small percentage of the bridge deck, and typically transportation officials limit the amount of coring to ensure the strength and durability of the deck. Core extraction and analysis can be expensive because road crews are required to extract the cores, along with trained experts to perform the laboratory analysis. Also, lane closures are required while road crews perform the core extraction and fill the core holes. These core holes can also create weakened zones in the deck and allow moisture and deicing salts to penetrate to the reinforcing steel if not properly filled.

2.3.2. Chloride Ion Concentration Measurements. Chloride ion concentration tests are commonly performed by many transportation agencies to determine the level of chloride intrusion into the bridge deck. Measurements are taken at different levels within the deck, providing a chloride ion concentration profile. If the concentration is high

enough near the reinforcing bars, corrosion can result as the protective passive layer of the reinforcement is broken.

There are two types of tests that can be performed to determine chloride ion contents. The first test determines the acid-soluble chloride ion content. The acid-soluble chlorides include chlorides present in the cement. ASTM C1152 can be followed to determine the acid-soluble chloride content [37]. Water-soluble chlorides are the other form of chloride ions that can be measured in bridge decks. They are known to lead to the initiation or acceleration of corrosion in metals [38]. These chloride ions can be a result of deicing chemicals. ASTM C1218 can be followed to determine the amount of chloride ions present in concrete [38].

Samples for testing can be obtained either from cores extracted from the deck, or directly from the bridge deck. If cores are used, vertical sectioning and pulverization is required before the samples can be tested. If the samples are removed directly from the bridge deck, a rotary hammer can be used to pulverize the concrete, and then the sample can be removed directly from the deck. In this process, samples are taken at specific depth increments, with cleaning of the sampling hole using a vacuum or compressed air in between samples. Figure 2.11 below shows the use of a rotary hammer to extract chloride ion samples.

Figure 2.11. Pulverization Using a Rotary Hammer (Left) and Sample Extraction (Right) for Chloride Ion Determination

Although chloride ion testing is commonly used to determine the likelihood of the steel reinforcement corroding, the exact threshold values for corrosion are difficult to determine [39]. According to Kepler, the concentration of chloride ions at the corrosion threshold is dependent on the ratio of chloride ions to hydroxide ions, however it is not generally presented in this way [39]. In this thesis, a threshold value of 0.15% water-soluble chloride ions by weight of cement will be used. This value comes from a study conducted by the FHWA [2].

2.4. METHODS OF BRIDGE DECK REHABILITATION

Departments of transportation have several methods that they use to repair and rehabilitate their bridge decks. Typically the most cost effective method is that chosen by transportation officials. If the deck is in very bad shape and the substructure is in good shape, a complete deck replacement is considered. In other cases, the deck surface may have deterioration that can be repaired at a lower cost than a complete replacement. Common deck repair strategies used by transportation officials are discussed in this section.

2.4.1. Complete Deck Replacement. In some cases, transportation officials determine that a complete bridge deck replacement is more cost effective than rehabilitation. When a deck replacement occurs, the existing deck is completely removed from the substructure of the bridge, and then it is replaced. In 2012, MoDOT completed their Safe and Sound project, in which 248 bridges were rehabilitated in 3.5 years, most of which consisted of complete deck replacements [40]. The average length of bridge closures during this project was 46 days, which also included 554 bridges that were completely replaced [41].

Whenever a bridge deck is replaced, it is critical that the closure time be as short as possible to ensure traffic disruption is minimized. Therefore, there are many construction methods available that can be considered in order to decrease the construction time of a bridge deck. One of those methods is to use precast prestressed panels. These panels can either be partial depth or full depth. MoDOT used full depth precast segments to replace a 1698 ft. bridge deck in 2004. The construction method

used closed the bridge Sunday through Thursday nights from 7 PM to 7 AM from Memorial Day to Labor Day 2004, allowing the bridge to be open during heavy traffic periods [42].

2.4.2. Removal and Replacement of Deteriorated Concrete. In some cases, transportation officials find it cost effective to repair deteriorated bridge decks rather than replace them. The level and type of repair varies for each case. There are two common methods to remove the loose and deteriorated concrete, traditional impact removal, and hydrodemolition.

2.4.2.1 Traditional impact removal. The most common way to remove deteriorated concrete during the rehabilitation of a bridge deck is to use impact sources, such as jackhammers, to break up the concrete. The repair process starts with a deck sounding using chains and/or hammers as discussed in Section 2.2.2. Sections that sound deteriorated are marked. Rectangular saw cuts are made around the deteriorated area. Jackhammers are then used to break apart the deteriorated concrete. After the concrete is removed, sandblasting of rusty or dirty reinforcing steel is required. Fresh concrete is then placed into the hole and allowed to cure before reopening to traffic. Concrete used for such patching operations is typically designed for early strength development, which in some instances can lead to early deterioration caused by shrinkage cracking [43].

2.4.2.2 Hydrodemolition. Hydrodemolition is increasing in popularity for the use of bridge deck rehabilitations. It provides several advantages over traditional impact removal techniques. Hydrodemolition utilizes a high pressure water jet stream with pressures in the range of 14,000 to 20,000 psi [44]. Prior to hydrodemolition, the deck must be scarified by using a milling machine. The hydrodemolition machine is then calibrated to remove all unsound concrete plus a little bit more (about 0.5 in.) into sound concrete. Removal of deteriorated concrete may include concrete that is spalled, cracked, delaminated, chloride contaminated, carbonated, or damaged by fires or cycles of freezing and thawing [44]. The machine typically removes the material in one pass, but if needed a second pass can be made. Figure 2.12 below shows a hydrodemolition machine being used to break apart deteriorated concrete. A vacuum is then used to remove all debris from the deck while it is still wet. The deck is then sounded, and any deteriorated concrete that still remains is removed with a jackhammer.

Figure 2.12. Hydrodemolition Machine [45]

Hydrodemolition is a faster, cleaner, and better way to remove deteriorated concrete from bridge decks than traditional impact methods [46]. The hydrodemolition process eliminates the need for saw cuts, sandblasting, and individual patching of deteriorated areas. Hydrodemolition does not induce micro fracturing like impact methods do, therefore the repairs are expected to last longer than when using impact methods [46]. MoDOT has experienced a lot of early deterioration on bridge decks rehabilitated using traditional impact methods, which they concluded is due to the micro fracturing caused by such methods [46]. After the hydrodemolition process, the concrete surface is sufficiently roughened to enhance the bond and help ensure composite action between the base concrete and the repair material [44]. After the deck is free of debris, a latex modified concrete overlay is then placed on top of the existing concrete.

3. BRIDGE INVESTIGATIONS

In order to determine the utility of GPR to predict bridge deck deterioration, comprehensive investigations of two bridge decks were undertaken. Section 3.1 discusses the methods used to investigate the bridge decks. Sections 3.2 and 3.3 discuss each bridge and show some of the investigation results, which are further discussed in Section 4.

3.1. METHODS OF INVESTIGATION

Bridges in this study were investigated in situ to evaluate the bridge deck condition using non-destructive and destructive methods described in Sections 3.1.1 through 3.1.5. Prior to field investigations, comprehensive CAD drawings were created with the computer program AutoCAD, using as-built bridge drawings supplied by MoDOT. The CAD base map drawings incorporated important structural elements of each bridge, including the bents, main support beams, deck outline, and deck reinforcement, along with the curb and barrier wall as illustrated in Figure 3.1 below. Typical cross sections of each bridge deck were also created as shown in Figure 3.2. Bridge deck field investigations commenced following the creation of the drawings and the determination of evaluation methods. At the start of each field investigation, chalk lines were drawn on the top surface of the deck to mark the locations of the GPR traverses. Reinforcing bars were then located with the GPR and marked with chalk to mark locations for the PSPA tests. It should be noted that PSPA is not within the scope of this thesis, however it is mentioned here for completion. The visual inspection, GPR scan, and PSPA tests were all performed simultaneously. Once all of the data were collected, core locations were chosen and cores were removed. The cores were then transported to Missouri S&T where they were carefully examined and later sent to MoDOT to measure chloride ion concentrations. Researchers from Missouri S&T's lidar crew scanned the bridges before and after hydrodemolition to document and determine the amount and locations of concrete removal. Researchers who performed the initial

investigation returned to the bridges after the hydrodemolition process to photograph and measure the depth of concrete removal for segments of the two bridge decks.

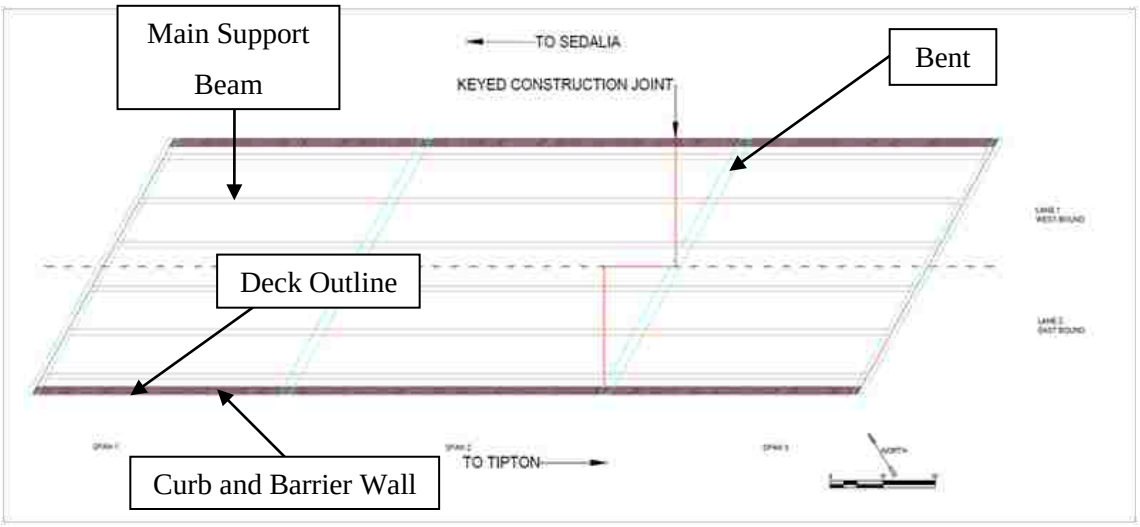

Figure 3.1. Sample Base Map CAD Drawing

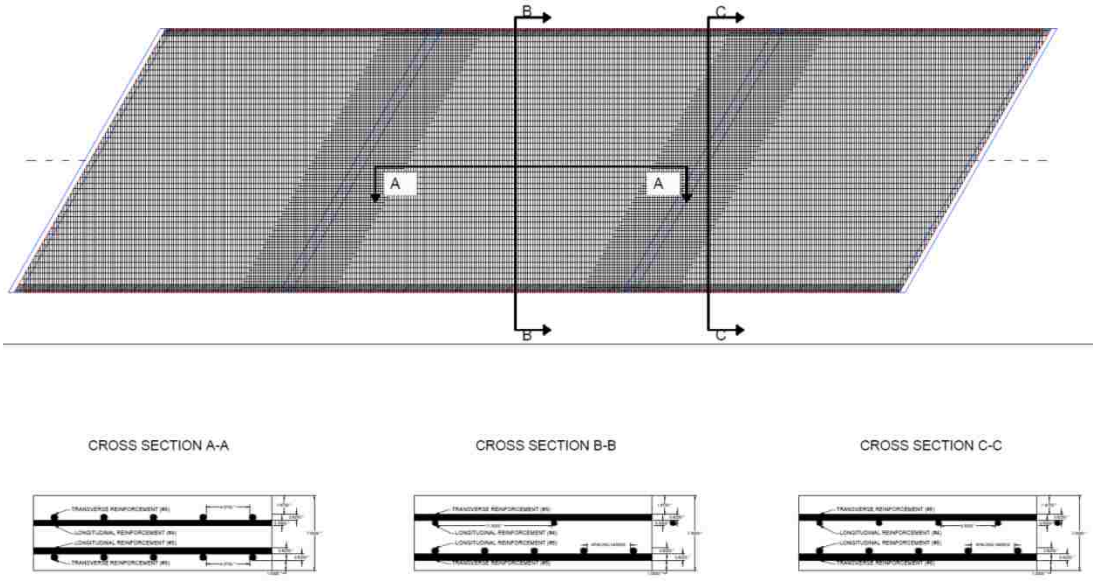

Figure 3.2. Sample Cross Section CAD Drawing of Bridge Deck

3.1.1. Visual Inspection. Each bridge was carefully examined for defects and deterioration by the researchers on site. The top of each bridge deck was thoroughly examined for signs of defects and deterioration including asphalt and concrete patches, cracks, unfilled spalls, and efflorescence. Where time and access allowed, the underside of the deck was quickly examined for concrete spalling, rust marks, efflorescence, and any other signs of deterioration. Each noted item on the top of the deck was numbered, measured, and photographed. These notes were later incorporated into CAD drawings of the bridge, showing the exact size, location, and type of defect or deterioration as shown in Figure 3.3 below.

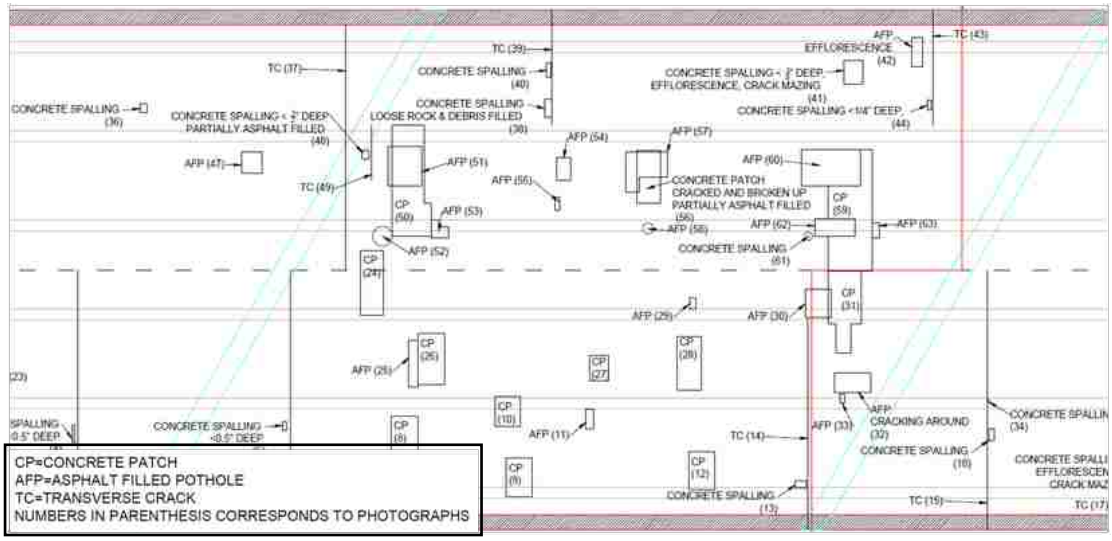

Figure 3.3. Sample Visual Inspection Results

3.1.2. Ground Penetrating Radar Scan. The GPR scan was performed using a GSSI 1.5 GHz ground coupled antenna mounted to a cart as shown in Figure 3.4 below. Profile lines were first marked with chalk on the deck surface, and then the antenna was pushed along the profiles to acquire data. The profiles were oriented parallel with the direction of traffic flow (i.e., longitudinal direction of the bridge). The top layer of reinforcing bar in the transverse direction of the bridge was used as a reflector for the analysis described in this thesis. The material, and therefore the dielectric constant, was

assumed uniform during the GPR data acquisition. Surfer, a computer program used for contouring and surface modeling, was then used to generate 2-D maps showing the reflection amplitude from the top transverse layer of reinforcing bar, which is how the GPR results are presented in this thesis. It is important to note that the results between GPR profiles are interpolated within the program, which could be a cause of misinterpretation and lack of correlation between some data sets as mentioned in the following sections. The program also generated a color scale to correspond to the normalized reflection amplitude presented in the contour maps. After correlating the GPR results with the visual evaluation of the cores, reflection amplitude ranges for three deterioration categories were defined. The three categories defined are no evidence of deterioration, evidence of moderate deterioration, and evidence of extensive deterioration, corresponding to relatively high amplitude, moderate amplitude, and low amplitude, respectively. The amplitude range for each category was determined by the researchers using core visual evaluation results.

Figure 3.4. GSSI 1.5 GHz Ground Coupled GPR System

3.1.3. Portable Seismic Property Analyzer. Data from the PSPA were obtained while the visual inspection and GPR scan were taking place. As mentioned in Section 3.1, PSPA is not within the scope of this thesis, but the description is included here for

completion. PSPA data were acquired in a grid formation over small sections of the bridges, typically 10 ft. by 8 ft., with a typical spacing between set points of 2 ft. Typically, one to three PSPA grids were set up per lane, depending on the allowed time. PSPA data were also acquired over most cores prior to their removal from the deck. As part of the final deliverable, PSPA data were plotted on the final bridge deck drawings as illustrated in Figure 3.5 below.

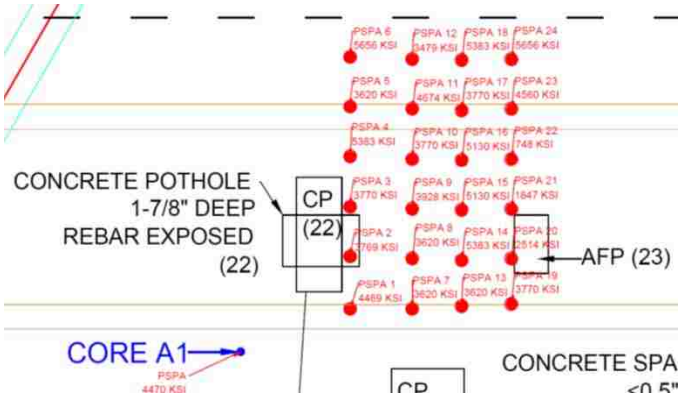

Figure 3.5. Sample PSPA Data Plotted on Bridge Deck Drawing

3.1.4. Cores. Core locations on the bridge deck were chosen based on the visual inspection, raw GPR data, and USW data from the PSPA tests. Core locations were chosen both from areas where the bridge deck appeared to be in good condition from the data, and areas where the deck appeared to be in bad condition. Six to twelve cores were removed from each deck, depending on the deck condition and the limit set by MoDOT. Cores were 2 in. diameter and were drilled to at least the bottom of the top transverse reinforcing bar where possible. MoDOT personnel extracted the cores after the locations were marked and measured by Missouri S&T researchers as shown in Figure 3.6 below. Cores were then individually labeled, bagged, and transported back to Missouri S&T for further testing. Cores were evaluated visually, tested for volume of permeable voids, and tested for chloride ion concentration as discussed in Sections 3.1.4.1 through 3.1.4.3.

Figure 3.6. Extraction of Cores

3.1.4.1 Visual evaluation. The bridge deck cores were carefully examined and documented at Missouri S&T. Visible properties examined included diameter, length, surface material, number of pieces and the length of each piece, presence of reinforcing bar, concrete roughness, number of voids, quality of aggregate coating with the paste mixture in the concrete, the volume of paste, signs of air entrainment, flaking surfaces, discolorations, delaminations, segregation of the aggregate, and presence of cracks. Based on this analysis the cores were then given a visual core rating defined for this project of either "Good", "Fair", or "Bad". A visual core rating of "Good" indicates that the core had no delaminations or visible deterioration present. "Fair" indicates that the core had some visible deterioration including delaminations, however the concrete is in a few large sections. "Poor" indicates that the core had a lot of deterioration and was in many pieces when extracted, including several small pieces. If asphalt was present on the surface of the core, only the concrete portion was rated using the visual inspection, however the bond and condition of the asphalt layer was noted in the "Other Comments" section. Figure 3.7 below illustrates the data collected from the visual inspection of the bridge deck cores.

Core	A1	A2	A3	B1	B2	B3
Diameter (in)	2.0	2.0	2.0	2.0	2.0	2.0
Length (in)	2.5-3.0	2.75-3.375	3.125-3.75	~3.0	5.25-6.0	3.875-4.125
Surface (Asphalt: A, Concrete: C)	C	C	C	C	C	C
Number of Pieces	1	1	2	5	2	1
#1 Length (in) and failure mode [1]	2.5-3.0, CEX	2.75-3.375, CEX	1.875, PRE	1.5, PRE-Non rebar metal in core	0.25-1.0, PRE	3.875-4.125, CEX
#2 Length (in) and failure mode	N/A	N/A	1.25-1.75, CEX	0.25, PRE- Non rebar metal in core	4.25-4.75, CEX	N/A
#3 Length (in) and failure mode	N/A	N/A	N/A	0.25, PRE	N/A	N/A
#4 Length (in) and failure mode	N/A	N/A	N/A	0.25, PRE	N/A	N/A
#5 Length (in) and failure mode	N/A	N/A	N/A	0.25, CEX- Rebar marks visible on edge	N/A	N/A
Rebar: diameter (in), length (in), orientation [2], corrosion [2]	None	None	None	None	None	None
Roughness (Smooth, Average, Very Rough)	Smooth	Average	Average	Rough	Average	Average
Voids (Number >0.25 in. diameter)	1	2	0	0	5	1, 0.875" long 0.5" wide, 0.5" deep
Coating of the Aggregate (good or bad)	Good	Good	Good	Good	Good	Good
Volume of Paste (good or bad)	Good	Good	Good	Good	Good	Good
Air Entrained (yes or no)	Yes	Yes	Yes	Yes	Yes	Yes
Flaking surface: thickness (in)	None	None	None	None	None	None
Discoloration: color, maximum length (in)	None	None	None	Rust, 1.5 @ Bottom of piece 1 and 2	None	None
Delaminations: depths (in)	None	None	1.875	1.5, 1.75, 2.0	1.0	None
Segregation of Aggregate: depths (in)	None	None	None	None	None	None
Cracks (excluding fracture planes): number, type, length (in)	None	None	None	None	None	None
Other Comments						
General Quality of Concrete[3] (good, fair, bad)	Good	Good	Fair	Bad	Fair	Good

[1]Preexisting Rupture (PRE), Induced during coring (IDC), Produced by shear from extracting the core (CEX), Generated during handling (HAN), Other cause (OTR)
[2]Orientation: traverse (Tr) or longitudinal (Lo); Corrosion: none (Co1), low (Co2), average (Co3), high (Co4)
[3]Good indicates no delaminations or visible deterioration, Fair indicates some visible deterioration including delaminations however concrete is in large sections, Bad indicates concrete shows a lot of deterioration and is in many pieces including several small pieces

Figure 3.7. Sample Visual Core Inspection Results

3.1.4.2 Volume of permeable pores. The volume of permeable pores in the concrete cores indicates the amount of water that is able to enter into the pore structure of the concrete. The more permeable the concrete, the more water can enter into the pore structure and deteriorate the concrete with freeze/thaw cycles, along with allowing deicing agents to enter and accelerate the concrete degradation. In this thesis, it was postulated that a higher percentage of permeable pores in the concrete corresponds to a higher level of deterioration in the concrete. Figure 3.8 illustrates the process followed to obtain the volume of permeable pores. This test was performed following ASTM C642-06 [47]. Steps taken to determine the volume of permeable pores were:

1. The mass of the cores was initially determined, and then the cores were placed into a 220°F oven for 24 hours. The cores were then cooled to room temperature, and the mass was determined again. If the percentage difference between final and initial mass was more than 0.5% then the cores were placed back into the oven for another 24 hours. If the percentage difference in mass with a 24 hour period of being in the oven was less than 0.5%, they were considered dry, and the

final mass was recorded. This process was repeated until all of the cores had a mass difference of less than 0.5% within a 24 hour drying cycle.

2. The concrete cores were immersed in room temperature water for 48 hours. The cores were then surface dried using a towel, and the mass was determined. If the mass in a 24 hour period of soaking increased by less than 0.5%, the cores were considered saturated. This process was repeated until all cores had an increase in mass of less than 0.5% in a 24 hour period. The final mass was recorded as the saturated mass after immersion.
3. A 30 qt. aluminum cylindrical container was used to boil the cores in water for 5 hours. The cores were allowed to cool to room temperature. After cooling, the surface of the cores was dried, and the saturated mass after boiling was determined.
4. The concrete cores were suspended in room temperature water, and the immersed apparent mass was determined.

Figure 3.8. Process of Determining Volume of Permeable Pores

3.1.4.3 Chloride ion concentration. Chloride ion concentration levels indicate the likelihood for corrosion of the reinforcement steel. Once corrosion of the reinforcing steel is initiated, further deterioration of the surrounding concrete will occur and eventually lead to a delamination of the concrete from the steel. GPR also responds to the presence of saline moisture, therefore the chloride ion concentration levels were expected to correlate with GPR results. Areas with higher chloride ion concentration levels were expected to correlate to lower reflection amplitudes in the GPR data, indicating higher likelihood of deterioration.

Tests to determine the chloride ion concentration of the concrete cores were completed by MoDOT. MoDOT followed ASTM C1218/ C1218M-99 to determine the water soluble chloride ion concentrations at different depths in the concrete [48]. After

the visual evaluation and the volume of permeable pores tests were completed (Sections 3.1.4.1 and 3.1.4.2, respectively), several cores were selected for chloride ion concentration measurements. Chloride ion concentration was measured on three to five cores per bridge, depending on the length of the bridge. Many of the cores were in multiple pieces after being extracted from the deck. Furthermore, due to the size of the core (2 in. diameter), it was difficult to obtain samples to conduct the tests. In order to allow samples to be removed from the cores, MoDOT personnel embedded the cores in fresh concrete. Even with the 2 in. diameter cores encased in concrete, damage occurred to the cores upon sampling. Therefore, chloride ion concentration measurements from few cores are reported in this thesis.

3.1.5. Concrete Removal by Hydrodemolition. MoDOT awarded contracts for the rehabilitation of three of the eleven bridge decks that were investigated in this project during the project duration. All of the construction to complete the three rehabilitations was completed by the same prime contractor within one year of the original bridge deck investigation. The rehabilitation process that was performed included removing deteriorated concrete via hydrodemolition, which was completed by a different contractor. The same contractor conducted the hydrodemolition for all three bridges decks. Prior to the hydrodemolition, the top 0.25 in. of concrete was removed using a mill. Milling the concrete left behind a rough and grooved surface as noted in Figure 3.9 below. After the milling process was complete, the contractor used a machine with high pressure water jets to remove loose and deteriorated concrete, which exposed corroded reinforcement bars in some locations as shown in Figure 3.10 below. The water pressure was set to remove 0.5 in. of sound concrete, therefore, at least 0.75 in. of material was removed from the entire bridge deck surface. A constant water pressure between 14,000 and 20,000 psi was used to remove material. Following the hydrodemolition, traditional hammer and chain sounding techniques were used to identify any areas of the deck that required further concrete removal.

Figure 3.9. Rough Grooved Concrete Surface Caused by Milling (a) and Original As-Built Concrete Surface (b)

Figure 3.10. Corroded Rebar Exposed After Removal of Loose and Deteriorated Concrete by Hydrodemolition

Hydrodemolition removes concrete that is not strong enough to stay intact when a high pressured water stream is applied. Low strength concrete, allowing for removal during the hydrodemolition process, could be a result of deterioration, such as cracking,

delaminations, and chloride intrusion. When MoDOT prepares quantity estimates for construction documents, it is important that the estimates be similar to actual construction quantities. Under or over estimating material quantities can cost MoDOT a significant amount of money. According to Mr. Bill Dunn, a Structural Preliminary and Review Engineer with MoDOT, the deck rehabilitations of the bridges discussed in this thesis were bid based on the following. Scarification of the top 0.25 in. using a mill was paid for the by square yard, and hydrodemolition of the top half inch minimum and all unsound concrete was paid for by the square yard. The new material placed onto the deck includes the material used to replace the removed concrete and complete the new grade rise was paid for as follows: overlay (1.75 in. thick with a 1.0 in. grade rise), partial depth repair, and full depth repair. The partial depth repair was defined as a region in which the thickness of replacement concrete was greater than 0.75 in. Full depth repair was defined as a region where the bottom mat of steel is exposed or the concrete is completely void. Full depth repair costs cover the removal and replacement of the concrete up to the elevation of the bottom of the overlay.

3.1.5.1 Manual measurements. After the loose and deteriorated concrete was removed by the hydrodemolition process, Missouri S&T researchers documented the concrete surface using video, photographs, and manual depth measurements. The manual depth measurements obtained were not indented to be accurate, but rather provide a general sense of the correlation between concrete removal and the data collected in the previous field investigations. Manual depth measurements were also a backup in case the lidar data were not able to be collected. The device used for manual depth measurements consisted of a 10 ft. by 10 ft. grid with 1 ft. grid spacing that was created using PVC pipe and rope as illustrated in Figure 3.11 below. The measuring grid was placed onto the post-hydrodemolition surface to obtain depth estimates for the amount of concrete that was removed. For these measurements, it was assumed that the top of the rope represented the pre-hydrodemolition concrete surface. The depth was measured from the top of the rope in the grid to the top of the concrete surface. A survey point was typically taken either every 4 or 25 square feet, depending on time constraints. The flags in Figure 3.11 are locations where depth measurements were taken when the survey interval was every four square feet. Only a 10 foot wide section of each lane was investigated using

this measurement method. Manual depth measurements were plotted using a spreadsheet and superimposed on the bridge deck drawings containing all of the nondestructive evaluation information.

Figure 3.11. Grid Used to Obtain Manual Depth Measurements

3.1.5.2 Lidar measurements. Missouri S&T's Lidar Applications Team was contracted to obtain depth measurements of concrete removal for the three bridge decks being rehabilitated. Lidar is a form of laser imaging that can be used to map surfaces, in this study the bridge deck surface. The lidar team performed two scans per lane on each bridge deck undergoing rehabilitation. The first scan was completed less than a week before the milling of the concrete bridge deck took place. The second scan was conducted after completion of the concrete removal by hydrodemolition but prior to placing the new concrete overlay. Using these two sets of lidar data, the lidar team was able to subtract the pre-rehabilitation lidar data from the post-hydrodemolition data to obtain the location and depth of material removal. The depth accuracy was determined to be less than 0.4 in. (1 cm.). Figure 3.12 below shows the image generated by subtracting

the second scan from the first scan. The reinforcement is visible in the figure, along with the rough, grooved surface created by the milling of the deck surface.

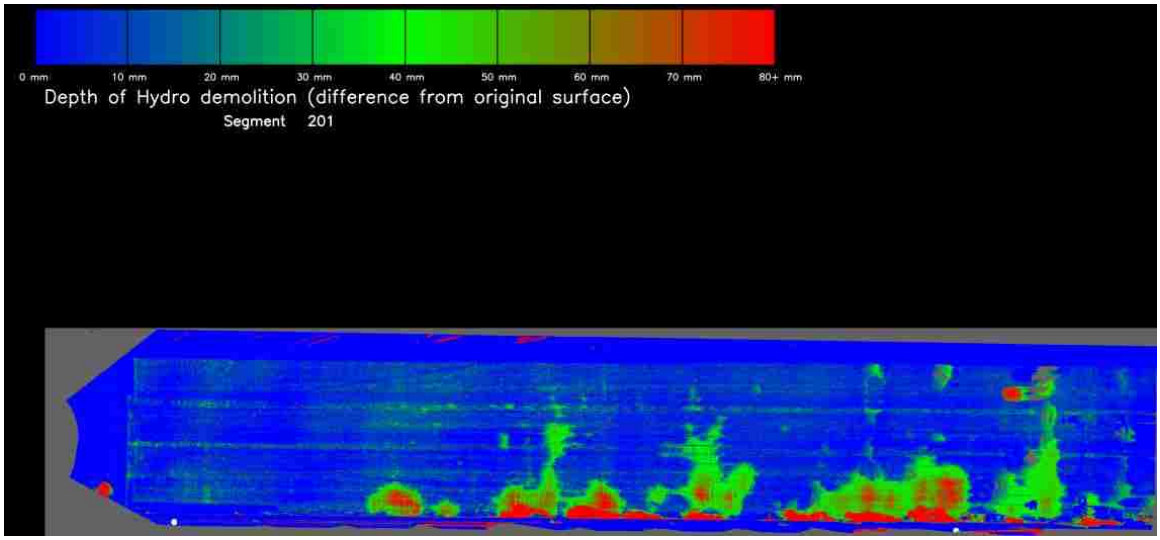

Figure 3.12. Lidar Image of Bridge Deck Showing Depth Difference Between Pre-Rehabilitation and Post-Hydrodemolition

Since MoDOT's bridge deck rehabilitation projects are bid based on the different categories as discussed in Section 3.1.5, the depth of material removal during the rehabilitation process was placed into three similar categories. The first category is a depth of removal less than 0.75 in., which is the depth of material removed by milling and hydrodemolition. The second category is material removal depths between 0.75 in. and the depth to the top of topmost layer of reinforcing bars. The third category is material removal depths greater than the depth to the top of the topmost layer of reinforcing bars. These categories are illustrated in Figure 3.13 below.

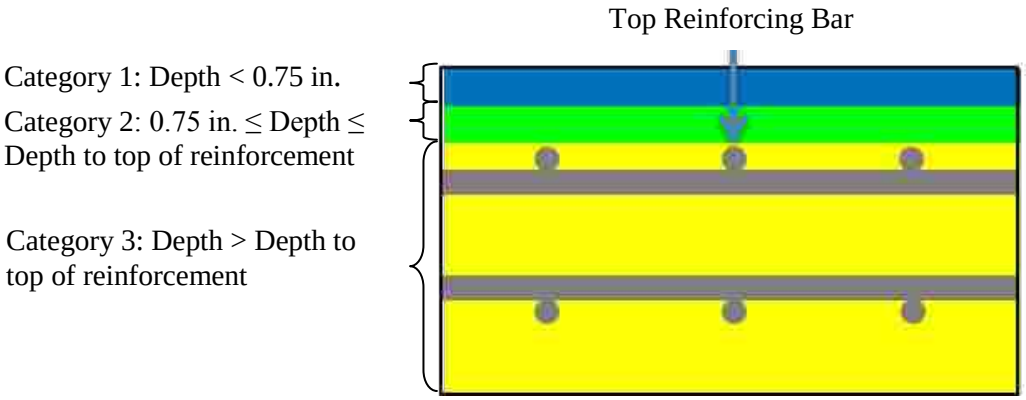

Figure 3.13. Categories of Material Depth Removal during Rehabilitation

3.2. OSAGE RIVER BRIDGE

Bridge A1479 is located near Lake Ozark City, in Miller County, Missouri. The bridge carries U.S. 54 West Bound traffic over the Osage River. Figure 3.14 below shows a side view of the bridge. In November 2012, the initial bridge investigation took place, which included visual inspection of the deck, PSPA, GPR, and coring. Eight researchers assisted in the seven hour long initial investigation. Approximately 0.25 in. of rain was reported in the area within the seven days prior to the investigation. The reported high and low temperatures for the day of the investigation were 64°F and 32°F, respectively. The deck was not prepared in any way prior to the investigation. Debris was minimal in the area of the GPR scan, which only included the two driving lanes.

Rehabilitation of the bridge commenced in March 2013 and was completed in May 2013, with a total project cost of $835,000 [49]. Hydrodemolition was used to remove loose and deteriorated concrete on the outside (West) lane in March 2013, and in April 2013 for the inside (East) lane. Each lane was scanned with lidar before and after the hydrodemolition process to document the concrete removal.

Figure 3.14. Bridge A1479 Side View

3.2.1. Bridge Description. Bridge A1479, as shown from satellite imagery in Figure 3.15 below, carries two lanes of West Bound traffic. The deck is 35 ft. - 4 in. wide, and the structure has a total length of 868 ft., with five spans. The main structural support is a continuous steel girder system. The reinforced concrete deck was cast-in-place. During the 2010 bridge inspection, MoDOT personnel rated the bridge deck a 6 (satisfactory condition) and the superstructure and substructure a 7 (good condition). See Table 2.1 for descriptions of these ratings. Table 3.1 below outlines details of the bridge.

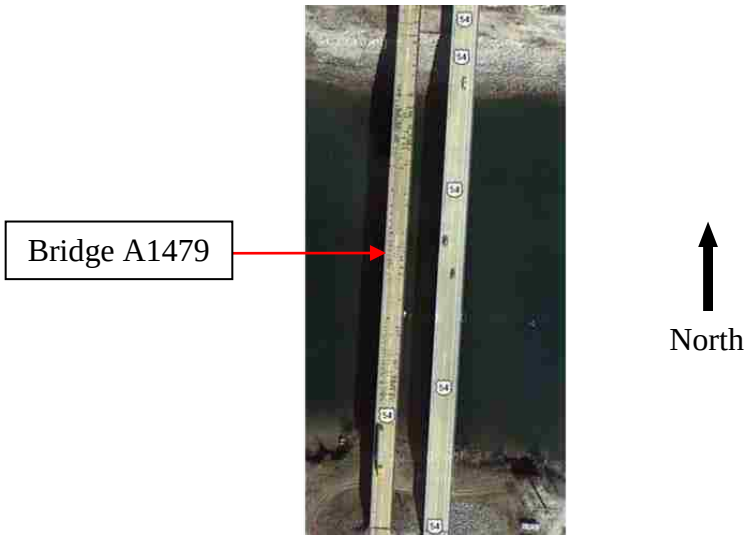

Figure 3.15. Bridge A1479 from Satellite Imagery [50]

Table 3.1. Bridge A1479 Details

Year Constructed	1966
Feature Intersected	Osage River
Number of Lanes	2
Traffic Direction	One-Way West Bound
Number of Spans	5
Deck Width	35 ft. – 4 in.
Inside Curb to Curb Width	32 ft.
Total Structure Length	868 ft.
Main Structural System	Continuous Steel
Deck Construction Type and Material	Cast-in-Place Reinforced Concrete

The bridge deck was designed to be 7.5 in. thick, with a concrete clear cover of 2 in. on top and 1 in. on bottom. Longitudinal (parallel to traffic flow) steel reinforcing bars spaced at 12 in. on center are positioned on top of the transverse (perpendicular to traffic flow) reinforcing bars spaced at 6 in. on center. There are additional longitudinal reinforcing bars in the deck over the bents, making the longitudinal bar spacing 6 in. on center in these areas. All longitudinal bars are #4 (0.5 in. diameter), and all transverse bars are #6 (0.75 in. diameter). All reinforcement bars were uncoated. Figure 3.16 below illustrates the deck reinforcement described above.

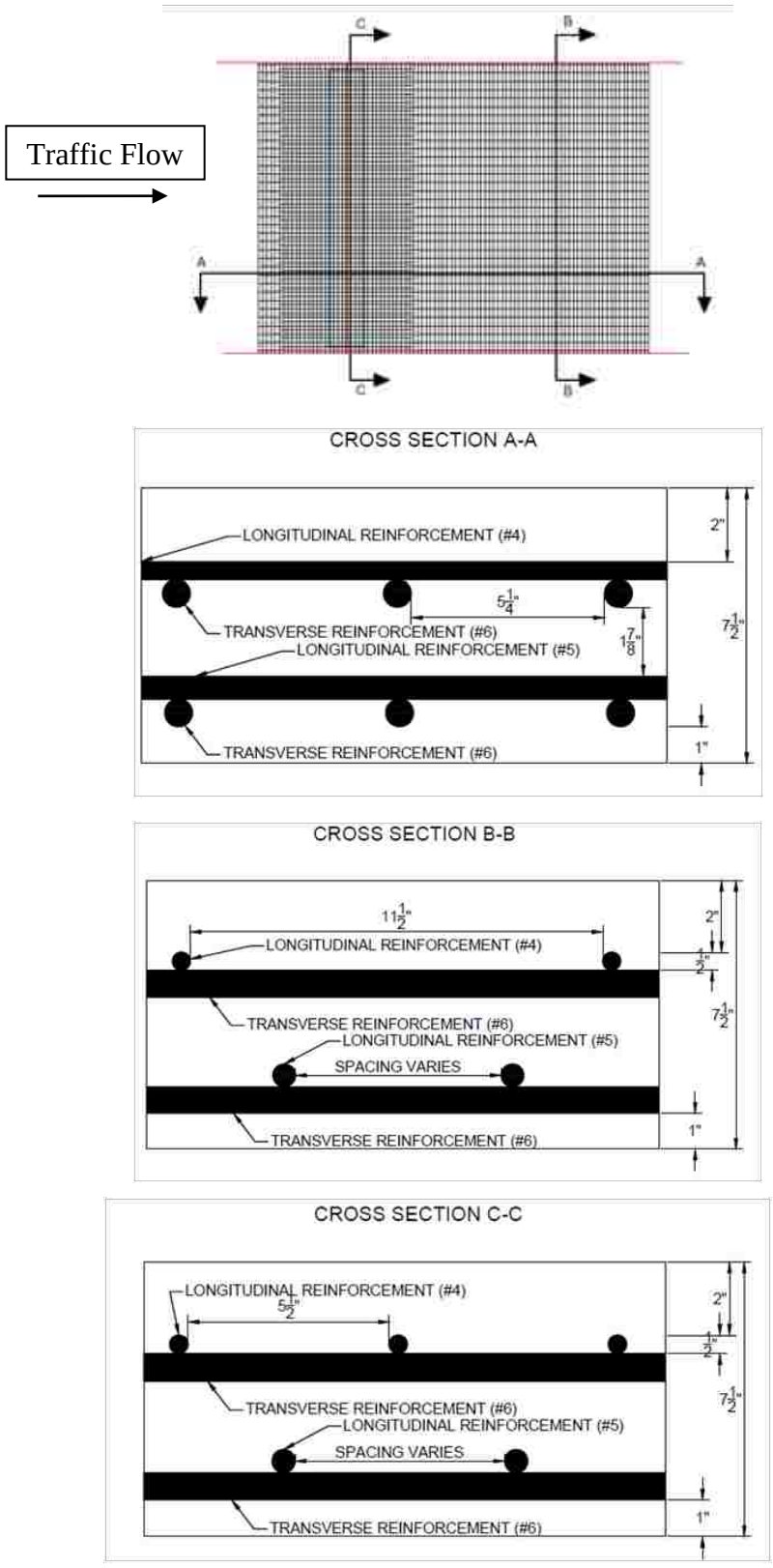

Figure 3.16. Bridge A1479 Deck Cross Sections

3.2.2. Findings. Bridge A1479 was investigated on November 8, 2012. During the investigation, it was noted by researchers that the bridge experienced a large amount of deflection or vibration during heavy traffic loading. The bridge also contained deck drains within the curb. These drains were spaced along both curbs of the bridge. Heavy deterioration was noted around these drains, especially on the side and bottom of the deck as shown in Figure 3.17 below. More detailed findings were noticed with the visual inspection, GPR, cores, and the survey of the post-hydrodemolition deck. See Appendix A for bridge drawings, which include visual inspection findings and GPR results, along with the lidar survey of material removal during the rehabilitation. A complete digital version of the A1479 Bridge Investigation Drawing is included in the Digital Appendix which is further discussed in Appendix F.

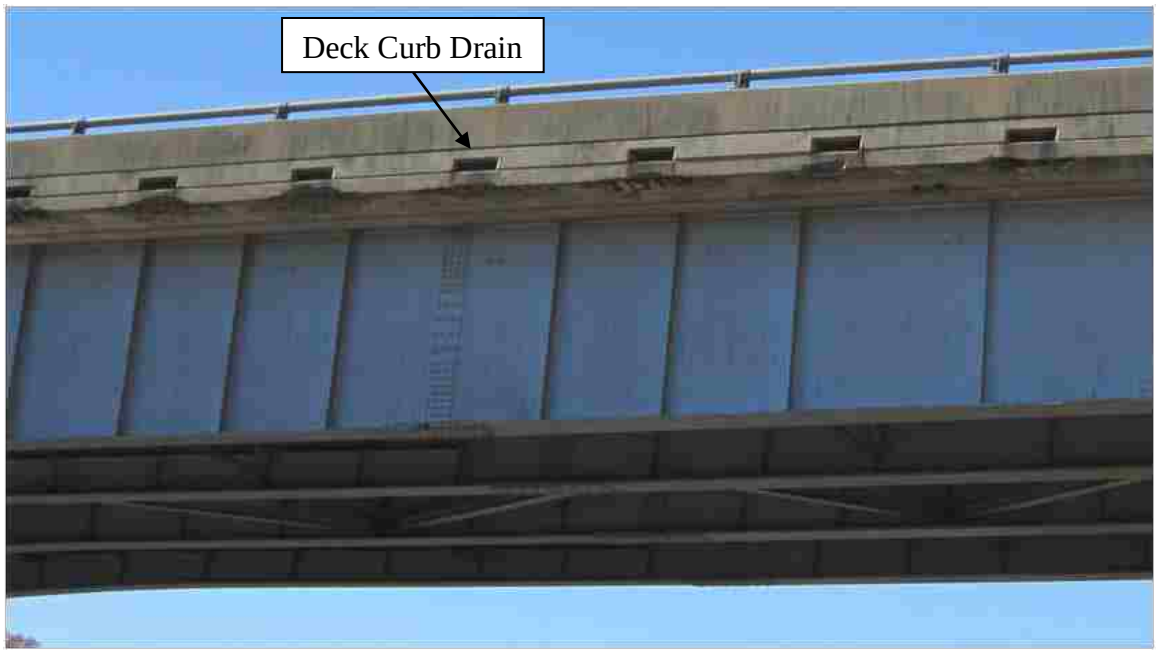

Figure 3.17. Bridge A1479 Deterioration of the Deck Soffit Around Curb Drains

3.2.2.1 Visual inspection. From the visual inspection of the top deck surface of Bridge A1479, 161 defects were documented. Those defects included transverse cracks, concrete patches, asphalt filled potholes, and concrete spalls, including some spalls with

reinforcing bars visible. The majority of the documented defects were located mid-span of the girders (i.e., between the bents). Few defects were noted near the bents as illustrated in Figure 3.18 below.

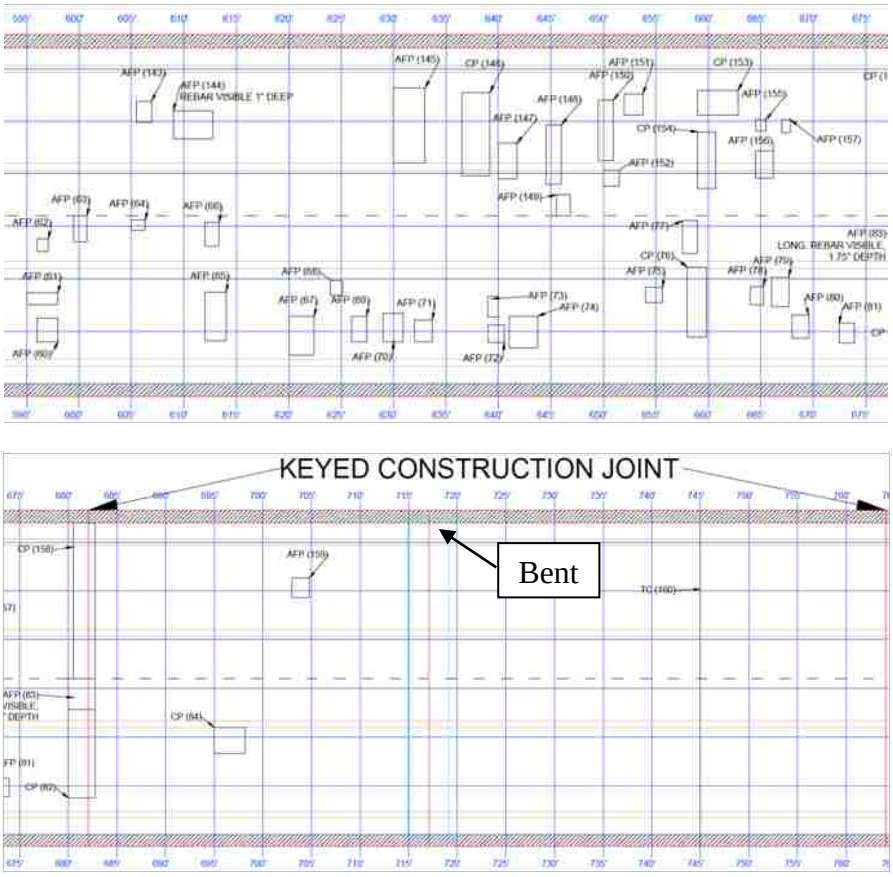

(a)

(b)

Figure 3.18. Bridge A1479 Visual Inspection Results Near Mid-Span (a) and Bent (b)

3.2.2.2 Ground penetrating radar. Both lanes of the bridge deck were scanned with GPR. Due to time constraints, 4.5 ft. of the West shoulder and 3.5 ft. of the East shoulder were not scanned. Therefore, the total width of the GPR scan was 24 ft., compared to the inside curb-to-curb width of 32 ft. The scan covered the entire length of the bridge deck. As discussed in Section 3.1.2, the GPR results included in this thesis were generated from the reflection amplitude from the top transverse layer of reinforcement, therefore the results pertain to the concrete cover above the top transverse

reinforcement. Figure 3.19 below illustrates the GPR results included in the bridge drawing. Increased evidence of deterioration based on the GPR results is more prevalent on the East side of the bridge deck than the West side.

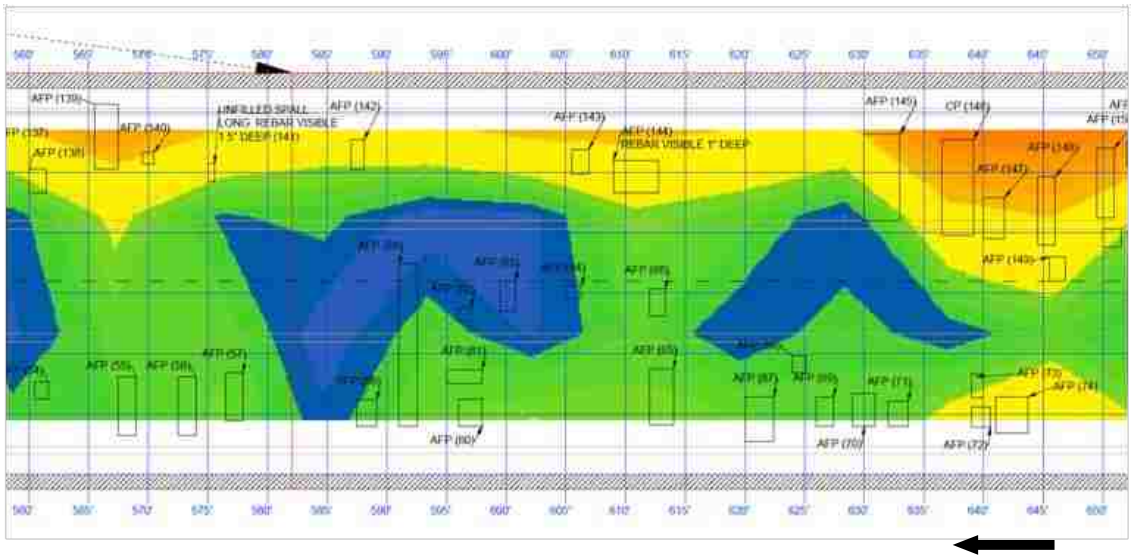

North

GPR Top Transverse Reinforcement
Reflection Amplitude Map Scale (NdB)

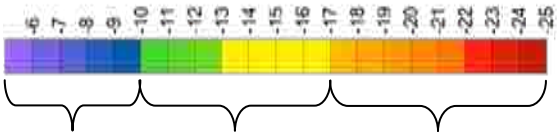

No evidence of deterioration	Evidence of moderate deterioration	Evidence of extensive deterioration

Figure 3.19. Section of Bridge A1479 GPR Results

Most sections of the bridge deck that showed no evidence of deterioration based on the GPR results also had few documented visual defects. Figure 3.20 (a) below shows a section of the bridge deck that has very few visual defects and also shows no evidence of deterioration based on the GPR results. In areas where many visual defects were documented, the GPR results indicate higher levels of deterioration as indicated in Figure 3.20 (b).

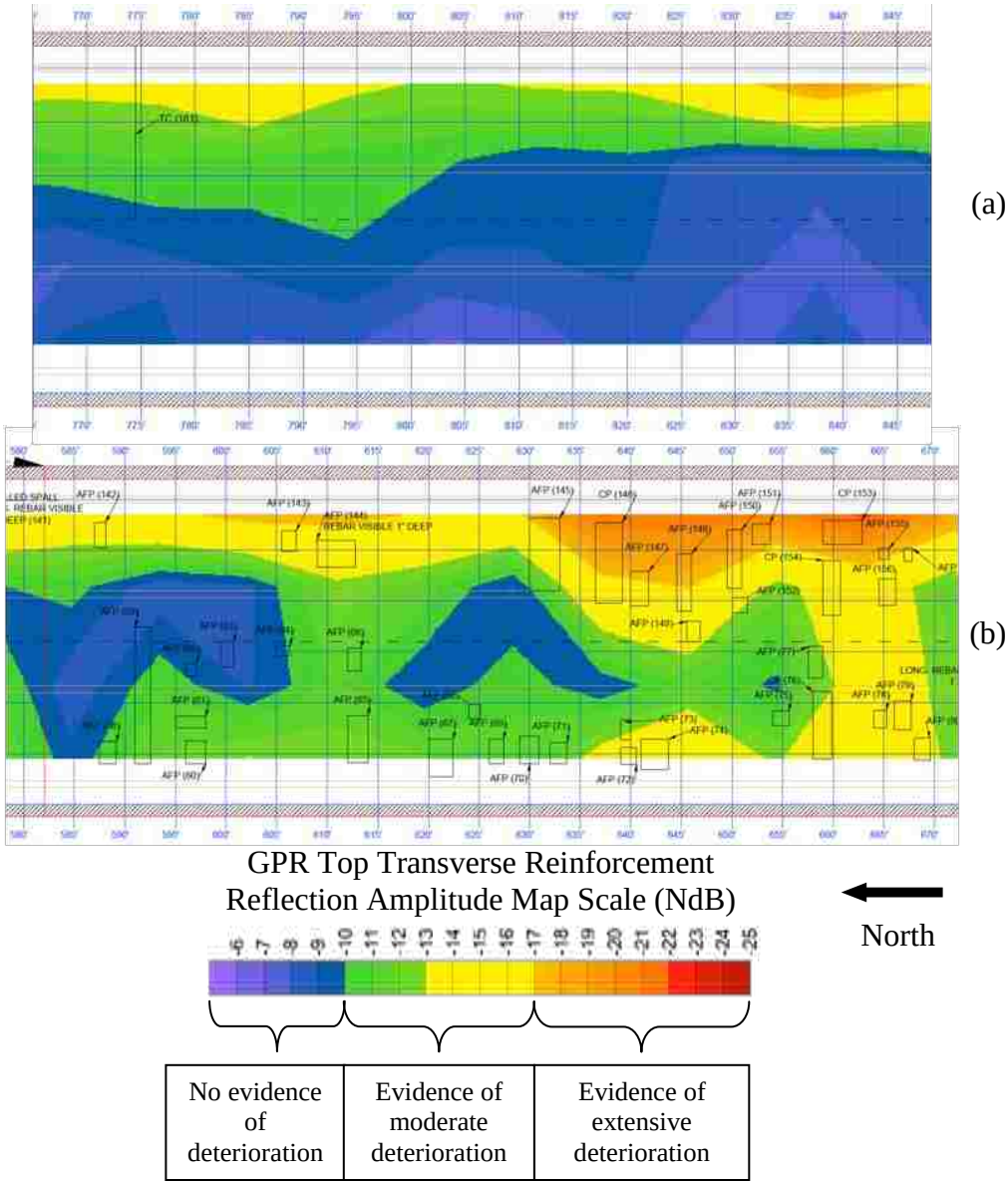

Figure 3.20. Bridge A1479 GPR and Visual Inspection Results with Low Levels of Deterioration (a), and with High Levels of Deterioration (b)

Of the 27,776 sq. ft. inside curb-to-curb area of the bridge deck, 20,760 sq. ft., or 75%, was scanned with GPR. Based on the GPR estimates, 5,398 sq. ft. or 26% of the scanned portion had no evidence of deterioration. 13,494 sq. ft. or 65% of the deck was estimated to have evidence of moderate deterioration, and 1,868 sq. ft. or 9% was estimated to have evidence of extensive deterioration. These values are illustrated in Figure 3.21 below.

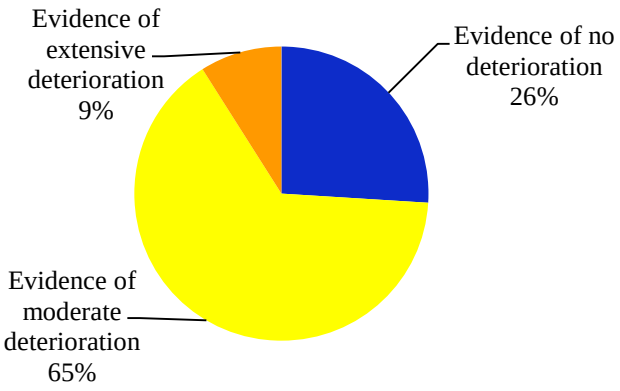

Figure 3.21. Bridge A1479 Deck Deterioration Levels Based on GPR

3.2.2.3 Cores. Nine cores were extracted from the deck of Bridge A1479. Of the nine cores, five were rated good based on visual evaluation, three fair, and one bad. Refer to Section 3.1.4.1 for the core rating criteria. Seven of the cores were composed of the as-built concrete, one of the cores was taken from a concrete patch as determined by the difference in aggregate, and one core was mostly asphalt, with a 0.5 in. piece of as-built concrete on bottom as shown in Figure 3.22 below. Figure 3.23 shows all nine cores extracted from Bridge A1479, along with the visual rating assigned to each during the visual evaluation. Complete core visual evaluation results are included in the Appendix B.

(a) (b) (c)

Figure 3.22. Material Types of Extracted Cores from Bridge A1479, (a) As-Built Concrete, (b) Concrete Patch, (c) Asphalt Overlaying As-Built Concrete

Core: A1 Visual Rating: Fair	Core: A2 Visual Rating: Good	Core: A3 Visual Rating: Fair

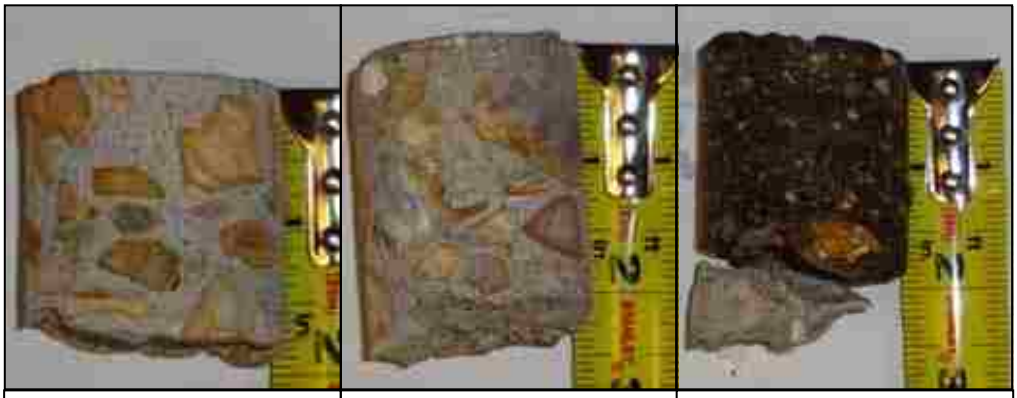

Core: A4 Visual Rating: Good	Core: B1 Visual Rating: Good	Core: B2 Visual Rating: Bad

Core: B3 Visual Rating: Good	Core: B4 Visual Rating: Fair	Core: B5 Visual Rating: Good

Figure 3.23. Bridge A1479 Cores and Visual Core Ratings

Based on the GPR results, four cores were extracted from areas of the bridge deck that had no evidence of deterioration, and five cores from areas with evidence of moderate deterioration. Figure 3.24 below illustrates the locations of Core B3 on the bridge deck drawing containing the visual investigation and GPR. Core B3 is located in an area with no evidence of deterioration based on GPR and no documented visible deterioration. Core B3 was rated good in the visual examination. Figure 3.25 illustrates Core B4, which is located in an area that has evidence of moderate deterioration based on GPR results. The core has a visual evaluation rating of fair due to a delamination. Concrete was not extracted below the delamination because the extraction process would have caused the concrete below the delamination to crumble.

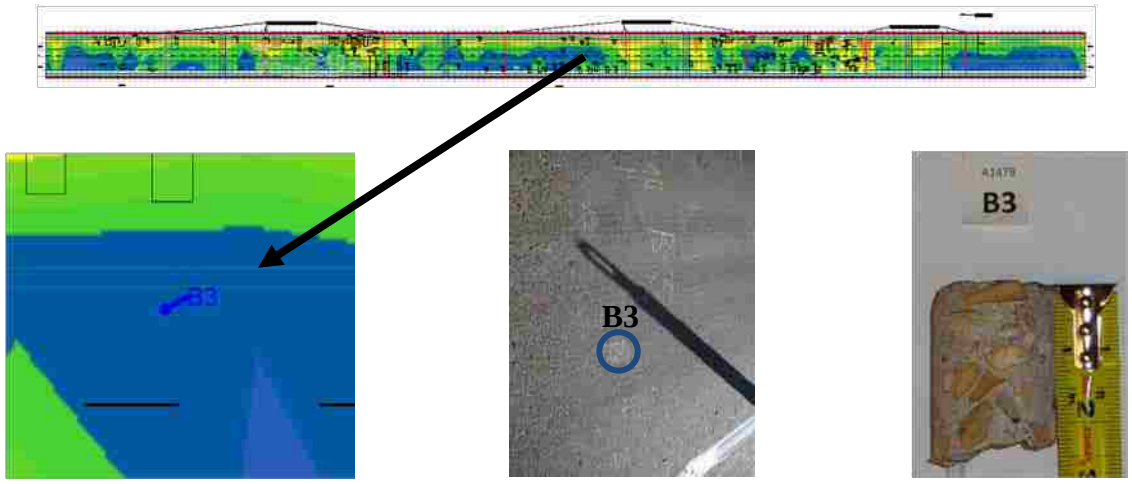

(a) (b) (c)

Figure 3.24. Bridge A1479 Core B3, (a) On Bridge Drawing, (b) Deck Image at Core Location, (c) Extracted Core

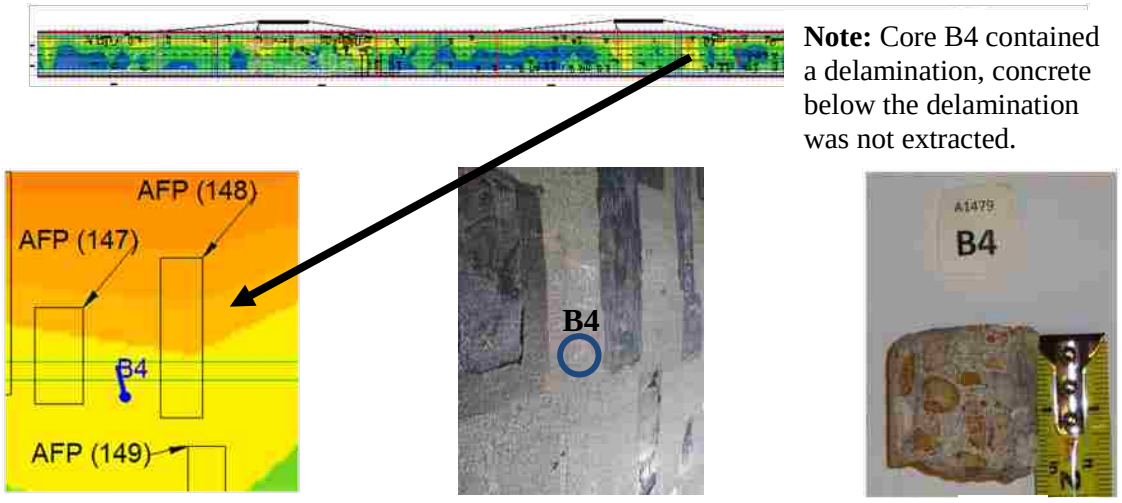

Figure 3.25. Bridge A1479 Core B4, (a) On Bridge Drawing, (b) Deck Image at Core Location, (c) Extracted Core

The volume of permeable pore space was determined for seven of the nine extracted cores. Volume of permeable pores space ranged from 13.01% to 15.32%. Core A2, which was composed of the concrete patch material, split apart during the testing for volume of permeable pores. Core B2 was asphalt, so it was not tested for the volume of permeable pores. Core A3, which was rated fair during the visual evaluation, had the highest volume of permeable pores at 15.32% and Core A4, which was rated good during the visual evaluation, had the lowest volume of permeable pores at 13.01%. Core A3 was extracted from an area with evidence of moderate deterioration based on GPR results, and Core A4 from an area with no evidence of deterioration. Figure 3.26 below illustrates the volume of permeable pore space for the cores. Complete results from the volume of permeable pore space test are included in Appendix E.

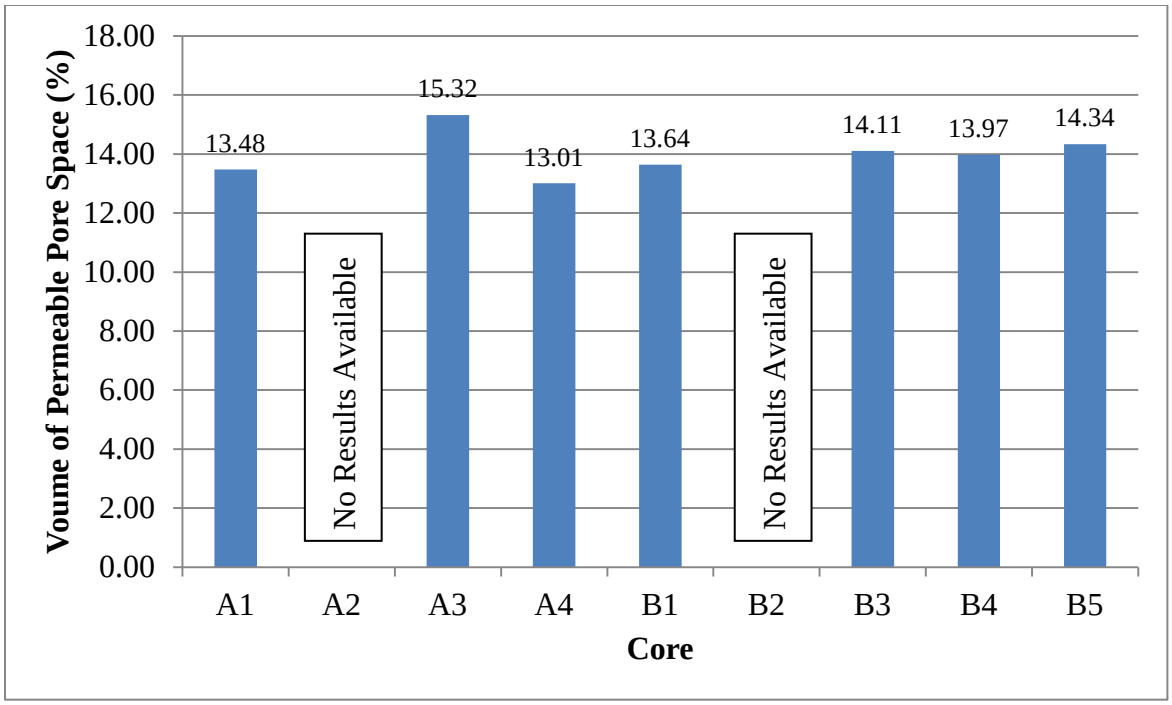

Figure 3.26. Bridge A1479 Volume of Permeable Pore Space Results

Chloride ion concentration test results were obtained for two cores from Bridge A1479, Cores B1 and B3. Both cores were rated good in the visual examination, however B1 showed evidence of moderate deterioration based on the GPR results, and B3 showed no evidence of deterioration. The chloride ion concentration results are illustrated in Figure 3.27 below. Core B3 had a higher initial chloride ion concentration than Core B1, but at a depth of 1.5 in., B1 has a slightly higher percent chloride. The bridge design specifies that the reinforcing bars have a clear cover of 2 in. As discussed in Section 2.3.2, a threshold value of 0.15% water-soluble chloride by weight of cement is used in this thesis as the threshold for the initiation of corrosion. Chloride ion concentrations at or above this level indicate the potential for corrosion of the steel reinforcing bars.

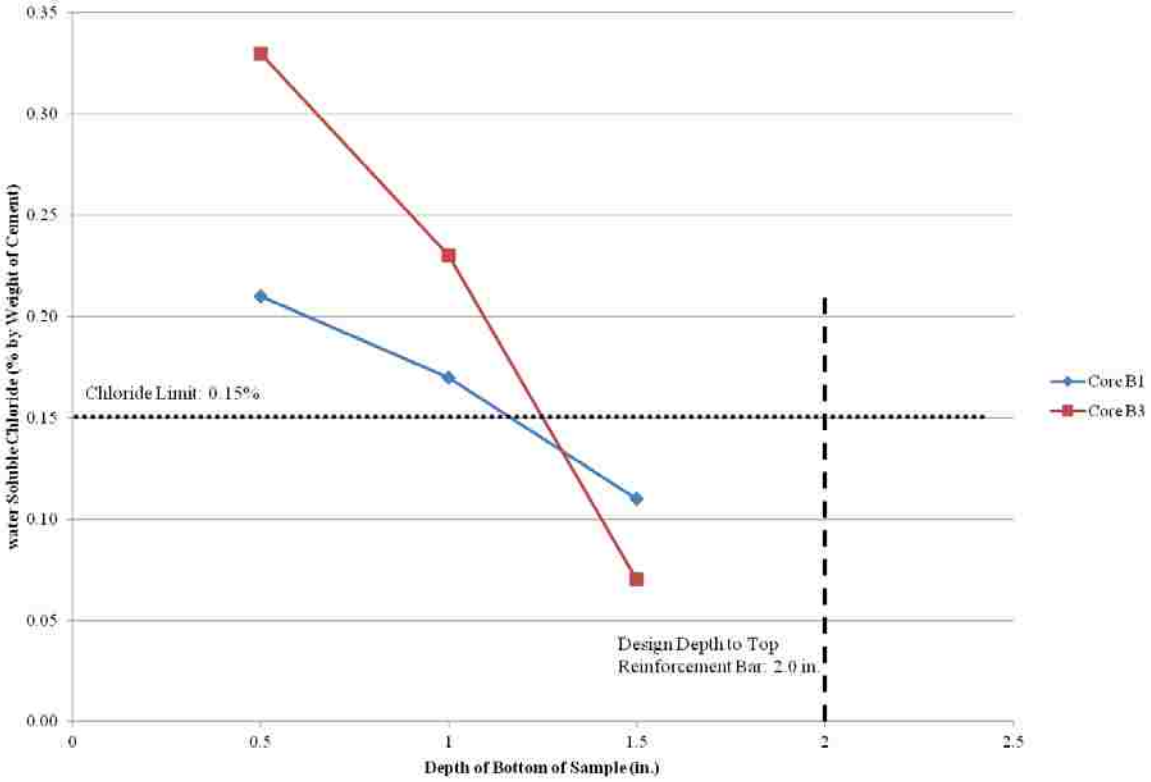

Figure 3.27. Bridge A1479 Chloride Ion Content Results

3.2.2.4 Hydrodemolition. Hydrodemolition was used as a method to remove loose and deteriorated concrete from the entire inside curb to curb area of Bridge A1479. The rehabilitation of the bridge deck was conducted one lane at a time, with the other lane remaining open to traffic during rehabilitation. When the first lane was finished being rehabilitated, it was reopened, and the second lane was closed to traffic. Lidar data were acquired before and after the hydrodemolition of each lane. All results given below were generated using the difference between the before and after hydrodemolition lidar scans. Three feet from the East and West edge of the lidar map was removed because of inaccurate data due to construction debris along the curbs during scanning. Therefore, all lidar images in this thesis cover only a 26 ft. width of the bridge. Figure 3.28 below shows a section of the bridge drawing with the lidar and visual inspection results.

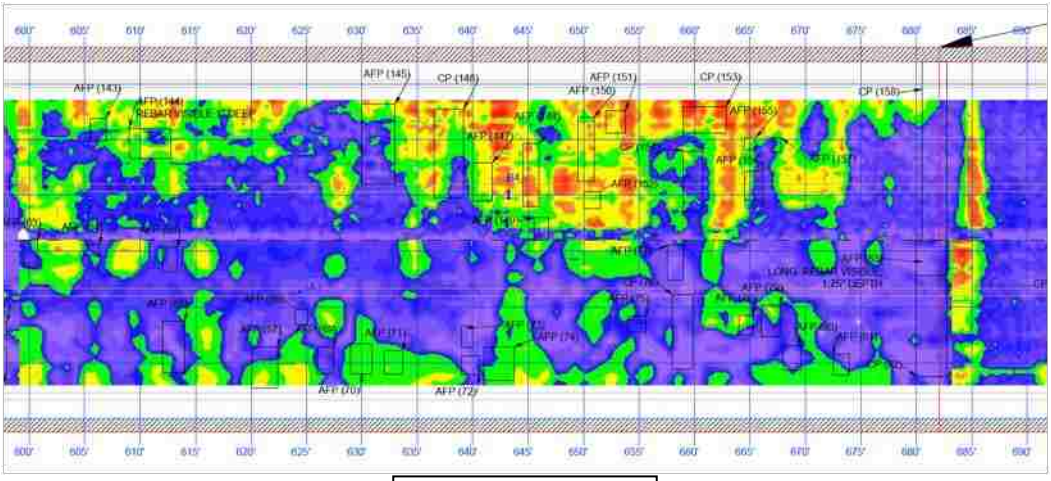

Figure 3.28. Section of Bridge A1479 Drawing Including Lidar Rehabilitation Survey and Visual Investigation Results

Several concrete patches remained in place on the bridge deck after the hydrodemolition process. Figure 3.29 below illustrates the correlation between the lidar results and visual investigation documentation in an area where concrete patches remained after the hydrodemolition. From the figure, it can be noted that the lidar and visual investigation results are congruent.

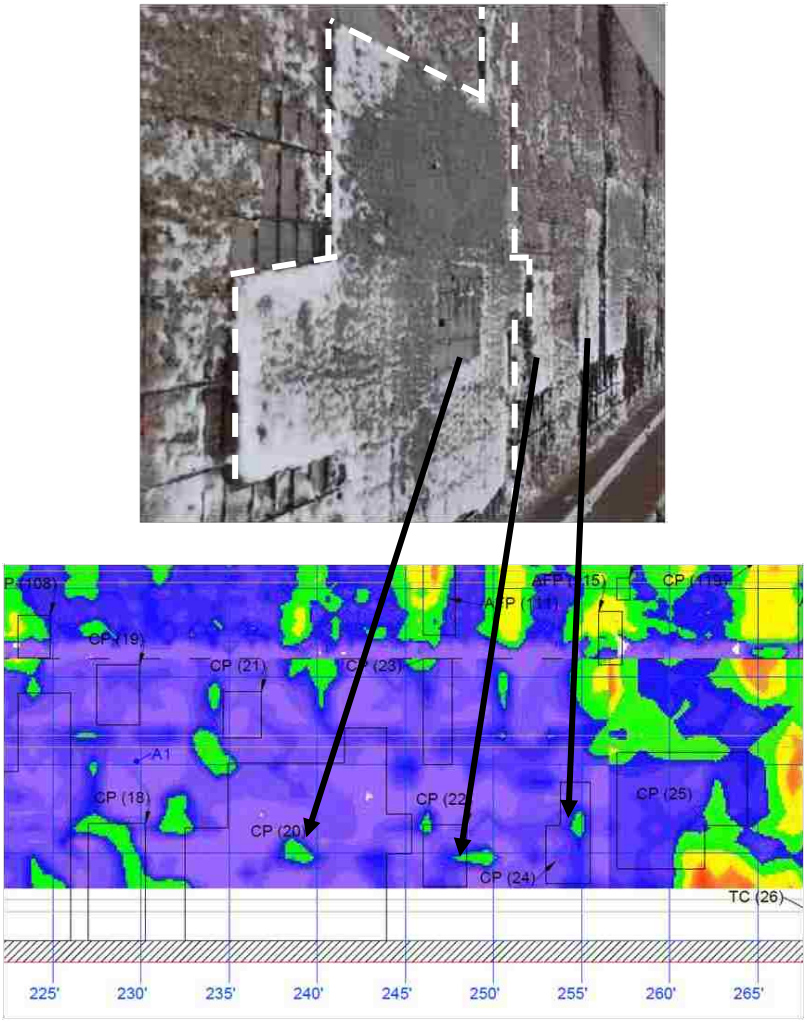

Figure 3.29. Image of Bridge A1479 Deck Surface After Hydrodemolition (a) Compared to Lidar Rehabilitation Survey and Visual Investigation Results (b)

Figure 3.30 shows Core B3 on the GPR and lidar maps. As mentioned in Section 3.2.2.3, Core B3 was rated good in the visual evaluation and was located in an area where there was no evidence of deterioration based on the GPR results. Figure 3.31 shows Core B4 on the GPR and lidar maps. Core B4 was rated fair in the visual evaluation due to a delamination at an approximate depth of 1.75 in. Based on the GPR results, the area where Core B4 was extracted from showed evidence of moderate deterioration.

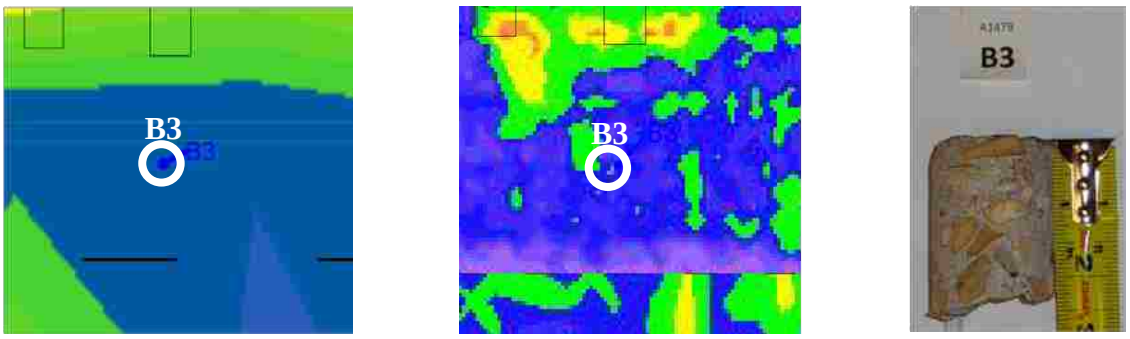

(a) (b) (c)

Figure 3.30. Bridge A1479 Core B3 on GPR Map (a), Lidar Map (b), and Core Photograph (c)

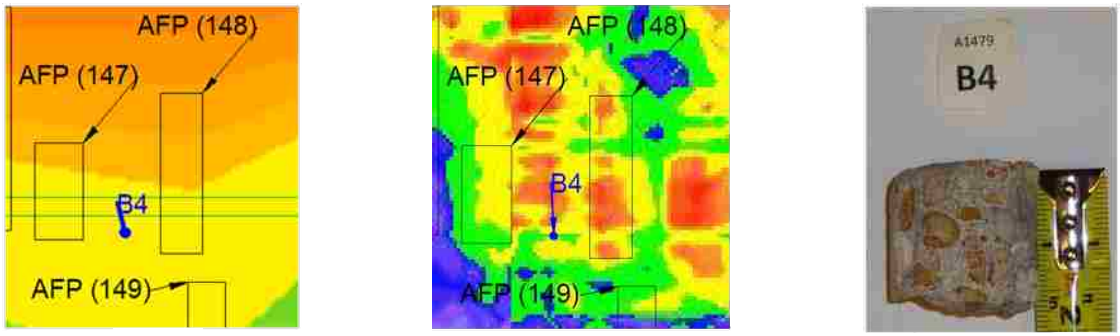

(a) (b) (c)

Note: Core B4 contained a delamination, concrete below the delamination was not extracted.

Figure 3.31. Bridge A1479 Core B4 on GPR Map (a), Lidar Map (b), and Core Photograph (c)

From the lidar results, it was possible to categorize the concrete removal into three categories based on depth, as discussed in Section 3.1.5. The categories include 0.75 in. depth or less, greater than 0.75 in. to the top of reinforcing bar, and deeper than the top of reinforcing bar. For this bridge, it is important to note that the top reinforcing bar is in the longitudinal direction, and the GRP data is based on the reflection amplitude from the top traverse rebar, which is 0.625 in. below the top of the top longitudinal bar. From this analysis, 58% of the deck was determined to have 0.75 in. or less concrete removed. Twenty seven percent of the deck had concrete removal depths greater than

0.75 in., but not below the top of reinforcing bar. Approximately 15% of the deck had concrete removal deeper than the top of reinforcing bar. The 0.75 in. category includes the milling of the entire bridge deck surface as discussed in Section 3.1.5. Figure 3.32 below summarizes the lidar results.

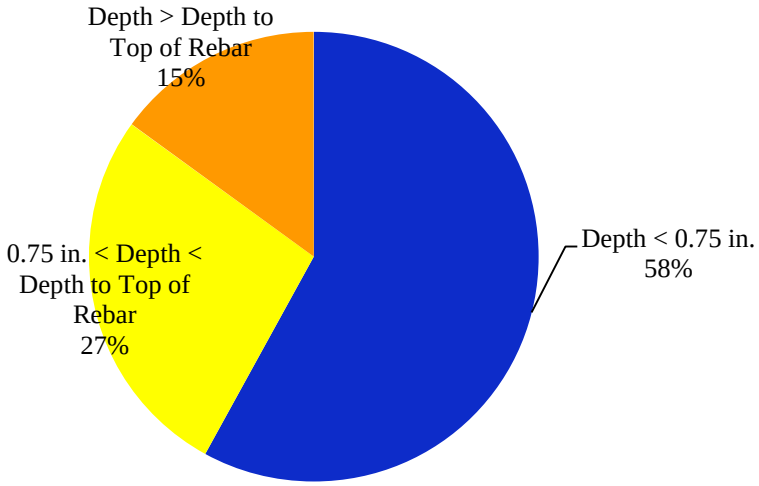

Figure 3.32. Bridge A1479 Lidar Depth of Concrete Removal Results

3.3. RAILROAD BRIDGE

Bridge A1297 is located approximately ten miles East of Sedalia, in Morgan County, Missouri. The bridge carries U.S. 50 East and West bound traffic over the Union Pacific Railroad. Figure 3.33 below shows a side view of the bridge. In October 2012, the initial bridge investigation took place, which included visual inspection of the deck, PSPA, GPR, and coring. Five researchers assisted in the five hour long initial investigation. Approximately 3.25 in. of rain was reported in the area within the seven days prior to the investigation. The reported high and low temperatures for the day of the investigation were 83°F and 67°F, respectively. Debris was removed from the deck with a push broom prior to the investigation.

Rehabilitation of the bridge commenced in May 2013 and was completed in September 2013, with a total project cost of $292,000, according to Mr. Bill Dunn, a

Structural Preliminary and Review Engineer with MoDOT. Hydrodemolition was used to remove loose and deteriorated concrete on the westbound lane in June 2013, and in July for the eastbound lane. Each lane was scanned with lidar to document the concrete removal during the rehabilitation.

Figure 3.33. Bridge A1297 Side View

3.3.1. Bridge Description. Bridge A1297, as shown from satellite imagery in Figure 3.34 below, carries two lanes of traffic. The deck is 46 ft. - 9 in. wide, and the structure has a total length of 157 ft., with three spans. The main structural support is a continuous steel girder system. The reinforced concrete deck was cast-in-place. During the 2011 bridge inspection, MoDOT personnel rated the bridge deck a 6 (satisfactory condition) and the superstructure and substructure a 7 (good condition). See Table 2.1 for complete descriptions of these ratings. Table 3.2 below outlines details of the bridge.

Figure 3.34. Bridge A1297 from Satellite Imagery [51]

Table 3.2. Bridge A1297 Details

Year Constructed	1972
Feature Intersected	Union Pacific Railroad
Number of Lanes	2
Traffic Direction	Two-Way
Number of Spans	3
Deck Width	46 ft. – 9 in.
Inside Curb to Curb Width	44 ft.
Total Structure Length	157 ft.
Main Structural System	Continuous Steel
Deck Construction Type and Material	Cast-in-Place Reinforced Concrete

The bridge deck was designed to be 7.5 in. thick, with a concrete clear cover of 1.875 in. on top and 1 in. on bottom. Transverse (perpendicular to traffic flow) steel reinforcing bars spaced at 5 in. on center are positioned on top of the longitudinal (parallel to traffic flow) reinforcing bars spaced at 12 in. on center. There are additional longitudinal reinforcing bars in the deck over the bents, making the longitudinal bar spacing 6 in. on center in these areas. All longitudinal bars are #4 (0.5 in. diameter), and all transverse bars are #5 (0.625 in. diameter). All reinforcing bars in the deck are uncoated. Figure 3.35 below illustrates the deck reinforcement described above.

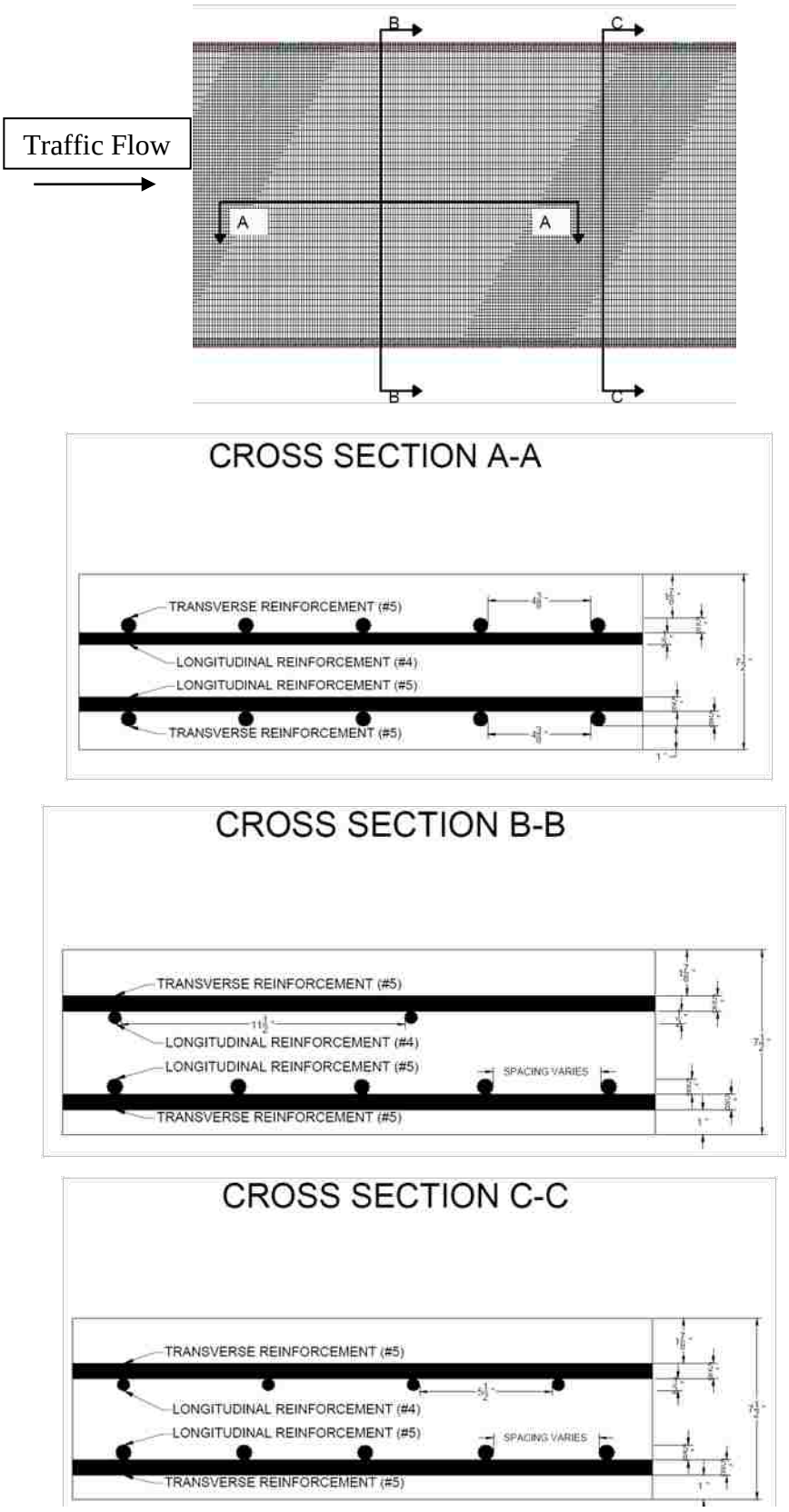

Figure 3.35. Bridge A1297 Deck Cross Sections

3.3.2. Findings. Bridge A1297 was investigated on October 24, 2012. During the investigation, researches noted that the bridge did not contain any deck drains and based on the crown in the bridge, water would run off to all 4 corners of the structure. Researchers also noted that no deflection or vibration of the bridge was noticeable while performing the investigation. More detailed findings were noted with the visual inspection, GPR, cores, and the survey of the post-hydrodemolition deck. See Appendix C for bridge drawings, which include visual inspection findings and GPR results, along with the lidar survey of material removal during the rehabilitation. A digital version of the A1297 Bridge Investigation Drawing is included in the Digital Appendix.

3.3.2.1 Visual inspection. From the visual inspection of the top deck surface of Bridge A1297, 69 defects were documented. Those defects included transverse cracks, concrete patches, asphalt filled potholes, efflorescence, and concrete spalls, including some spalls with reinforcing bars visible. The majority of the documented defects were located in the middle span (span 2) of the girders. Fewer defects were noted in the two end spans (span 1 and 3) of the girders as illustrated in Figure 3.36 below.

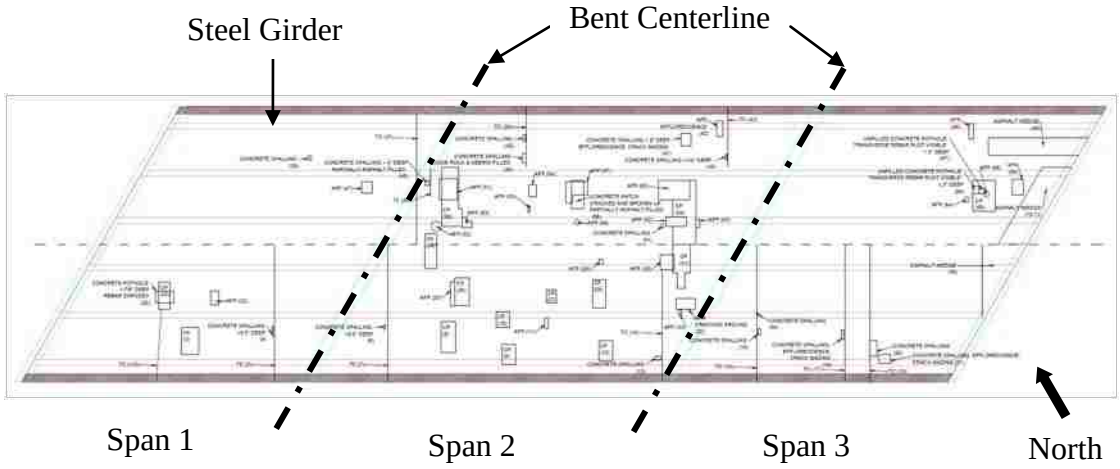

Figure 3.36. Bridge A1297 Visual Inspection Results

3.3.2.2 Ground penetrating radar. Both lanes of the bridge deck were scanned with GPR. Due to size constraints of the GPR push cart, 1.3 ft. of the South shoulder and 1.2 ft. of the North shoulder were not scanned. Therefore, the total width of the GPR scan was 41.5 ft., compared to the inside curb-to-curb width of 44 ft. The scan covered the entire length of the bridge deck. Figure 3.37 below illustrates the GPR results included in the bridge drawing. Increased evidence of deterioration based on the GPR results is more prevalent on the South side of the bridge deck than the North side. One theory for this phenomenon is the South edge of the bridge deck is shaded more often due to the shadow of the barrier wall created by the sun being located in the southern sky, especially in the winter when snow and deicing chemicals are piled on the shoulder.

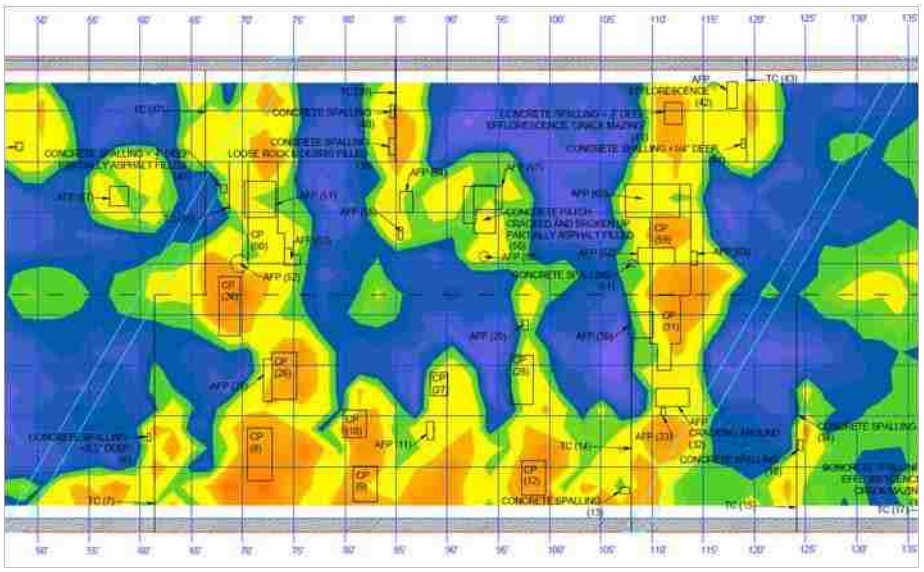

GPR Top Transverse Reinforcement
Reflection Amplitude Map Scale (NdB)

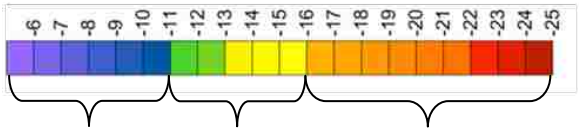

No evidence of deterioration	Evidence of moderate deterioration	Evidence of extensive deterioration

Figure 3.37. Section of Bridge A1297 GPR Results

Similar to the GPR results of Bridge A1479 in Section 3.2.2.2, the GPR results of A1297 show a correlation with the documented visual defects. Sections of the deck that showed no evidence of deterioration on the GPR results had few documented visual defects. In areas where many visual defects were documented, the GPR results indicate higher levels of deterioration.

Of the 6,908 sq. ft. inside curb-to-curb area of the bridge deck, 6,515 sq. ft., or 94%, was scanned with GPR. Based on the GPR estimates, 3,258 sq. ft. or 50% of the scanned portion had no evidence of deterioration. 2,671 sq. ft. or 41% of the deck was estimated to have evidence of moderate deterioration, and 586 sq. ft. or 9% was estimated to have evidence of extensive deterioration. These values are illustrated in Figure 3.38 below.

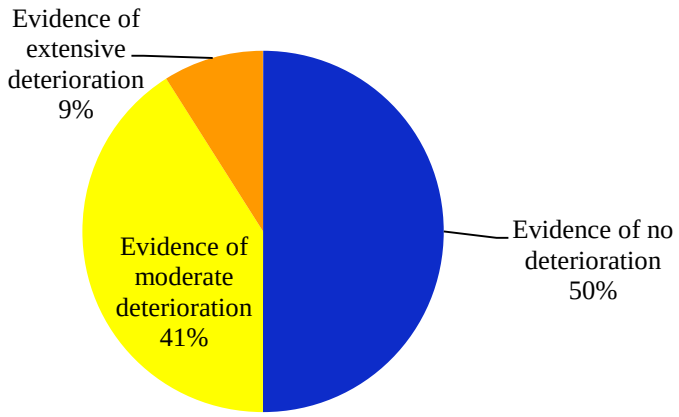

Figure 3.38. Bridge A1297 Deck Deterioration Levels Based on GPR

3.3.2.3 Cores. Six cores were extracted from the deck of Bridge A1297. Of the six cores, three were rated good based on visual evaluation, two fair, and one bad. Refer to Section 3.1.4.1 for the core rating criteria. All six of the cores were composed entirely of the as-built concrete. Figure 3.39 below shows photographs of all six cores and their ratings based on the visual evaluation. The complete visual evaluation results are included in the Appendix D.

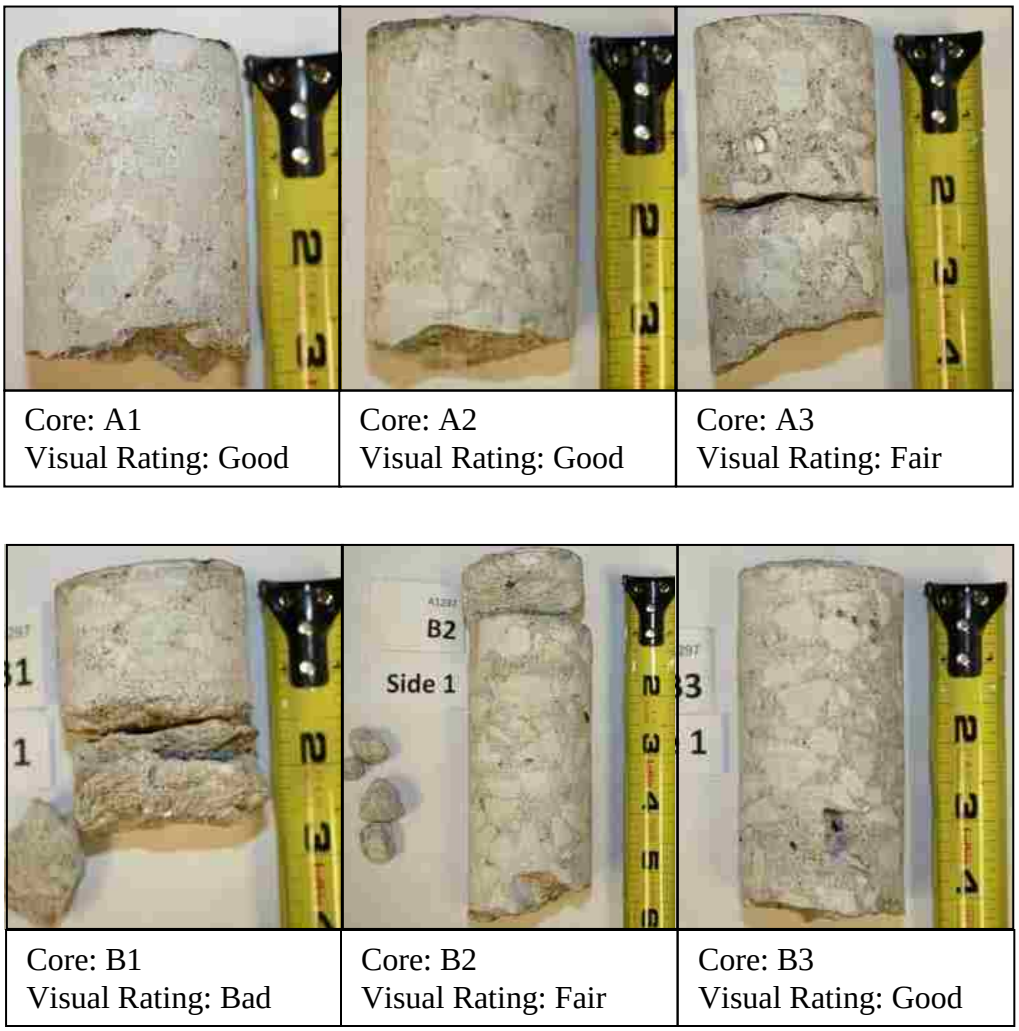

Core: A1 Visual Rating: Good	Core: A2 Visual Rating: Good	Core: A3 Visual Rating: Fair
Core: B1 Visual Rating: Bad	Core: B2 Visual Rating: Fair	Core: B3 Visual Rating: Good

Figure 3.39. Bridge A1297 Cores and Visual Core Ratings

Based on the GPR results, one core was extracted from an area of the bridge deck that had no evidence of deterioration, and five cores from areas with evidence of moderate deterioration. Figure 3.40 below illustrates the locations of Core A1 on the bridge deck drawing containing the visual investigation and GPR. Core A1 is located in an area with no evidence of deterioration based on GPR and no documented visible deterioration. Core A1 was rated good in the visual examination. Figure 3.41 illustrates Core A2, which is located in an area that has evidence of moderate deterioration based on GPR results. The core has a visual evaluation rating of good.

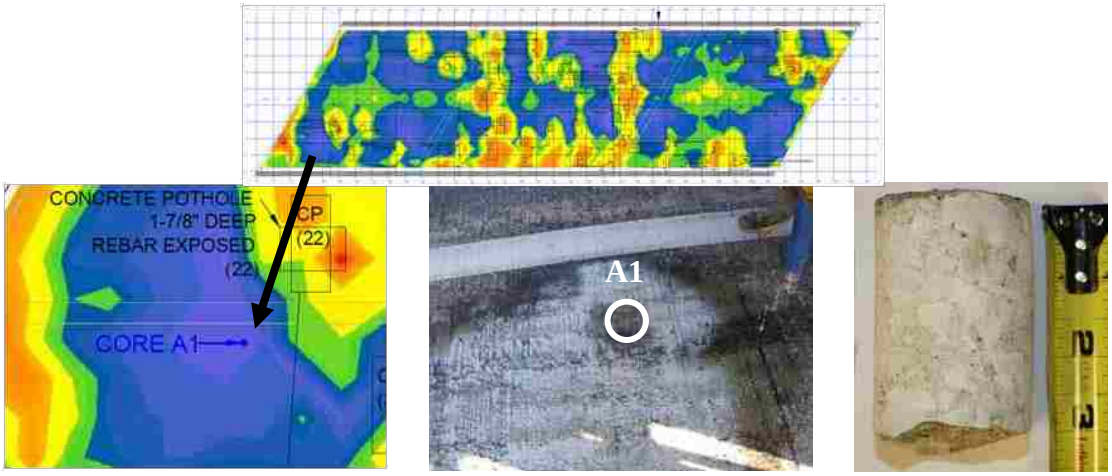

(a) (b) (c)

Figure 3.40. Bridge A1297 Core A1, (a) On Bridge Drawing, (b) Deck Image at Core Location, (c) Extracted Core

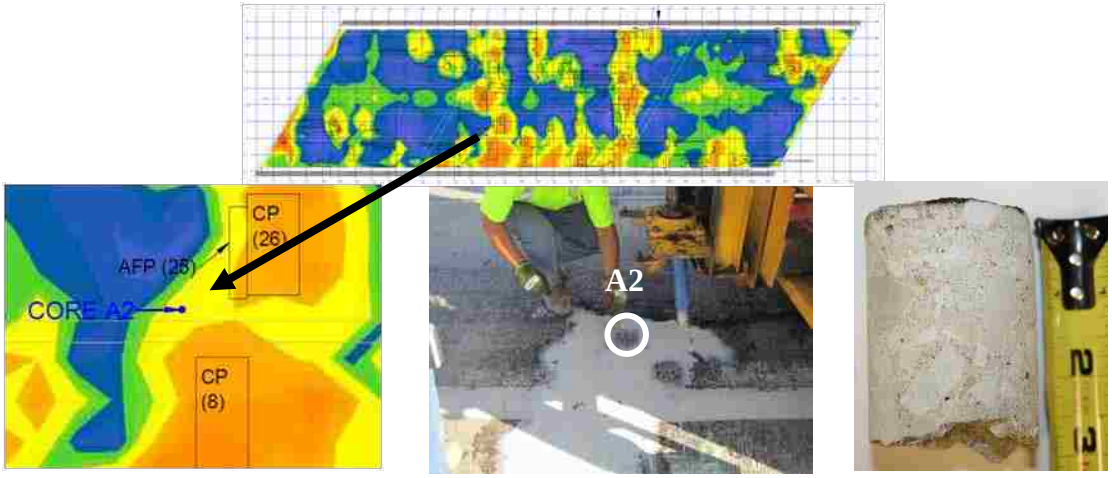

(a) (b) (c)

Figure 3.41. Bridge A1297 Core A2, (a) On Bridge Drawing, (b) Deck Image at Core Location, (c) Extracted Core

The volume of permeable pore space was determined for all six of the extracted cores. Volume of permeable pore space ranged from 13.20% to 15.72%. Core B1, which was rated bad during the visual evaluation, had the highest volume of permeable pores at 15.72% and Core B2, which was rated fair during the visual evaluation, had the lowest

volume of permeable pores at 13.20%. Both Cores B1 and B2 were extracted from areas with evidence of moderate deterioration based on GPR results. Figure 3.42 below illustrates the volume of permeable pore space for the cores. Complete results from the volume of permeable pore space test are included in the Appendix E.

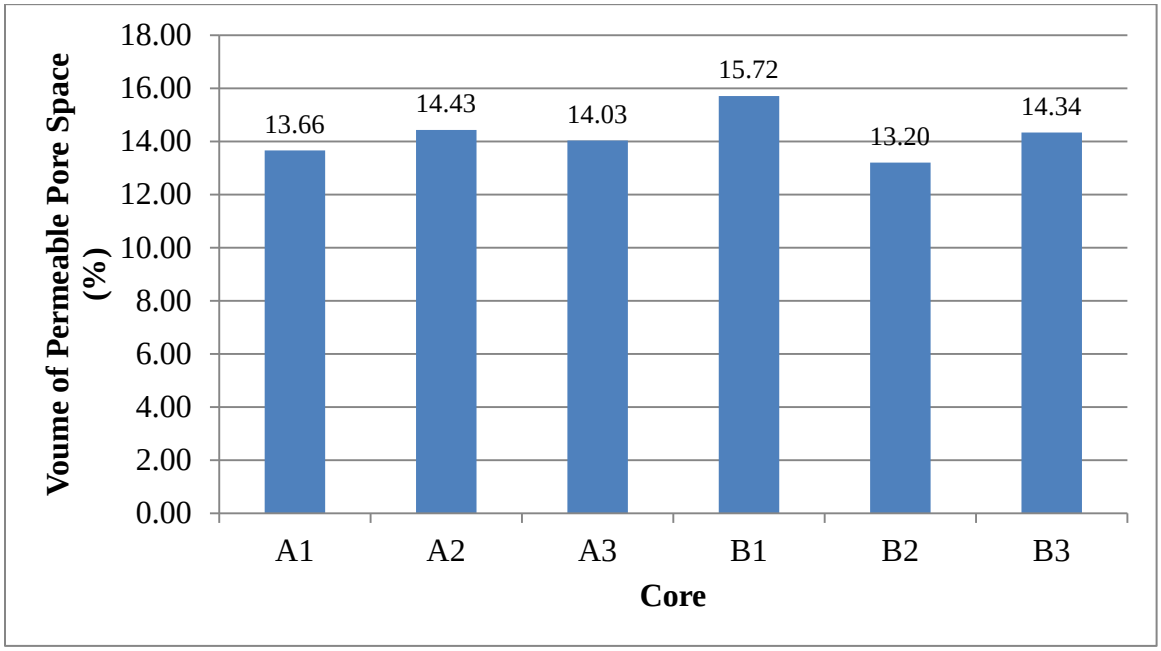

Figure 3.42. Bridge A1297 Volume of Permeable Pore Space Results

Chloride ion concentration test results were obtained for two cores from Bridge A1297, Cores A1 and A2. Both cores were rated good in the visual examination, however Core A1 showed no evidence of deterioration based on the GPR results, and Core A2 showed evidence of moderate deterioration. The chloride ion concentration results are illustrated in Figure 3.43 below. Both cores had low values of percent chloride, all values were below 0.06%. The bridge design specifies that the reinforcing bars have a clear cover of 1.875 in. As discussed in Section 2.3.2, a threshold value of 0.15% water-soluble chloride by weight of cement is used in this thesis as the threshold for the initiation of corrosion. Chloride ion concentrations at or above this level indicate the potential for corrosion of the steel reinforcing bars.

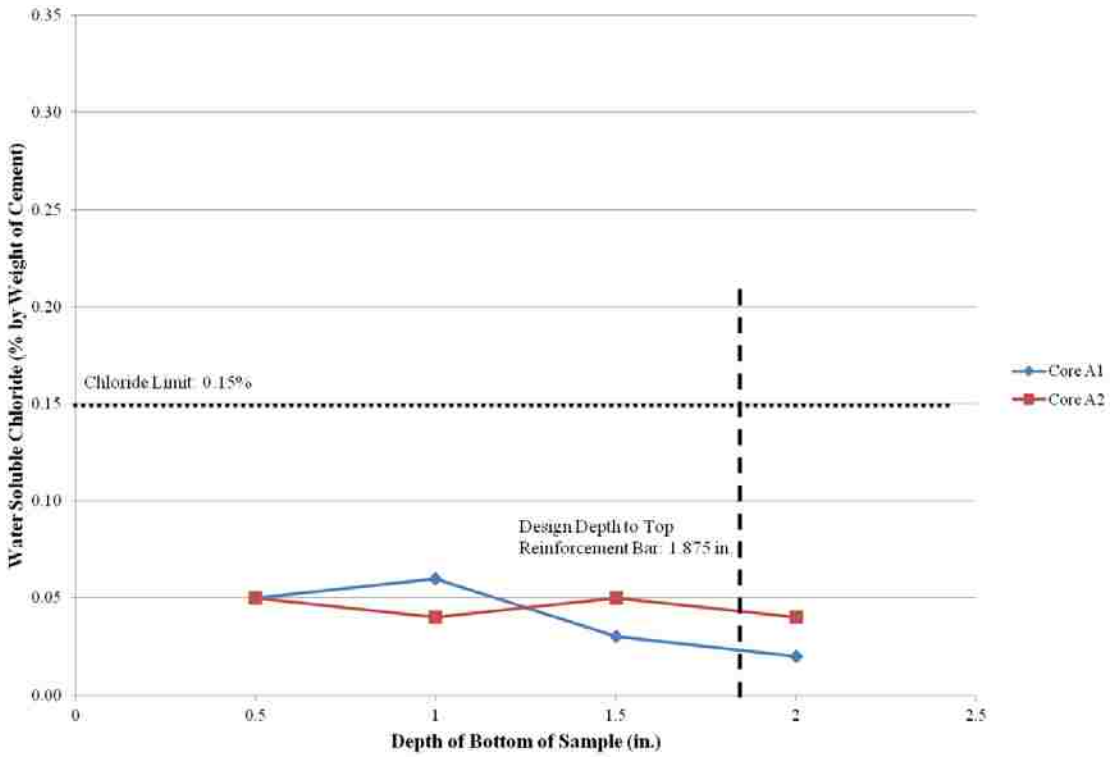

Figure 3.43. Bridge A1297 Chloride Ion Content Results

3.3.2.4 Hydrodemolition. Hydrodemolition was used as a method to remove loose and deteriorated concrete from the entire inside curb to curb area of Bridge A1297. The rehabilitation of the bridge deck was conducted one lane at a time, with the other lane remaining open to traffic during rehabilitation. When the first lane was finished being rehabilitated, it was reopened, and the second lane was closed to traffic.

Due to scheduling constraints, the eastbound lane of this bridge was not scanned with lidar before the hydrodemolition took place. A synthetic image of the eastbound lane before hydrodemolition was created to allow the depth of material removal to be calculated. The final lidar results for the eastbound lane were compared with photographs taken of the deck after hydrodemolition and the results appeared to be accurate, therefore all lidar data for this lane is considered valid. Lidar data were acquired before and after the hydrodemolition of the westbound lane.

All results given below were generated using the difference between the lidar scans before and after hydrodemolition. The lidar data were trimmed to match the GPR map curb offsets of 1.3 ft. from the South curb and 1.2 ft. from the North curb.

Therefore, all lidar images in this thesis cover only a 41.5 ft. width of the bridge. Figure 3.44 below shows a section of the bridge drawing with the lidar and visual inspection results.

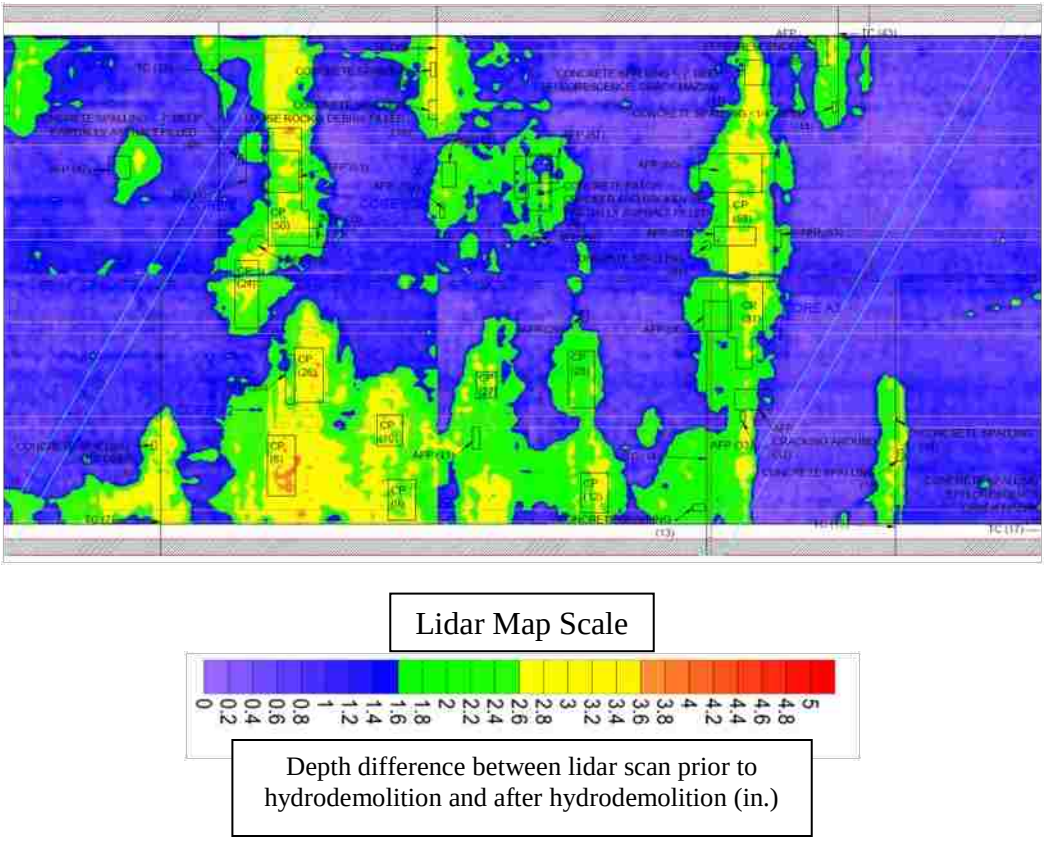

Figure 3.44. Section of Bridge A1297 Drawing Including Lidar Rehabilitation Survey and Visual Investigation Results

Figure 3.45 below shows Core A1 on the GPR and lidar maps, as well as the core hole after the hydrodemolition. As mentioned in Section 3.2.2.3, Core A1 was rated good in the visual evaluation and was in an area where there was no evidence of deterioration based on the GPR results. Approximately 1.6 in. of concrete was removed during the hydrodemolition process in the deck where Core A1 was extracted. Figure 3.46 shows Core A2 on the GPR and lidar maps. Core A2 was rated good in the visual evaluation. Based on the GPR results, the area where Core A2 was extracted from

showed evidence of moderate deterioration. Approximately 2.3 in. of concrete was removed from the hydrodemolition process in the area where Core A2 was extracted.

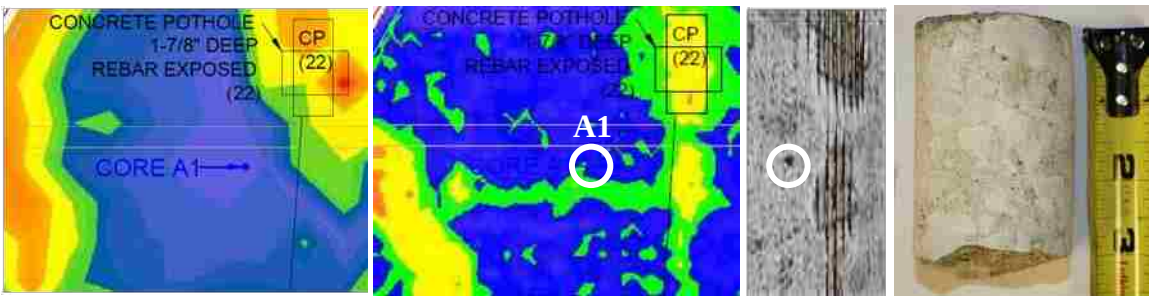

(a) (b) (c) (d)

Figure 3.45. Bridge A1297 Core A1 on GPR Map (a), Lidar Map (b), Image of Deck Around Core Location after Hydrodemolition(c), and Core Photograph (d)

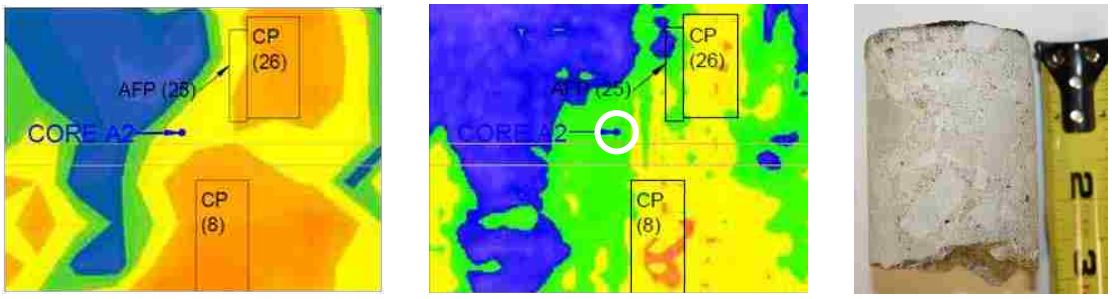

(a) (b) (c)

Figure 3.46. Bridge A1297 Core A2 on GPR Map (a), Lidar Map (b), and Core Photograph (c)

As discussed in Section 3.1.5, the lidar survey results were placed into three categories. The categories include 0.75 in. depth or less, greater than 0.75 in. to the top of reinforcing bar, and deeper than the top of reinforcing bar. From this analysis, 28% of the deck was determined to have 0.75 in. or less concrete removed. Forty eight percent of the deck had concrete removal depths greater than 0.75 in., but not below the top of reinforcing bar. Approximately 24% of the deck had concrete removal deeper than the

top of reinforcing bar. The 0.75 in. category includes the milling of the entire bridge deck surface as discussed in Section 3.1.5. The average depth to the top of the reinforcement bars was 1.80 in. Figure 3.47 below summarizes the lidar results.

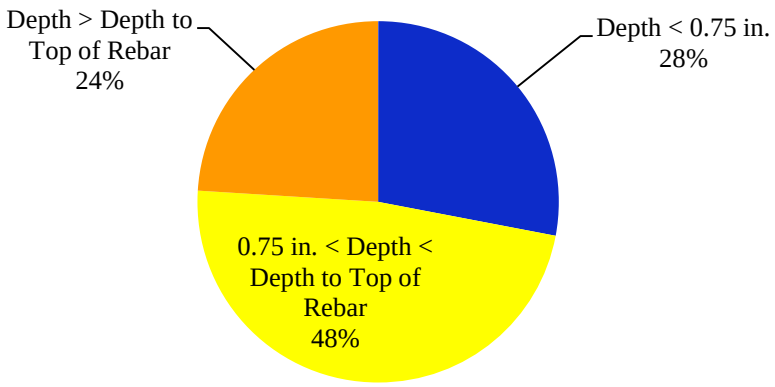

Figure 3.47. Bridge A1297 Lidar Depth of Concrete Removal Results

4. DISCUSSION OF RESULTS

The investigations of Bridges A1479 and A1297 (Section 3) produced a variety of data sets from both nondestructive and destructive test methods that can be used to correlate testing methodologies and assess the ability of GPR to detect deterioration of bridge decks as well as improve rehabilitation estimates. Correlation between GPR and the visual investigation is discussed in Section 4.1, GPR and cores in Section 4.2, and GPR and hydrodemolition in Section 4.3.

4.1. CORRELATION BETWEEN GPR AND VISUAL INVESTIGATION

As discussed in Sections 3.2.2.2 and 3.3.2.2, there is a strong correlation between the defects noted in the visual investigation and the GPR results. Areas with more visible deterioration or defects from the top bridge deck surface tend to be located in areas where the GPR indicated lower reflection amplitudes, which were interpreted as higher levels of deterioration. Sections of the bridge deck where no deterioration was noted are areas where the GPR indicated higher reflection amplitudes, which were interpreted as no evidence of deterioration.

These results were expected, since a defect visible on the bridge deck surface is most likely caused from concrete degradation below the surface, such as a delamination, which can be located using GPR. It is also important to note that the GPR will respond to changes in material, since electromagnetic waves travel at different velocities through different materials. Asphalt has a lower wave velocity than concrete, therefore the reflected signal appears more attenuated and has a longer two-way travel time compared to non-deteriorated concrete if the material (and thus the dielectric constant) is assumed to be uniform, as was the case in this study (Section 3.1.2). This could explain why areas with several asphalt filled potholes on the deck surface were highlighted as areas where there was evidence that the concrete was experiencing moderate to severe deterioration from the GPR results. Even though the signal reflections through the asphalt are being evaluated as though they were reflections from concrete, and therefore making the asphalt appear bad based on the GPR results, it is important to remember that

the asphalt patches on the bridge deck add no structural value to the bridge deck, they are simply there to make the ride smoother for motorists until repairs or rehabilitation with concrete takes place. Several of the asphalt patches on the bridge deck were also deteriorating, and in certain areas the reinforcing bar in the deck was visible as illustrated in Figure 4.1 below.

Figure 4.1. Reinforcing Bars Visible in Asphalt Filled Pothole

4.2. CORRLEATION BETWEEN GPR AND CORES

Cores extracted from the bridge deck provided a method to determine local deterioration in the bridge deck. Since the cores represent a very small percentage of the entire volume of the bridge deck, the deterioration estimates are very localized, but can still assist in the interpretation of GPR results. As discussed throughout Section 3, nine cores were extracted from the deck of Bridge A1479 and six cores from Bridge A1297. These cores were then visually evaluated, tested for volume of permeable pore space, and sent to MoDOT to obtain chloride ion concentration measurements. All of these core evaluation methods were compared to the GPR results to determine if any correlations exist between the data sets.

4.2.1. GPR and Visual Evaluation. There was a noticeable correlation between the GPR results and the visual evaluation of the cores. This correlation was analyzed by using the visual core rating (good, fair, and bad) and GPR deterioration level (evidence of no deterioration, evidence of moderate deterioration, and evidence of extensive deterioration) as discussed in Sections 3.1.4.1 and 3.1.2, respectively. One method used to evaluate the correlation between the GPR results and the visual evaluation of cores is illustrated below in Tables 4.1 and 4.2. In the tables, the cores are compared in terms of the visual core rating and the GPR deterioration level estimate at the location the core was extracted. For this evaluation, the ideal match is a core rated good during the visual evaluation to be extracted from an area with no evidence of deterioration based on the GPR results, a core rated fair to be extracted from an area with evidence of moderate deterioration, and a core rated bad to be extracted from an area with evidence of extensive deterioration. Cells indicating the ideal match described here are shaded in the tables. In the tables, cores that were within 6 in. of a different GPR deterioration level were indicated as border line. As mentioned in Section 3.1.2, the computer program used to generate the GPR contour maps interpolates the data between the GPR profiles, which were spaced 2 ft. and 1 ft. for Bridges A1479 and A1297, respectively. The interpolation could cause slight errors in the GPR results, especially when the results are being compared to a 2 in. diameter core as those extracted in this project.

Table 4.1. Bridge A1479 GPR and Visual Core Evaluation Comparison

	A1479	VISUAL CORE RATING		
		Good	**Fair**	**Bad**
GPR MAP CLASSIFICATION	**No Evidence of Deterioration**	A2, A4, B3	A1 (Border Line Moderate)	
	Moderately Deteriorated	B1, B5 (Border Line No Deterioration)	A3, B4	B2 (asphalt core)
	Extensively Deteriorated			
	% Ideal Match	**% Ideal Match with Border Line Correct**		
	56%	**78%**		

Table 4.2. Bridge A1297 GPR and Visual Core Evaluation Comparison

	A1297	VISUAL CORE RATING		
		Good	**Fair**	**Bad**
GPR MAP CLASSIFICATION	**No Evidence of Deterioration**	A1		
	Moderately Deteriorated	A2, B3 (Border Line No Deterioration)	A3, B2	B1
	Extensively Deteriorated			
	% Ideal Match	**% Ideal Match with Border Line Correct**		
	50%	**67%**		

The visual core evaluation and GPR estimated deterioration level comparison illustrated in Tables 4.1 and 4.2 above show there is a correlation between the cores and GPR results. Bridge A1479 had 56% of the cores with an ideal match with GPR estimated deterioration levels, and Bridge A1297 had 50% of the cores with an ideal match. If the border line cores are considered to fall into a different GPR estimated deterioration level, Bridge A1479 had 78% of the cores with an ideal match and 67% for Bridge A1297.

The visual examination of the cores was not expected to completely match the GPR estimated deterioration levels. Visible signs of concrete deterioration are the easiest to locate, but just because concrete appears to be in good condition visually does not necessarily mean there is no deterioration taking place. The visual examination does not take into account the pore structure of the concrete, where the degradation of the concrete can start as discussed in Section 2.1. The visual examination also gives no indication of concrete strength or the amount of chlorides present in the pore structure. Another important aspect of this comparison to note is the scale used to estimate the GPR deterioration level. The cutoff values for the different GPR levels (no evidence of deterioration, evidence of moderate deterioration, and evidence of extensive deterioration) were developed for each bridge individually by researchers. Calibration of the cutoff values for the GPR estimated deterioration levels is a complex process and is

ongoing at the time of writing this thesis using all data sets available, including core results, hydrodemolition results, and weather conditions during and prior to the investigation.

4.2.2. GPR and Volume of Permeable Pores. The volume of permeable pore space was determined for 14 of the 15 cores extracted from the decks of Bridges A1479 (Section 3.2.2.3) and A1297 (Section 3.3.2.3). In Figure 4.2 below, the volume of permeable pore space is compared to the visual core ratings (good, fair, and bad). Cores from both bridges were combined into the visual core rating categories where the average volume of permeable pores was calculated and plotted. A correlation between the visual core rating and volume of permeable pore space is visible in Figure 4.2. The core rated bad in the visual examination has a higher volume of permeable pores than the average of the cores rated fair. And likewise, the cores rated fair during the visual examination have a slightly higher average volume of permeable pore space than those rated good. This result was expected, because concrete with higher deterioration levels typically have damage to the pore structure from freezing and thawing cycles and chloride intrusion, which increases the volume of permeable voids, as discussed in Section 2.1.

Figure 4.2. Volume of Permeable Pore Space Compared to Visual Core Rating for Bridges A1479 and A1297 Combined

The volume of permeable pore space results were also compared to the GPR reflection amplitude from the top traverse reinforcement bar at the core location. Since the GPR contour map scales were individualized and calibrated to each bridge deck as discussed in Section 3.1.2, the results must be plotted individually for each bridge. The results for Bridge A1479 are shown in Figure 4.3 below. The volume of permeable pore space was determined for eight of the nine cores extracted from Bridge A1479. Three of the cores were located in areas where the GPR had a normalized reflection amplitude between -7 and -10 NdB, three cores from -10 to -13 NdB, and 2 cores from -13 to -17 NdB. Although the cores in the -10 to -13 NdB range have a higher volume of permeable pores than the average of the cores in the -7 to -10 NdB range, the cores in the -13 to -17 NdB category have a lower average volume of permeable pore space. Therefore, there is no visible correlation between GPR reflection amplitude and volume of permeable pores for Bridge A1479.

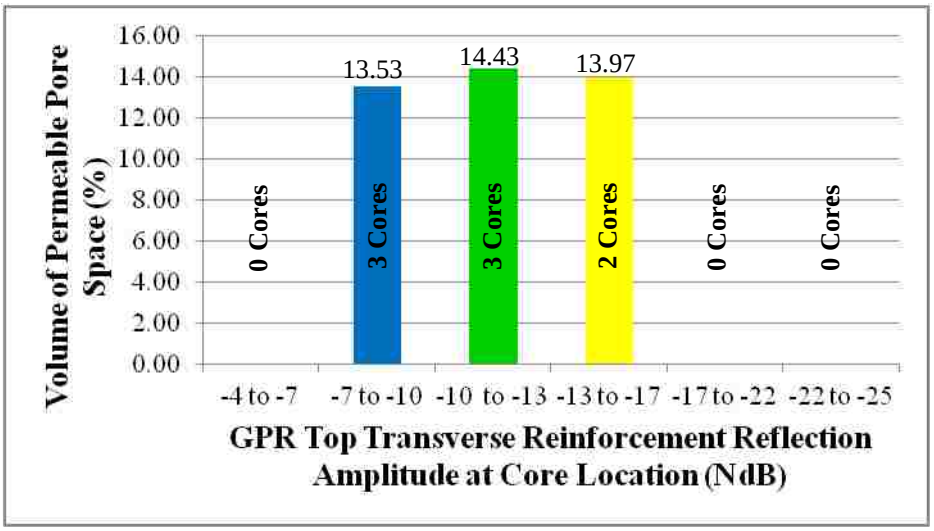

Figure 4.3. Volume of Permeable Pore Space Compared to GPR Amplitude for Bridge A1479

Similar to Figure 4.3 discussed previously, Figure 4.4 below illustrates the comparison between the GPR amplitude at core locations compared to the average volume of permeable pore space for the cores located in various ranges of GPR reflection

amplitude for Bridge A1297. The volume of permeable pores was determined for all six of the cores extracted from the deck of Bridge A1297. One core was extracted from an area where the normalized GPR reflection amplitude was in the -5 to -7 NdB range, three cores in the -11 to -13 NdB range, and two cores in the -13 to -16 NdB range. The average volume of permeable pores for the cores in the -11 to -13 NdB range is higher than the average of the cores in the -5 to -7 NdB range. However, the average volume of permeable pores for the cores in the -13 to -16 NdB range is the same as those in the -11 to -13 NdB range. Based on the results from Bridge A1297 illustrated in Figure 4.4, no conclusions can be made about the correlation between GPR reflection amplitude and the volume of permeable pore space.

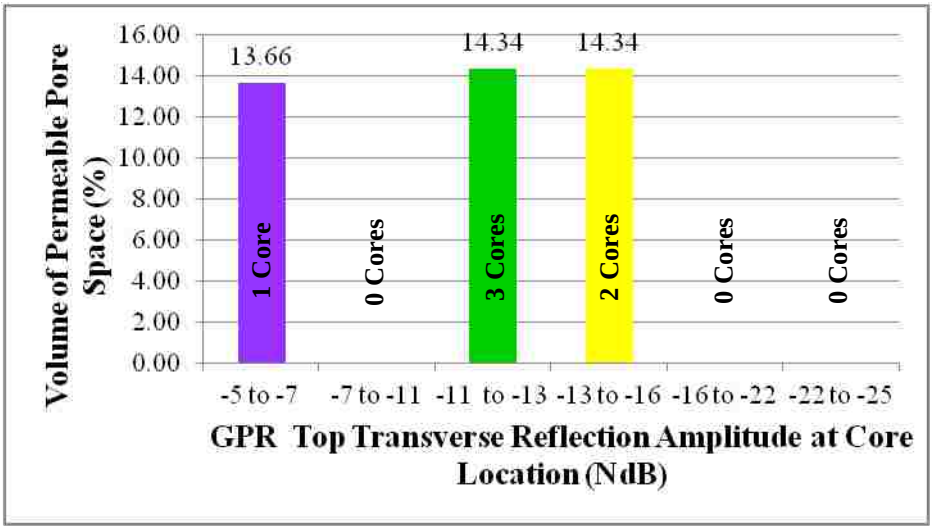

Figure 4.4. Volume of Permeable Pore Space Compared to GPR Amplitude for Bridge A1297

From Bridge A1297, Core A2 had the second highest volume of permeable pore space of the six cores extracted. As discussed in Section 3.3.2.3, Core A2 was rated good during the visual evaluation, and was in an area with evidence of moderate deterioration based on the GPR results. The depth of material removal during the rehabilitation at the location of this core was approximately 2.3 in. Interestingly, as discussed in Section 3.3.2.3, Core A1 from Bridge A1297 was also rated good during the visual evaluation,

had the second lowest volume of permeable pore space of the six extracted cores, and was in an area with no evidence of deterioration based on GPR results. During the rehabilitation process, approximately 1.6 in. of material was removed at the location of Core A1. From the same bridge, Core B1 had the highest volume of permeable pores at 15.72%. Core B1 was rated bad during the visual evaluation, and came from an area with evidence of moderate deterioration based on the GPR results. During the rehabilitation process, approximately 2.6 in. of material was removed at the location where Core B1 was extracted. Volume of permeable pore space, visual core evaluation, GPR, and rehabilitation results for Bridge A1297 at core locations are listed in Table 4.3 below. The cores are in order from lowest volume of permeable pore space to greatest. This information alludes that higher volumes of permeable pore space will show up as more deteriorated based on the GPR, and will have greater material removal depths during the rehabilitation process, however Cores B2 and B3 do not follow this trend.

Table 4.3. Bridge A1297 Results at Core Locations (Shaded cells are discussed in previous paragraph)

Core	Volume of Permeable Pore Space (%)	Visual Core Rating	Approximate GPR Reflection Amplitude Range (NdB)	Approximate Depth of Material Removal During Rehabilitation (in)
B2	13.20	Fair	-13 to -16	2.1
A1	13.66	Good	-5 to -7	1.6
A3	14.03	Fair	-13 to -16	1.6
B3	14.34	Good	-11 to -13	1.2
A2	14.43	Good	-13 to -16	2.3
B1	15.72	Bad	-13 to -16	2.6

When interpreting the results from the volume of permeable pore test, it is important to note that Section 4.1 of ASTM C642-06 states that test specimens used to determine the volume of permeable pores shall not have a volume less than 350 cm^3 (21.4 $in.^3$) and shall be free from observable cracks, fissures, or shattered edges [47]. In order for a 2 in. diameter core to meet this requirement, it would have to have a length of approximately 6.7 in., and most of the cores extracted in this project were 3 in. or less in

length. Extracting cores this deep was not permitted by MoDOT, therefore tests were performed on the samples available to see if any there were any trends between the GPR and volume of permeable pore space. Also, some of the cores that were tested for the volume of permeable pore space were later sent to MoDOT to have the chloride ion concentration determined. Therefore, it was desired not to alter the core in any way prior to the determination of chloride ion concentrations.

Even though the volume of permeable pore space was expected to increase as the evidence of concrete deterioration based on GPR increased (decreasing GPR reflection amplitude), no trends were visible between the two data sets in Figures 4.3 and 4.4. One possible explanation for the lack of correlation is the few number of cores in the data set. The data set contains only eight cores for Bridge A1479 and six cores for Bridge A1297. The different volumes of test specimens could also cause discrepancy in the results. Proof of this discrepancy may be visible in the results of Core B2 from Bridge A1297. The extracted Core B2 was approximately 5.5 in. long, and contained a delamination at a depth of approximately 0.5 in. In the testing to determine the volume of permeable pores, the entire 5.5 in. long core was tested, where other cores were typically no longer than 4 in. Core B2 had a resulting volume of permeable pore space of 13.2%, which was the lowest of all the cores extracted from Bridge A1297. Table 4.4 below shows a revised version of Table 4.3 with Cores B2 and B3 removed since they were approximately 5.5 in. and 4 in. in length respectively, where the remaining cores had a length between 2.75 and 3.5 in.

Table 4.4. Bridge A1297 Revised Results at Core Locations to Eliminate Core Volume Discrepancies

Core	Volume of Permeable Pore Space (%)	Visual Core Rating	Approximate GPR Reflection Amplitude Range (NdB)	Approximate Depth of Material Removal During Rehabilitation (in)	Approximate Core Length (in)
A1	13.66	Good	-5 to -7	1.6	2.75
A3	14.03	Fair	-13 to -16	1.6	3.0
A2	14.43	Good	-13 to -16	2.3	3.5
B1	15.72	Bad	-13 to -16	2.6	3.0

From Table 4.4 above, a relationship between the volume of permeable pore space and GPR results becomes more visible. The GPR amplitude tends to decrease (indicating more evidence of deterioration) as the volume of permeable pore space increases. Even though two cores were excluded from this data set to make the trend visible, the cores that were excluded had a substantially larger volume and surface area than the remaining four cores, which is believed to have caused bias in their volume of permeable pore space results. Therefore, based on the results listed in Table 4.4, it can be concluded that higher volumes of permeable pore spaces will correspond to estimates of greater deterioration based on GPR results.

4.2.3. GPR and Chloride Ion Concentration. Chloride ion concentrations were determined for four of the fifteen total cores extracted from Bridges A1479 and A1297. All four of the cores were rated good in the core visual evaluation. Two of the cores came from areas where the GPR showed no evidence of deterioration, and two came from areas with evidence of moderate deterioration. All of the cores had chloride ion concentrations lower than the threshold of 0.15% by weight of cement. Figure 4.5 below illustrates these results.

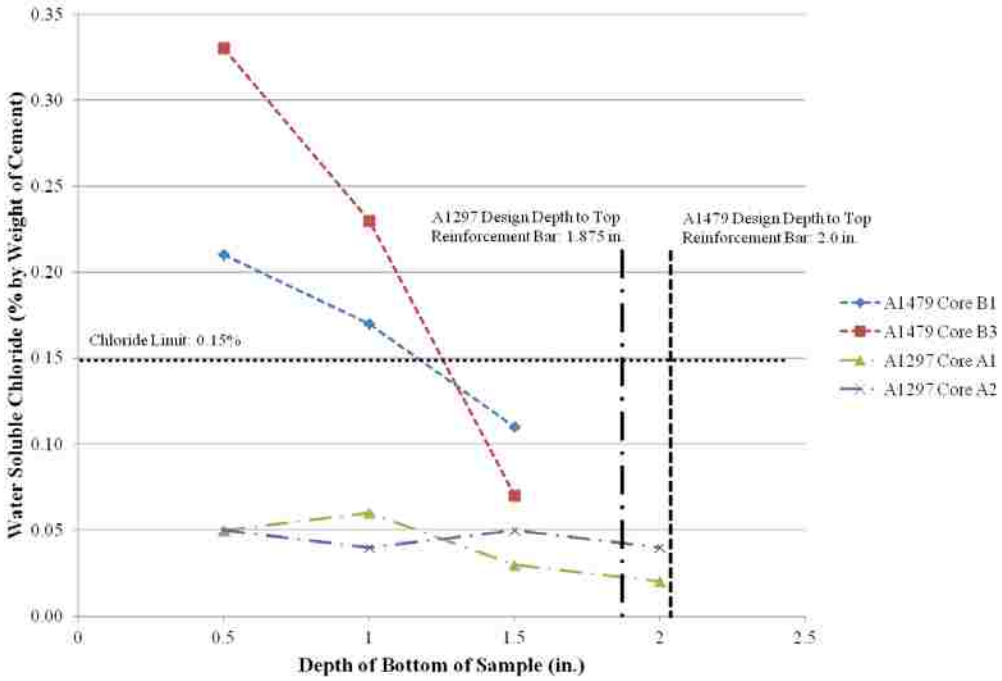

Figure 4.5. Bridges A1479 and A1297 Chloride Ion Concentration Results

Due to the limited amount of chloride ion concentration measurements available, no conclusions can be made on the impact of chloride ion levels on other forms of deterioration noted in this study. The chloride ion data available is from cores that showed no deterioration during the visual core evaluations, therefore, no data is available from cores that visually showed signs of deterioration which would indicate corrosion of reinforcing bars could be occurring. In order to effectively determine how chloride ion concentrations relate to GPR and visual investigations, data from cores with a variety of deterioration levels are needed.

4.3. CORRELATION BETWEEN GPR AND HYDRODEMOLITION

Bridges A1479 and A1297 both underwent deck rehabilitations after being investigated using visual evaluations, GPR, and core extractions as discussed in Section 3. Rehabilitation of both bridge decks included milling 0.75 in. of the surface, followed by hydrodemolition to remove any loose and deteriorated concrete. Lidar was used to determine the volume and location of material removal from the bridge decks. By plotting the lidar data onto contour maps and overlaying them on the bridge drawing, correlations with the visual inspection, GPR, and core results were able to be determined.

Figure 4.6 below shows the GPR results and rehabilitation lidar survey for a section of Bridge A1479. Due to the size of the bridge, only a 100 ft. section of the 868 ft. long bridge is shown. Complete results are located in the Digital Appendix discussed in Appendix F. In the figure, a strong correlation between the GPR results and rehabilitation lidar survey is visible. Areas where the GPR estimated higher evidence of deterioration correspond to areas where more material was removed during the rehabilitation process. And likewise, areas where the GPR estimated lower evidence of deterioration correspond to areas where less material was removed during the rehabilitation process.

(a) GPR Top Transverse Reinforcement Reflection Amplitude Results (NdB)

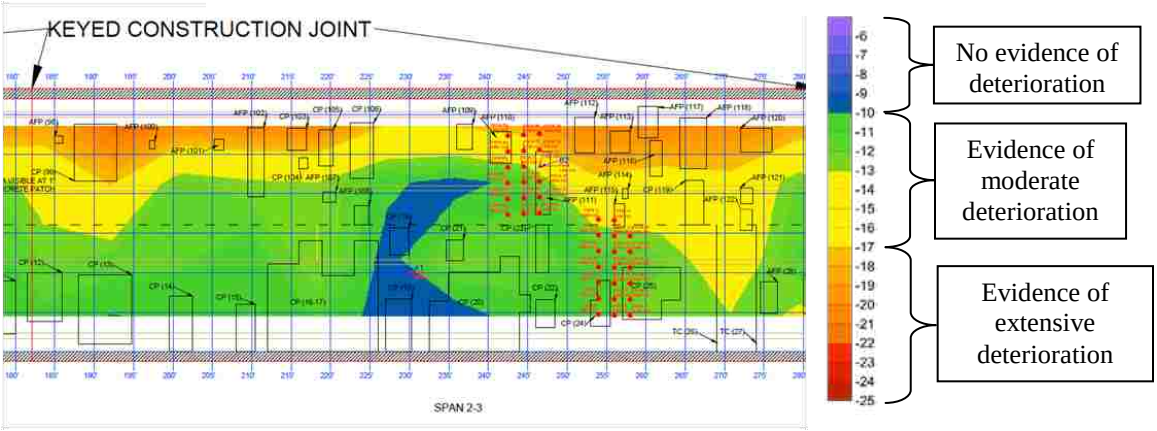

(b) Rehabilitation Lidar Survey

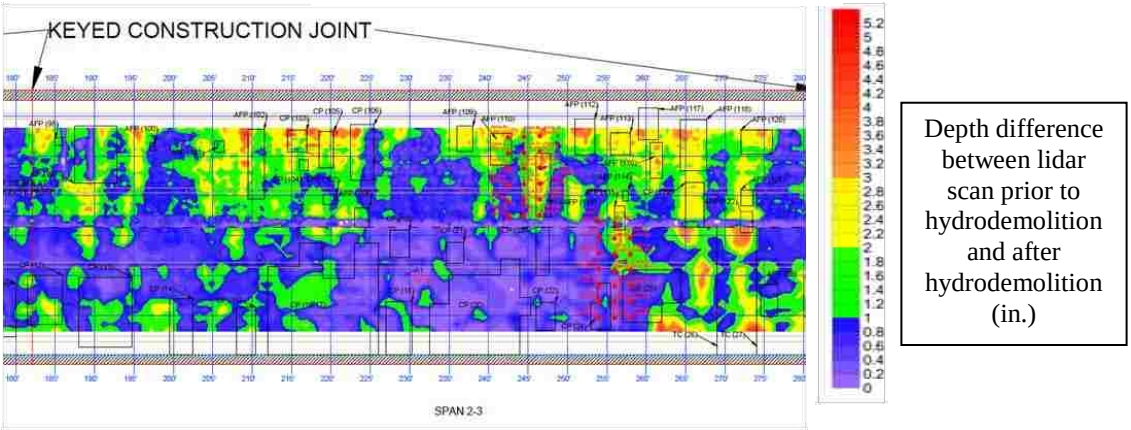

Figure 4.6. Visual Comparison Between GPR Results (a) and Rehabilitation Lidar Survey (b) From Bridge A1479

The GPR results and rehabilitation lidar survey for Bridge A1297 are shown in Figure 4.7 below. Results are show for 100 ft. of the 157 ft. long bridge. Complete results are available in the Digital Appendix described in Appendix F. Similar to Bridge A1479, the GPR and lidar results for Bridge A1297 have a visual correlation. Areas where the GPR estimated higher evidence of deterioration correspond to areas with greater material removal depths from the lidar survey of the rehabilitation. Similarly, areas where the GPR estimated lower evidence of deterioration correspond to areas with lower material removal depths from the lidar survey.

(a) GPR Top Transverse Reinforcement Reflection Amplitude Results (NdB)

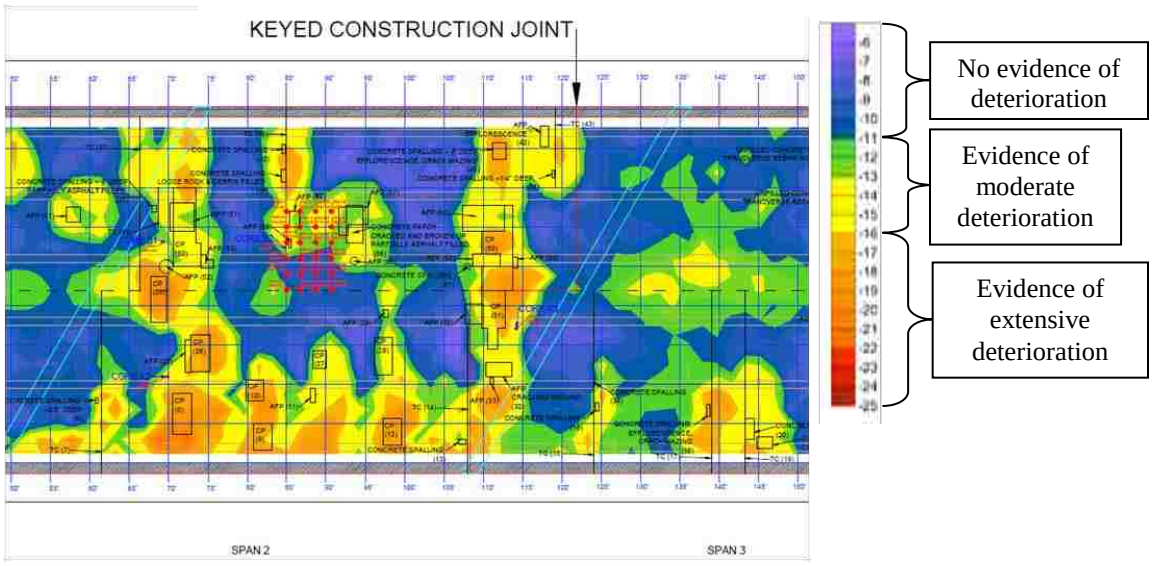

(b) Rehabilitation Lidar Survey

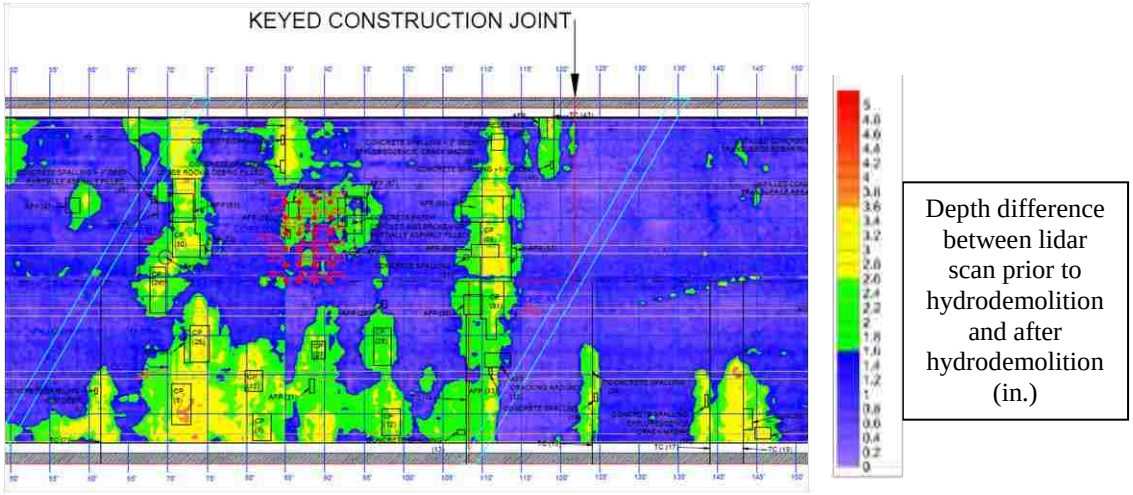

Figure 4.7. Visual Comparison Between GPR Results (a) and Rehabilitation Lidar Survey (b) From Bridge A1297

The correlation between GPR results and the rehabilitation lidar scans was expected. The GPR responds to areas of saline moisture present in the deck, and for the moisture to ingress into the deck, some form of degradation of the concrete has to be taking place.

In order to better understand the visual correlation between the GPR results and rehabilitation lidar survey, both data sets were grouped into three categories, and the percentage of the deck area that fell into each of these categories was determined. The three categories for the GPR results are: no evidence of deterioration, evidence of moderate deterioration, and evidence of extensive deterioration. The rehabilitation lidar survey data was also placed into three categories based on the depth of material removal. The three rehabilitation material removal categories are: material removal depths less than or equal to 0.75 in., material removal depths greater than 0.75 in but less than the depth to the top of the topmost reinforcement bar, and material removal depths greater than or equal to the depth to the top of the topmost reinforcement bar. The results for Bridges A1479 and A1297 are illustrated in Figures 4.8 and 4.9 respectively.

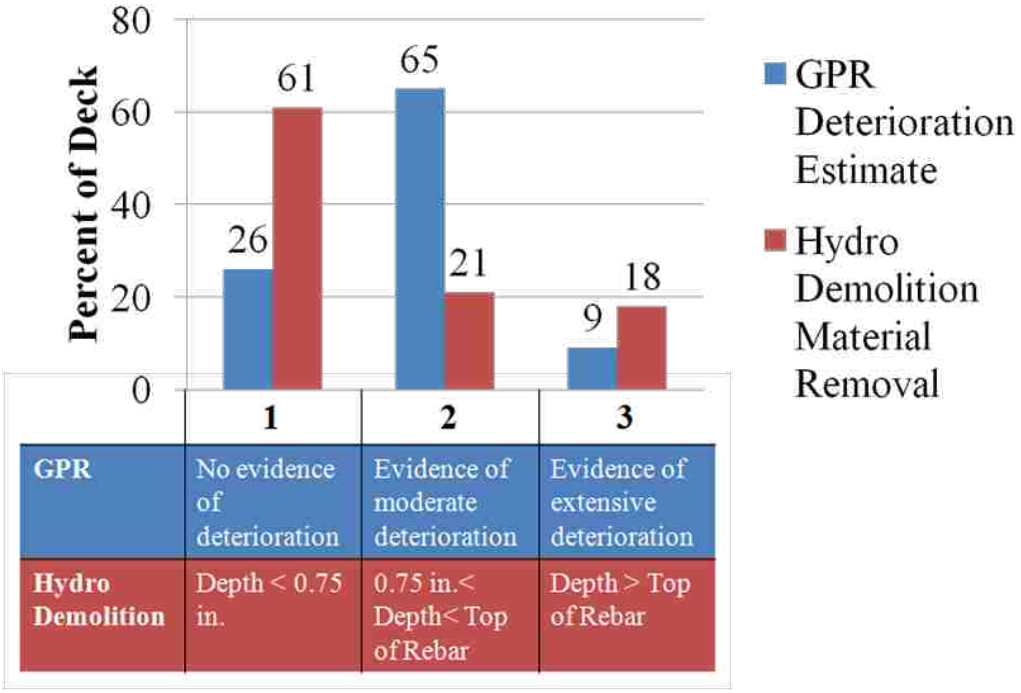

Figure 4.8. Percentage of Deck Area for Bridge A1479 Categorized by GPR Results and Rehabilitation Lidar Survey

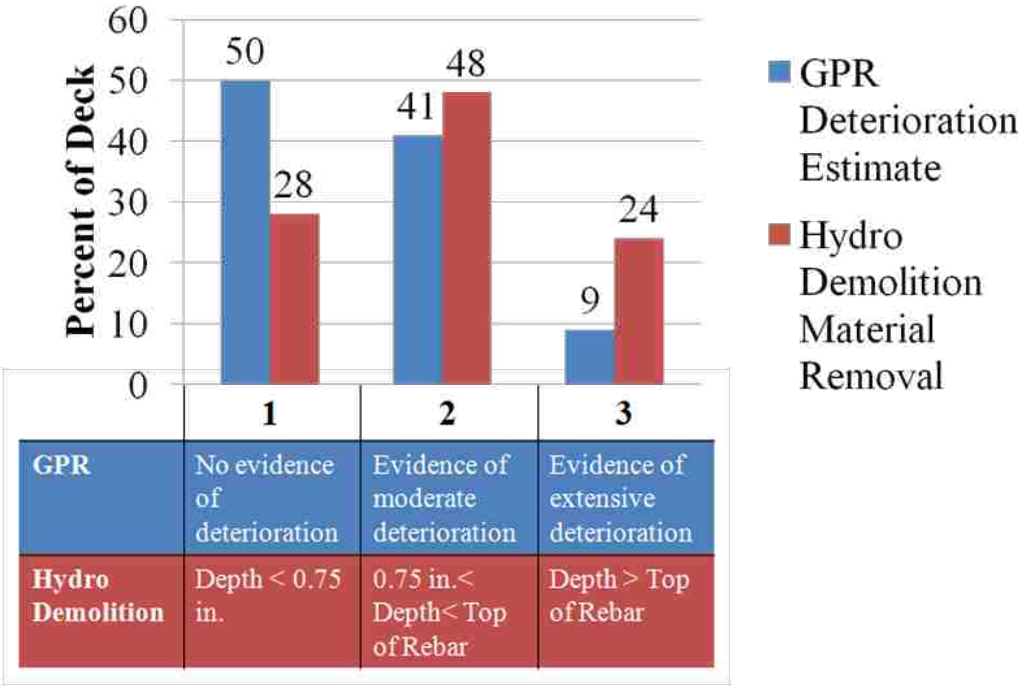

Figure 4.9. Percentage of Deck Area for Bridge A1297 Categorized by GPR Results and Rehabilitation Lidar Survey

Figures 4.8 and 4.9 above were expected to show a trend between the GPR results and the rehabilitation lidar survey because of the visual correlation noted in Figures 4.6 and 4.7. However, no trend between the three different categories of GPR results and rehabilitation lidar surveys is visible.

While interpreting the results shown in Figures 4.8 and 4.9 above, there are several crucial factors that need to be acknowledged. As discussed in Section 3.2, the GPR results used in this thesis are the reflection amplitude from the top transverse layer of reinforcement, therefore these results do not represent the condition of the concrete below the top transverse reinforcement. Because of this, category 3 of the rehabilitation lidar survey is not reflected in the GPR results, because the GPR results presented in this thesis do not extend deeper than the top transverse reinforcement bar. It is also important to note that the topmost layer of reinforcing bars in Bridge A1479 is in the longitudinal direction, which is what the percentages for the three depth removal categories are based on. However, the GPR results are based off of the top transverse reinforcement, which is located 0.625 in. below the top of the longitudinal bars. Also, the GPR results presented

in this thesis do not show the depth at which saline moisture is present in the deck causing the different GPR reflection amplitudes. As discussed in Section 4.2.1, the calibration of the GPR estimated deterioration levels is complex and is ongoing at the time of writing this thesis. The GPR results are being compared with the rehabilitation lidar survey to develop a GPR estimated deterioration level scale that is calibrated with concrete removal rates to assist transportation officials better estimate material removal quantities for rehabilitation projects. Results in this thesis support the general correlation and need for further calibration of the results in order to achieve this goal.

5. CONCLUSIONS, ONGOING STUDIES AND RECOMMENDATIONS FOR FUTURE STUDIES

This study investigated the use of nondestructive and destructive evaluation techniques for bridge deck condition assessments. Two bridge decks in Missouri were investigated in this study using visual inspections, GPR, core extraction, chloride ion concentration measurements, and surveys of material removal during the rehabilitation processes using lidar. The cores underwent a careful visual evaluation along with tests to determine the volume of permeable pore space. The Osage River bridge (A1479) was relatively long at 868 ft. compared to the railroad bridge (A1297) at 157 ft. Both bridge decks were experiencing heavy deterioration as noted during the visual inspections. All data sets were compared to determine correlations between bridge deck evaluation methods.

5.1. CONCLUSIONS

1. There were common areas in both bridge decks where heavier deterioration was noticed with the visual investigation, GPR, and the survey of the rehabilitation. These areas included construction joints, areas near girder mid-spans where traffic-induced vibration was noted during the investigation, and areas where deicing chemicals would remain on the deck for extended periods of time.
2. In both bridges discussed in this thesis, the GPR top reinforcement reflection amplitude indicated deterioration in areas where visual deterioration was noticed.
3. The majority of cores with delaminations were extracted from sections where the GPR top reinforcement reflection amplitude indicated greater evidence of deterioration based on lower amplitude values.
4. There was a correlation between the GPR reflection amplitude and the volume of permeable pore space when cores of similar lengths were compared. Cores with lower volumes of permeable pore space were extracted from areas with higher reflection amplitudes, indicating less deterioration.
5. As shown by the lidar survey of the material removed during rehabilitation, the GPR top reflection amplitude accurately predicted regions of deterioration.

Regions with lower reflection amplitudes, indicating more evidence of deterioration, corresponded to regions with greater depths of material removal during the rehabilitation.

5.2. ONGOING STUDIES

Additional studies related to the Nondestructive Evaluation of MoDOT Bridge Decks – Pilot Study are ongoing at the time this thesis was completed. These studies are aimed at better calibrating GPR results so that it can be used more accurately in the monitoring of bridge decks and planning of rehabilitation. The following is a list of ongoing studies.

1. Estimation of through thickness deterioration: Analysis of the through thickness of deterioration of the bridge decks is ongoing. Researchers are using different reflectors, such as the bottom of the slab, to estimate the depth of deterioration. Results from this study could be used to monitor deterioration for the full slab depth as well as better prepare estimates for repair and rehabilitation.
2. Calibration of GPR results to material removal from hydrodemolition results: This analysis could improve the interpretation of GPR results for future bridge scans as well as better calibrate results of the eight bridges investigated in this study that did not undergo rehabilitation.
3. Determination of climate effects on GPR results: Analysis of this study will determine the significance that climate changes have in GPR results, as well as aide in the calibration of GPR results to reflect climate conditions at the time of scanning.
4. Analysis of how reinforcing bar depth influences GPR reflection amplitude: This study is being performed to see how great of an impact varying depths of reinforcing bars has on GPR results. Results from this study can be used to either further validate that reinforcing bars with varying amounts of clear cover do not significantly impact GPR results, or that the impact on results is significant.
5. Ability of air launched GPR antenna to detect bridge deck deterioration: This study is a separate project, however some of the bridges evaluated in this study

will also be evaluated in the new study so results can be compared. If proven effective, the collection of air launched GPR data could enable more efficient evaluation of bridge decks.

5.3. RECOMMENDATIONS FOR FUTURE STUDIES

Although correlations between data sets were visible in this study, several factors were noted that would help to increase the accuracy of the interpretations. The following is a list of changes or additions that should be considered for future studies.

1. One concern with the interpretation of GPR results is the impact of climate effects, especially the amount of moisture present in the deteriorated areas of a bridge deck. Deteriorated areas without moisture present may not indicate deterioration with the GPR. One way to constrain the effect moisture has on GPR studies would be to apply a known dosage of water to the bridge deck prior to the GPR investigation. This would allow water to penetrate into the concrete and allow for more enhanced GPR imaging. By using a standard water dosage at a specific time before the GPR scan, certain climate factors could be normalized from the interpretation of GPR results.
2. More information regarding the volume of permeable pore space is needed to study how pores in the concrete affect GPR results. The volume of permeable pore tests performed in this study showed conflicting results, possibly due to variation in specimen size. Future studies should ensure that concrete tested is of equal volume and from locations of equal depth in the concrete.
3. When performing the GPR scan, it would be helpful to have GPR data exactly over the cores, and the cores marked in the profiles. In this study, the cores locations were chosen after the GPR scan, but for future studies, random core locations could be marked along GPR profiles before scanning, so marks can be placed in the data to ensure exact alignment between GPR and core locations.
4. When performing the lidar survey to measure material removal during rehabilitation, it would have been helpful to have an object next to the core locations so that the core locations could be located exactly on the lidar contour

maps, instead of relying on accurate aligning of core locations and lidar contour maps.

5. Studies should focus on determining specific causes of deterioration, such as design or construction aspects of the bridge that cause earlier than expected deterioration. Bridge designers could then use these findings to design longer lasting bridges by understanding problems with existing bridges.

APPENDIX A.

BRIDGE A1479 INVESTIGATION DRAWINGS

A. BRIDGE A1479 INVESTIGATION DRAWINGS

1. INTRODUCTION

This appendix provides the bridge deck design, including the location of bents and girders, visual investigation results, GPR and PSPA results, core locations, and depth of material removal during the rehabilitation process results obtained by lidar. Each drawing includes a grid with five foot spacing. See Figure 3.1 and the corresponding discussion in Section 3.1 for descriptions of the drawings. The drawing is included in 75 foot segments. There are three images per figure. The top image is the bridge drawing with the visual investigation results. The middle image is the bridge drawing with visual investigation results and the contour map of the GPR top transverse reinforcement reflection amplitudes. The bottom image is the contour map generated from the lidar survey measuring the depth of material removal during the rehabilitation process. All of the drawings included in this appendix are from a comprehensive PDF file which is included in the Digital Appendix discussed in Appendix F.

2. CONTENTS

Page

GPR Top Transverse Reinforcement Reflection Amplitude Map Scale (NdB)

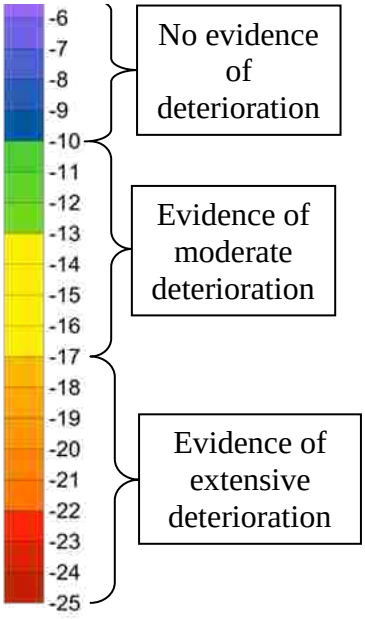

(b) Rehabilitation Lidar Survey Scale

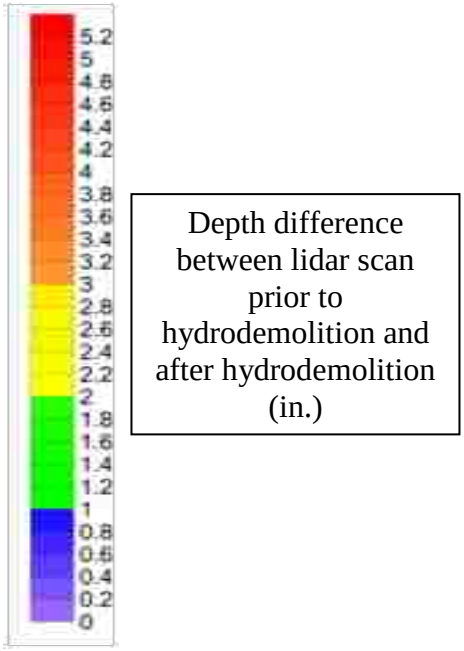

Figure A.1. Bridge A1479 GPR Map Scale (a) and Lidar Survey Scale (b)

North

Figure A.2. Bridge A1479 North for all Drawings in Appendix A

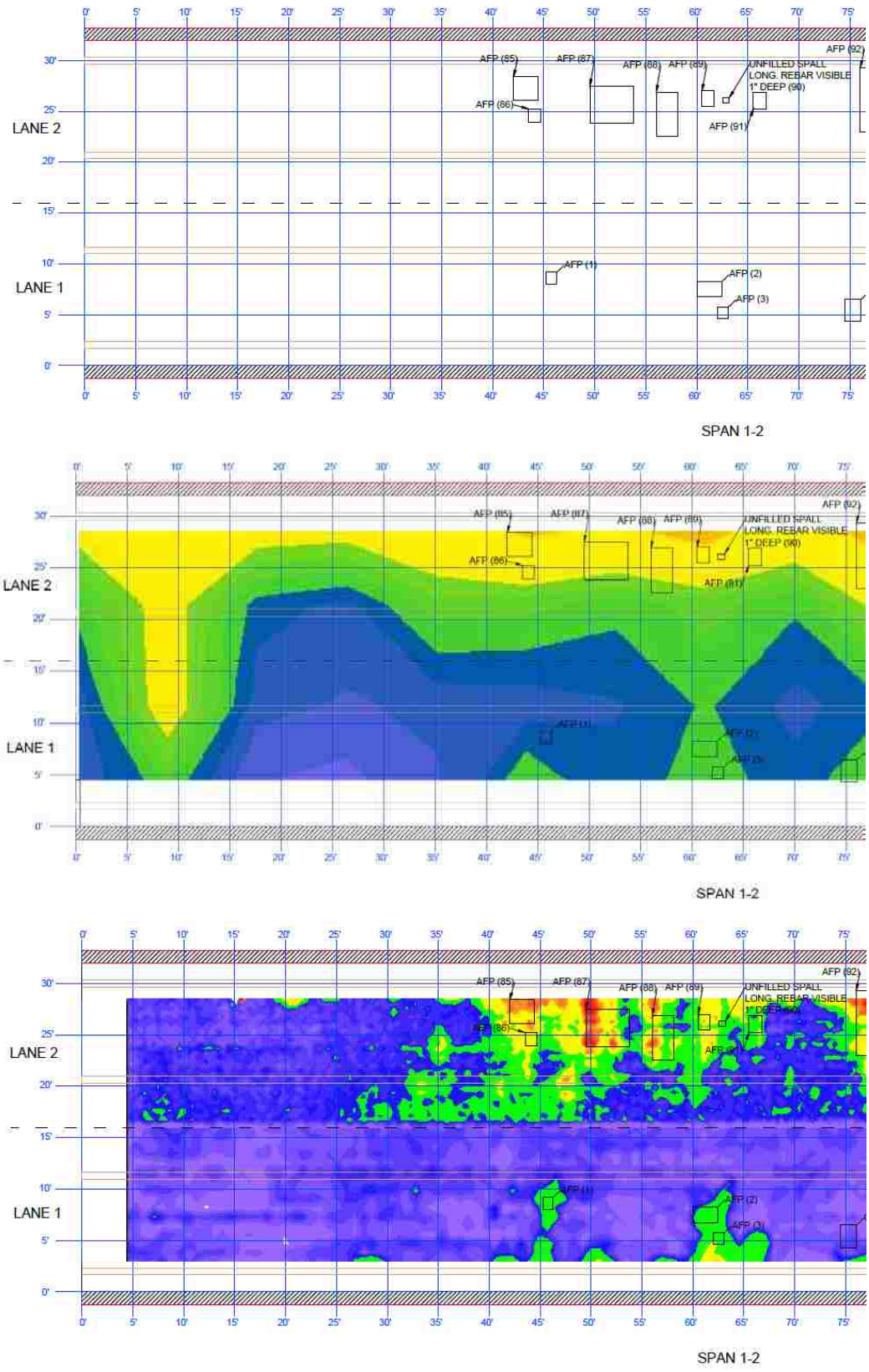

Figure A.3. Bridge A1479 Drawing Segment, 0 ft. – 75 ft.

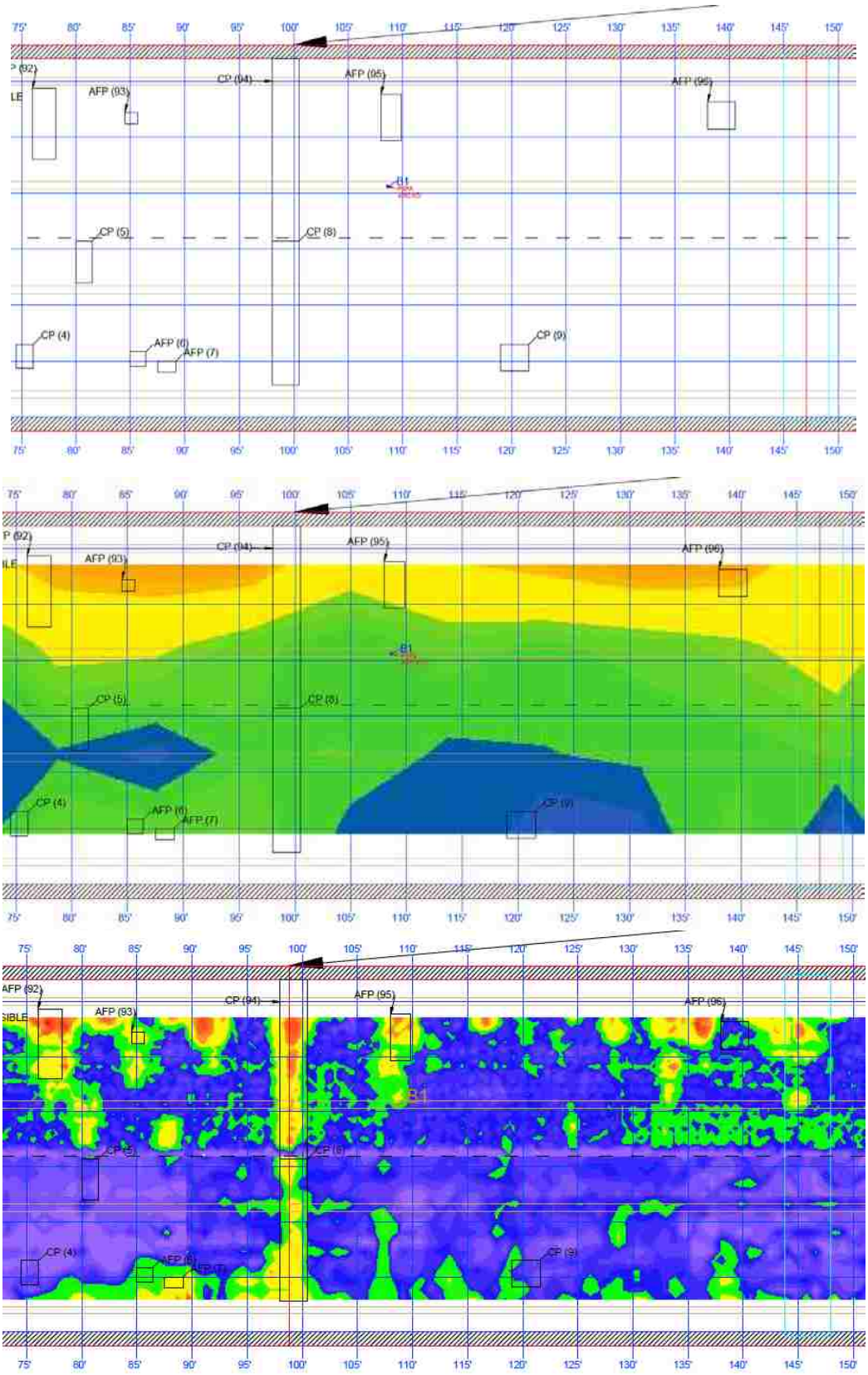

Figure A.4. Bridge A1479 Drawing Segment, 75 ft. – 150 ft.

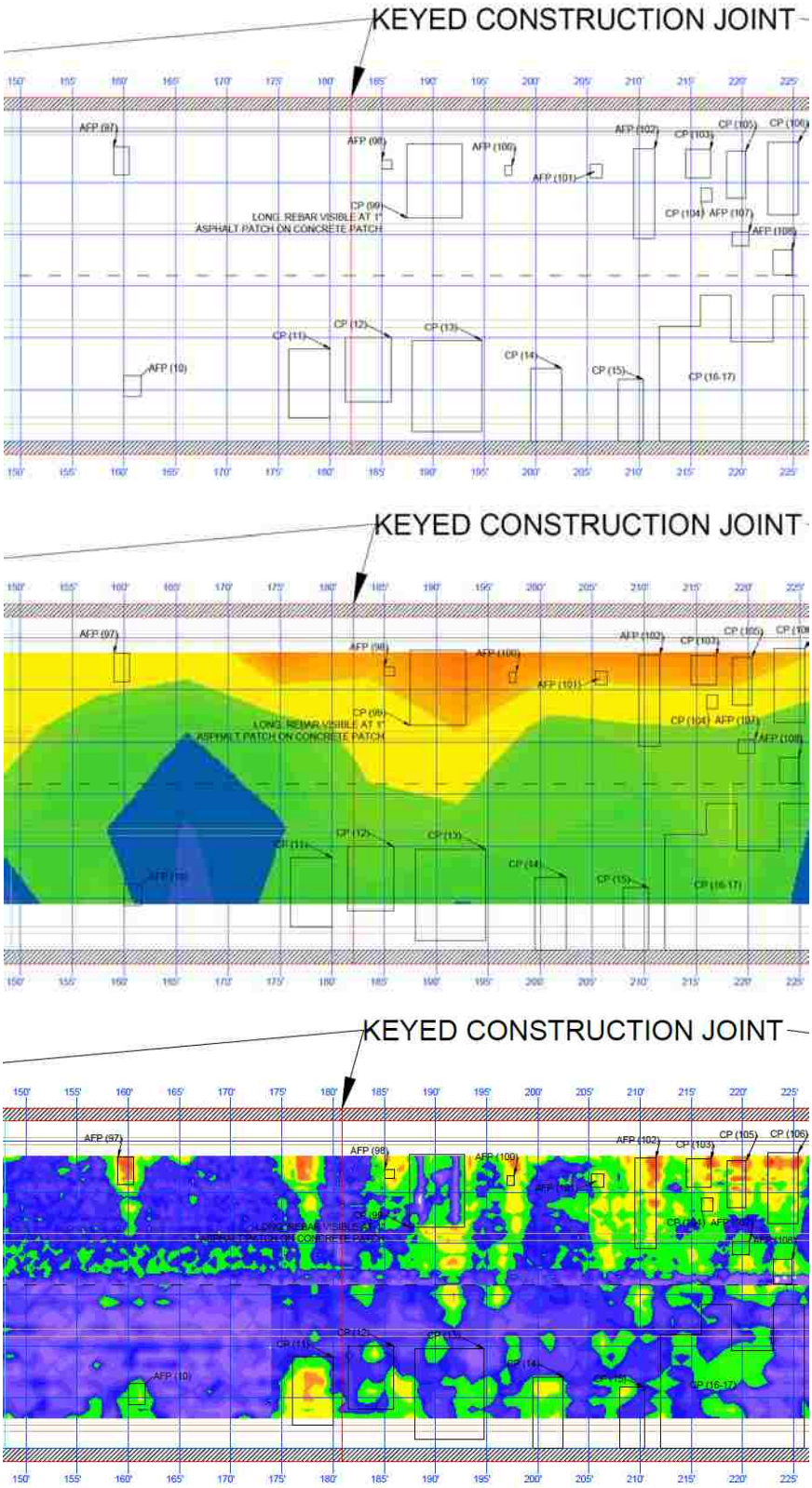

Figure A.5. Bridge A1479 Drawing Segment, 150 ft. – 225 ft.

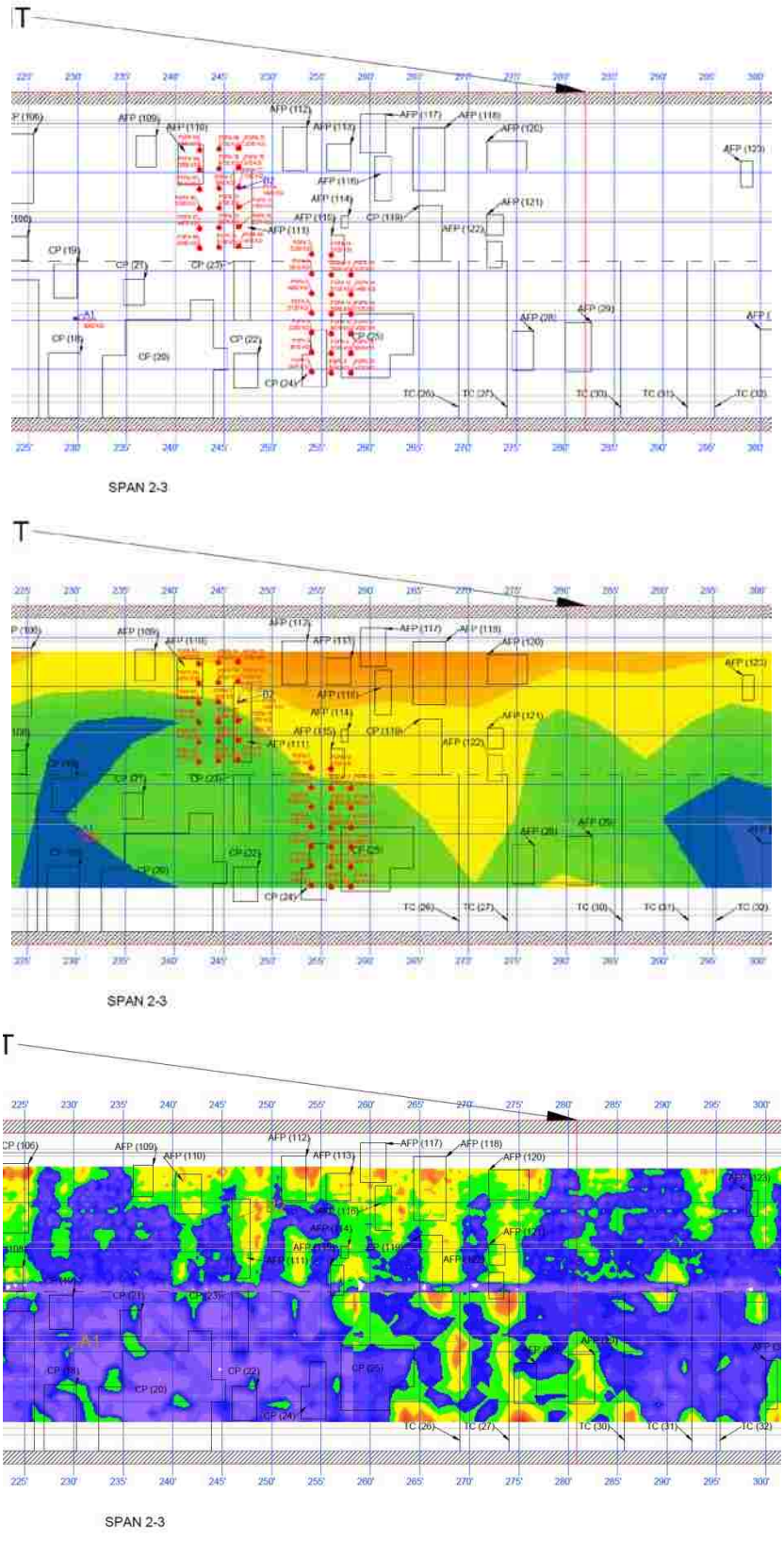

Figure A.6. Bridge A1479 Drawing Segment, 225 ft. – 300 ft.

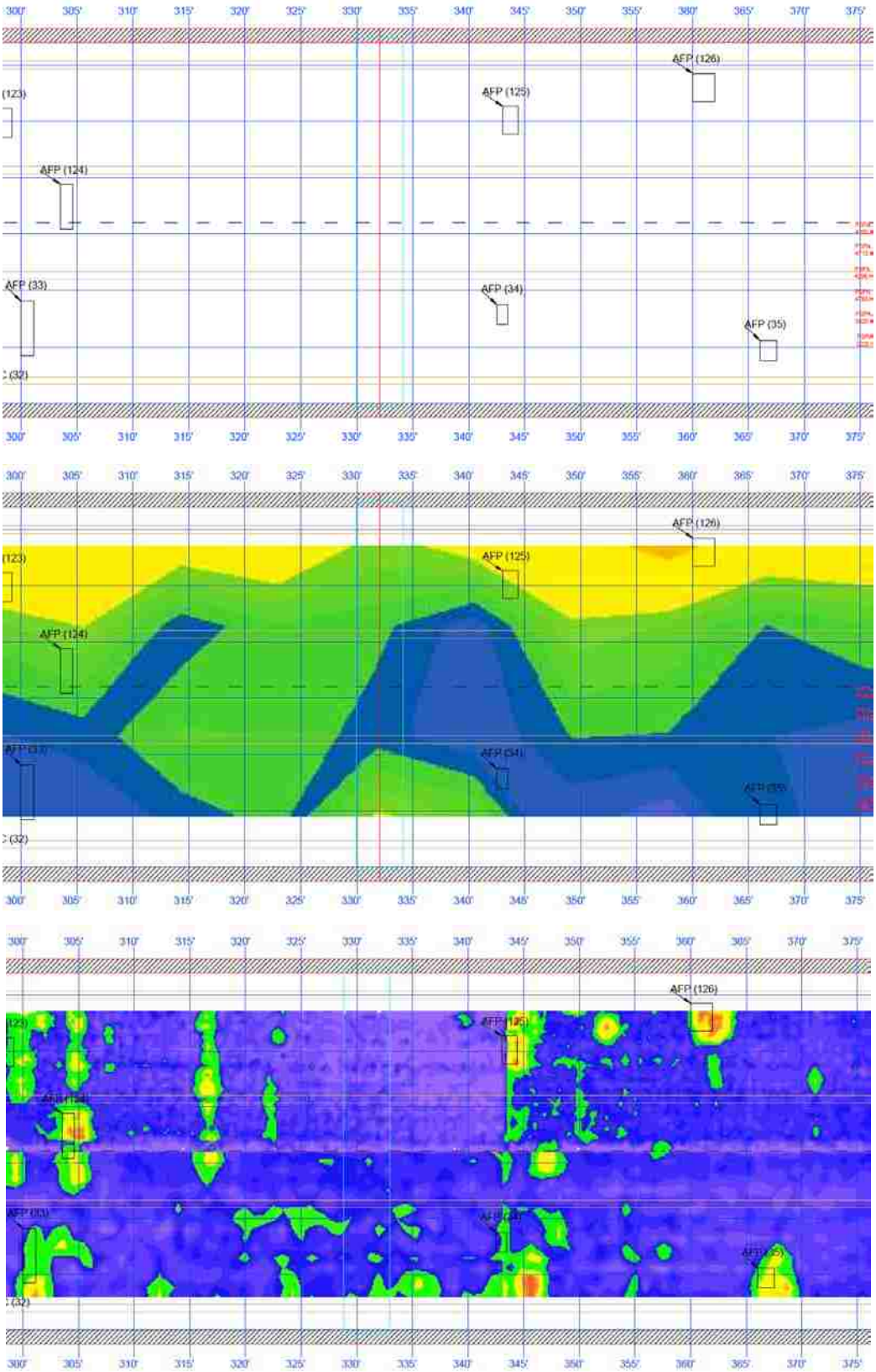

Figure A.7. Bridge A1479 Drawing Segment, 300 ft. – 375 ft.

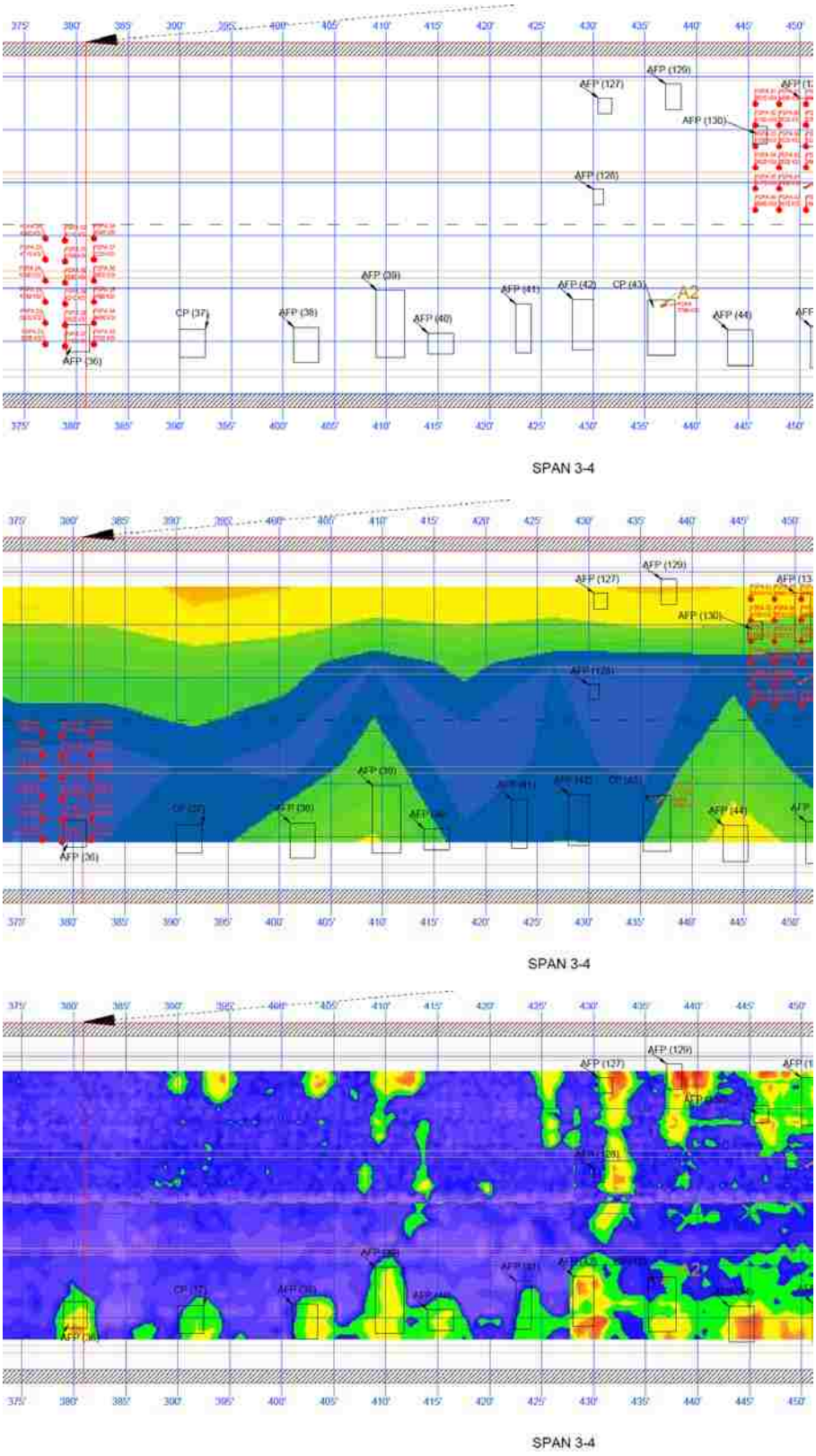

Figure A.8. Bridge A1479 Drawing Segment, 375 ft. – 450 ft.

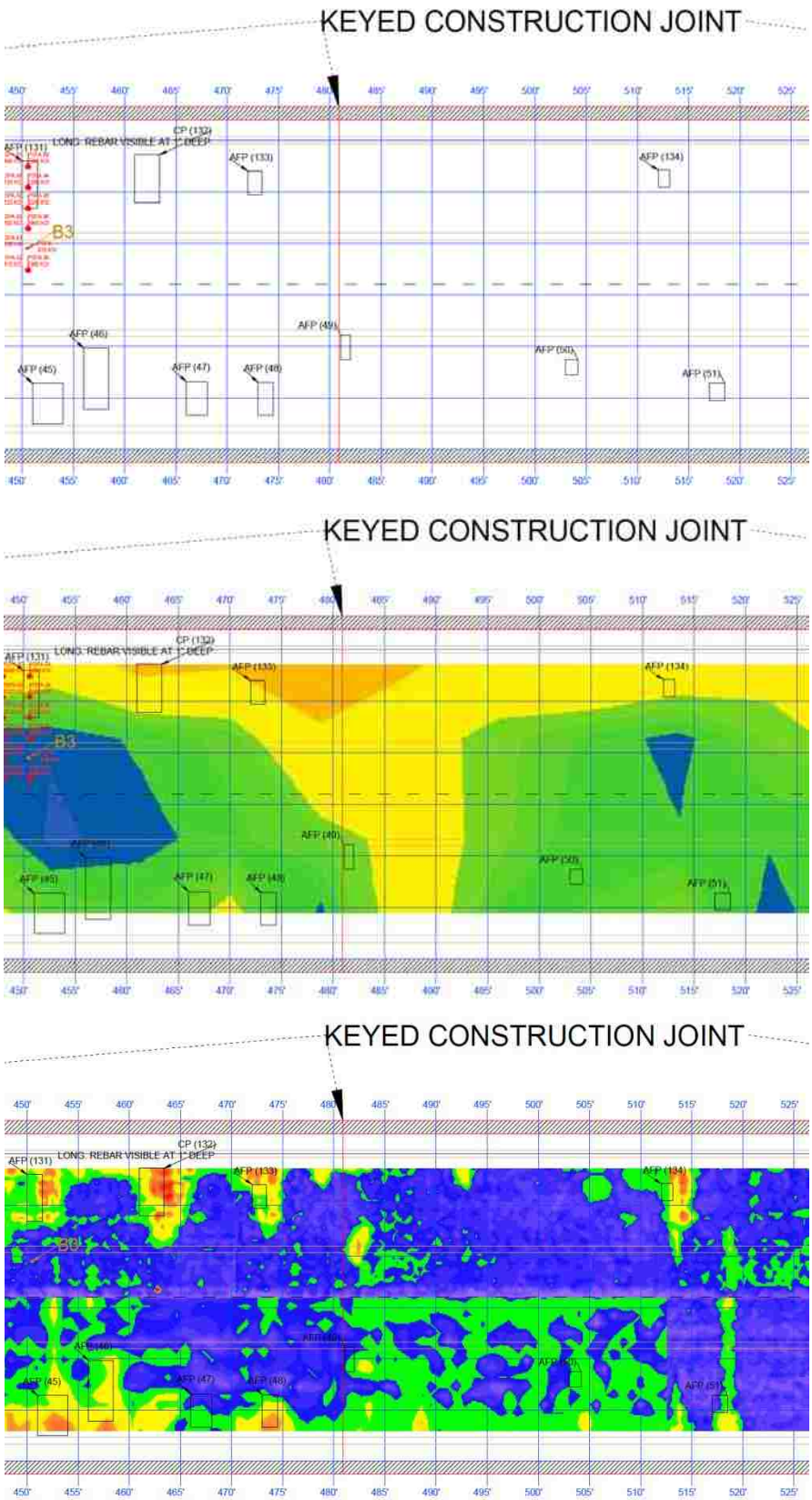

Figure A.9. Bridge A1479 Drawing Segment, 450 ft. – 525 ft.

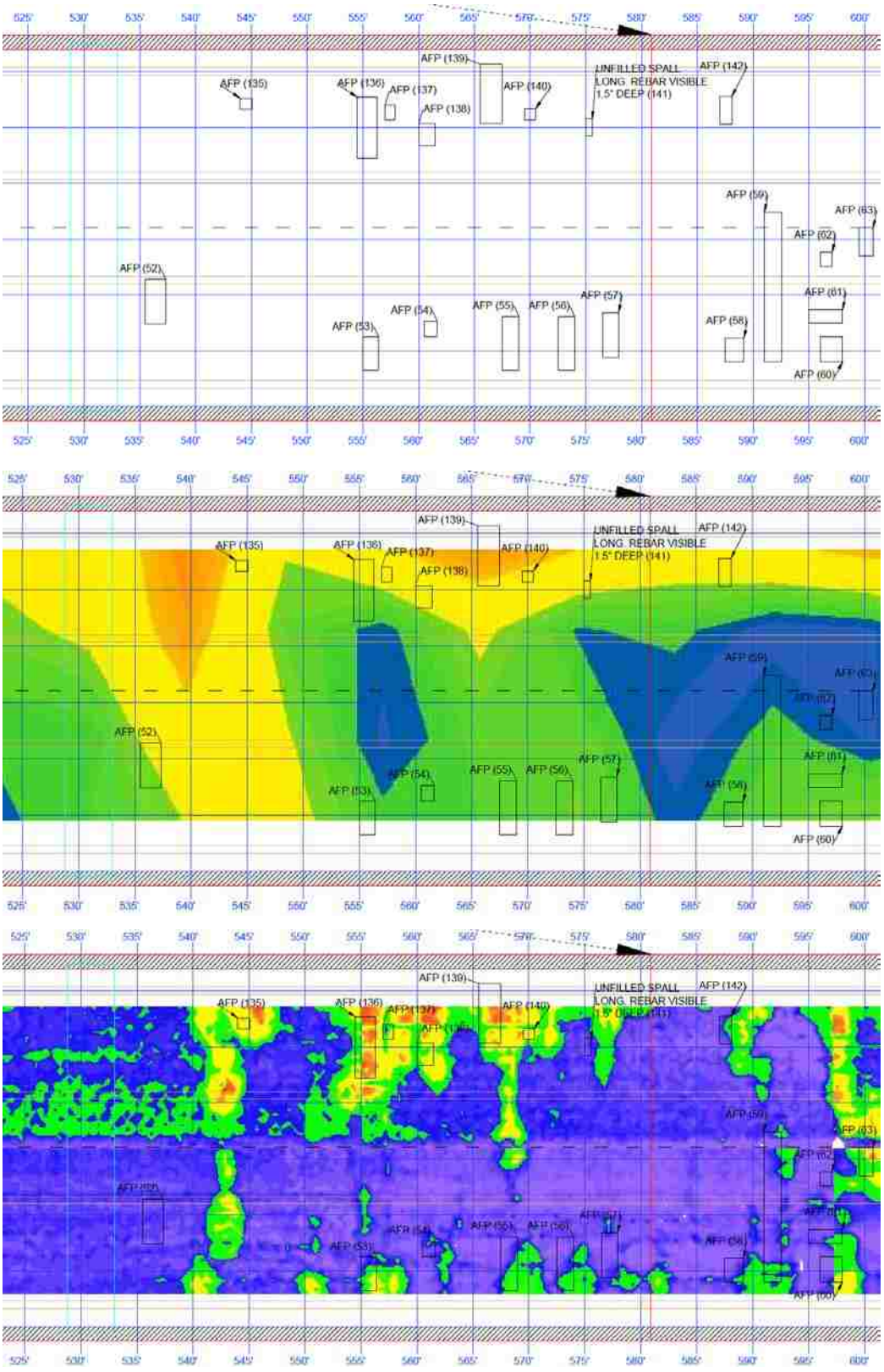

Figure A.10. Bridge A1479 Drawing Segment, 525 ft. – 600 ft.

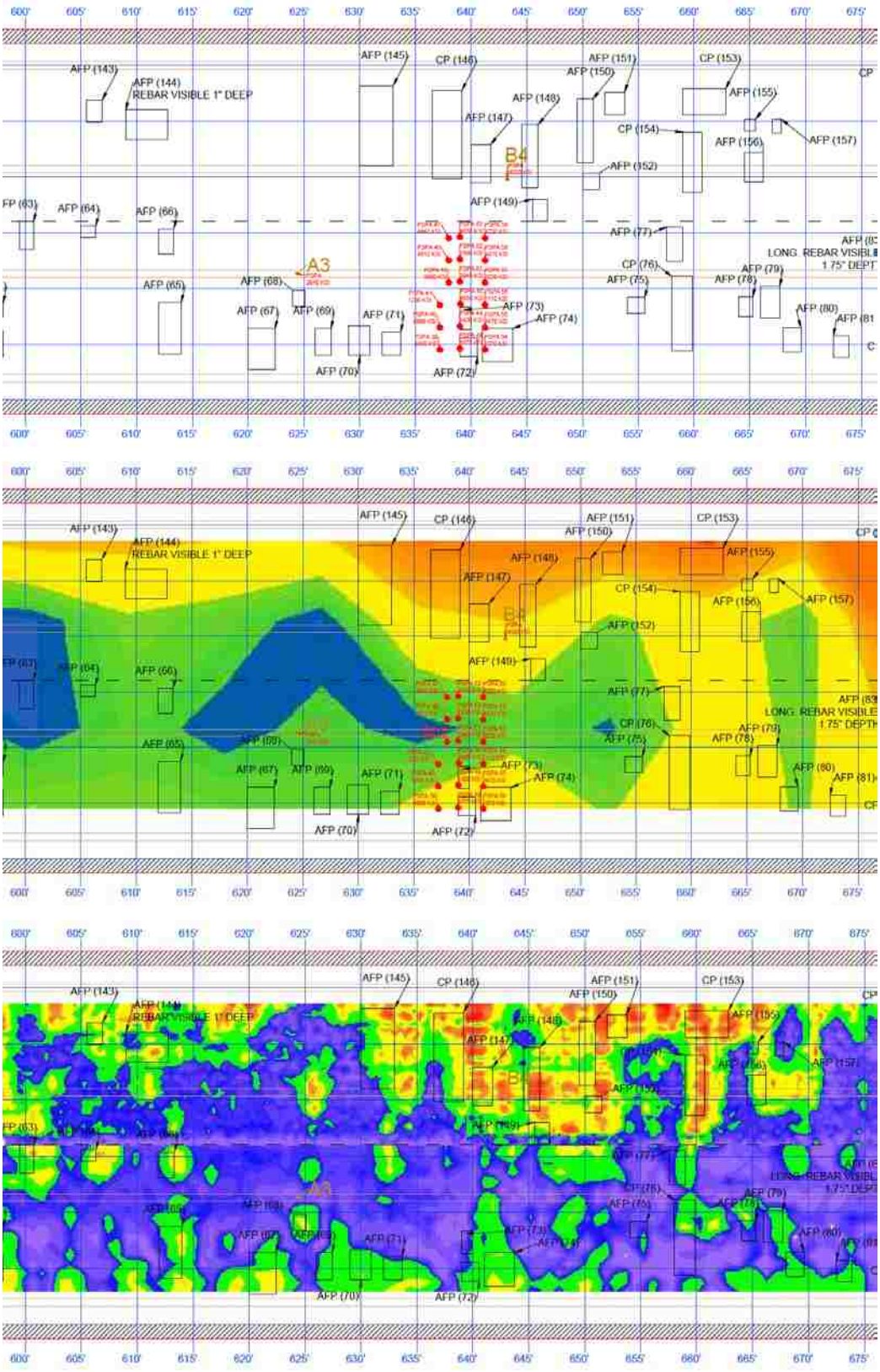

Figure A.11. Bridge A1479 Drawing Segment, 600 ft. – 675 ft.

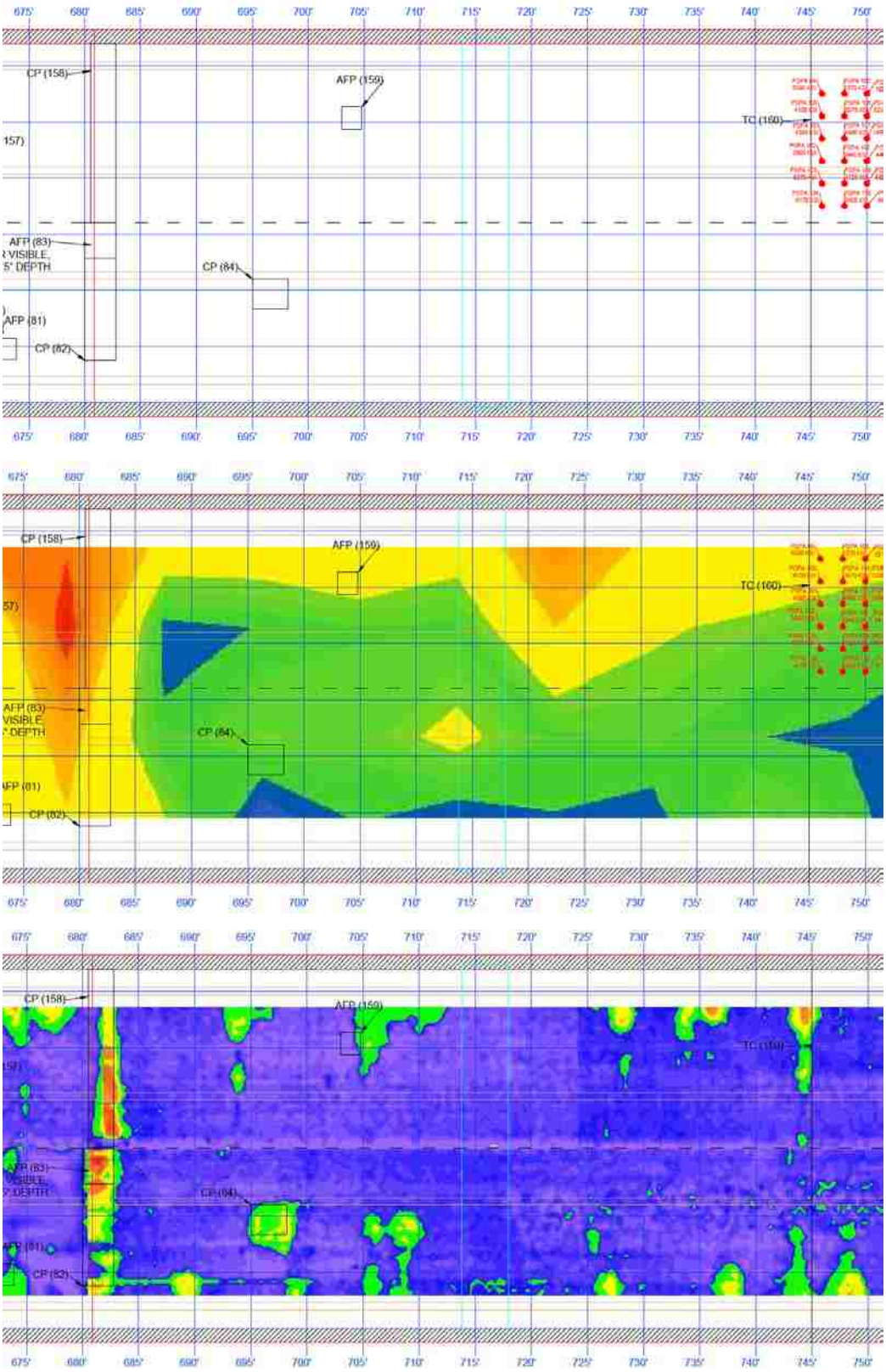

Figure A.12. Bridge A1479 Drawing Segment, 675 ft. – 750 ft.

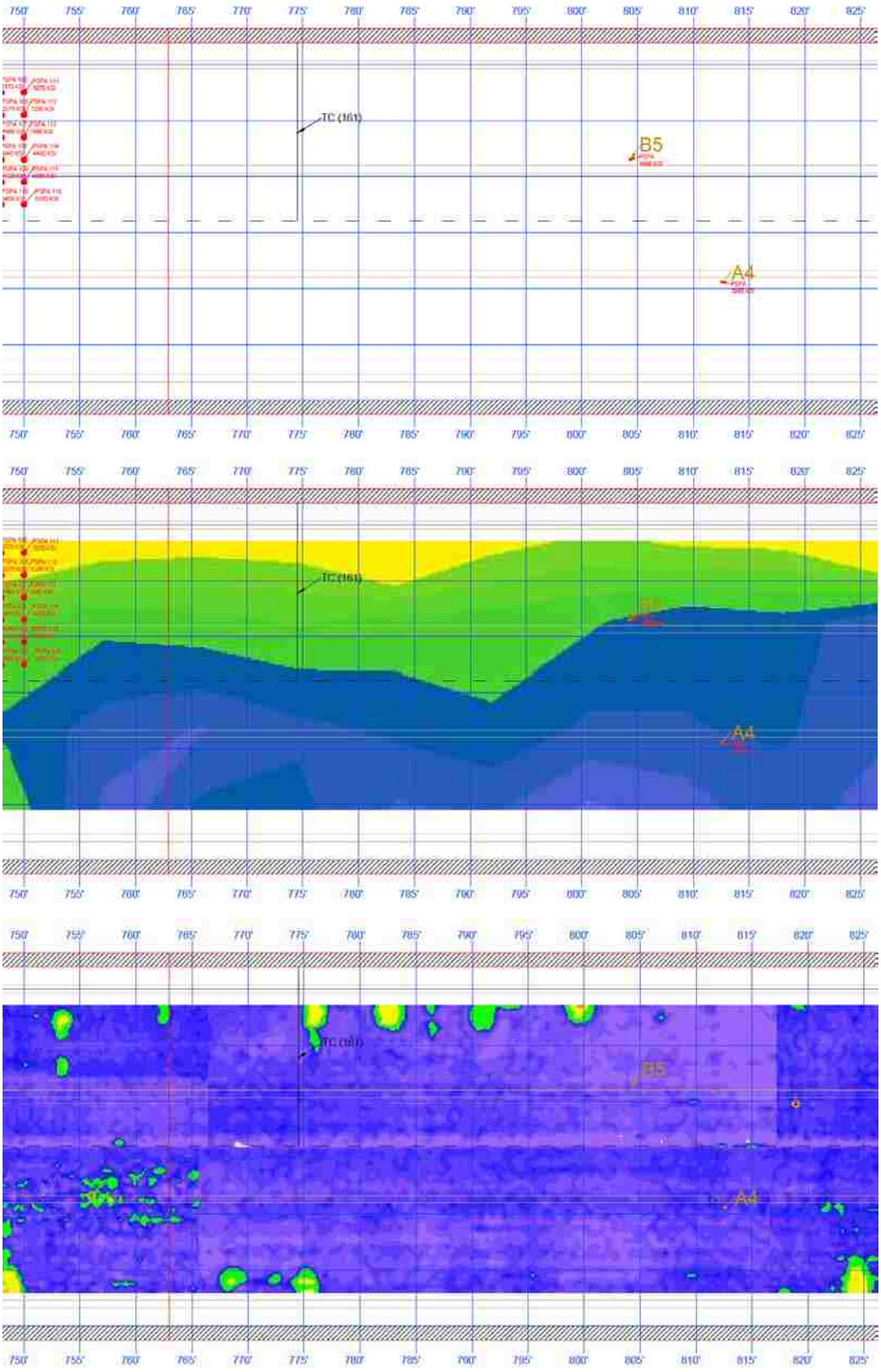

Figure A.13. Bridge A1479 Drawing Segment, 750 ft. – 825 ft.

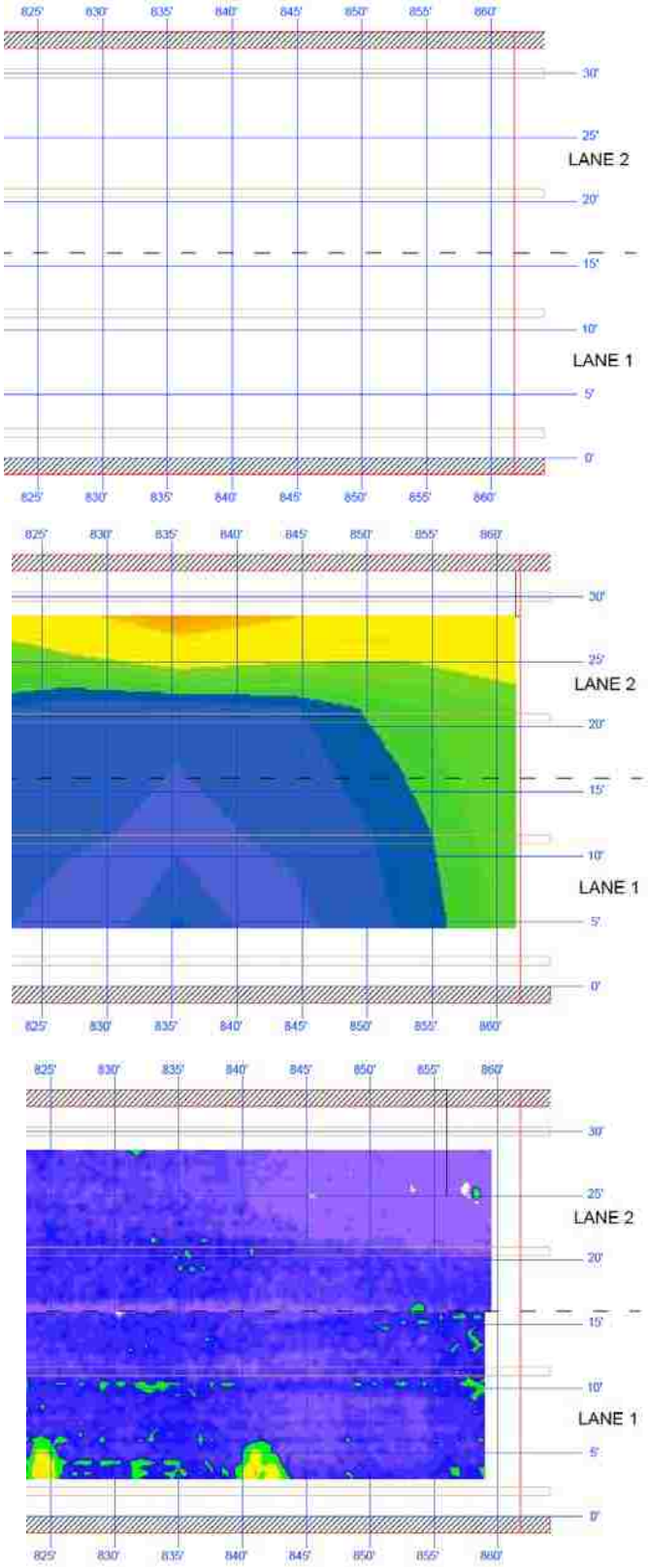

Figure A.14. Bridge A1479 Drawing Segment, 825 ft. – 864 ft.

APPENDIX B.
BRIDGE A1479 VISUAL CORE EVALUATIONS

B. BRIDGE A1479 VISUAL CORE EVALAUTIONS

1. INTRODUCTION

This appendix provides the complete visual core evaluation results from Bridge A1479, along with photographs of each core.

2. CONTENTS

Page

Table B.1. Bridge A1479 Visual Core Evaluations, Cores A1 – A4

Core	A1	A2	A3	A4
Diameter (in)	2.0	2.0	2.0	2.0
Length (in)	1.0	2.25-2.5	2.0-2.75	2.875
Surface (Asphalt: A, Concrete: C)	C	C	C	C
Number of Pieces	1	1	2	1
#1 Length (in) and failure mode [1]	1.0, PRE	2.25-2.5, CEX	1.0, PRE	2.875, CEX
#2 Length (in) and failure mode	N/A	N/A	1.0-1.75, CEX	N/A
#3 Length (in) and failure mode	N/A	N/A	N/A	N/A
#4 Length (in) and failure mode	N/A	N/A	N/A	N/A
#5 Length (in) and failure mode	N/A	N/A	N/A	N/A
Rebar: diameter (in), length (in), orientation [2], corrosion [2]	None	Welded Wire, 0.1875 Diam., Lo, Co1	None	None
Roughness (Smooth, Average, Very Rough)	Average	Average	Average	Average
Voids (Number >0.25 in. diameter)	0	2	1	1
Coating of the Aggregate (good or bad)	Good	Good	Good	Good
Volume of Paste (good or bad)	Good	Good	Good	Good
Air Entrained (yes or no)	Yes	Yes	Yes	Yes
Flaking surface: thickness (in)	None	None	None	None
Discoloration: color, maximum length (in)	None	None	None	None
Delaminations: depths (in)	1.0	None	1.0	None
Segregation of Aggregate: depths (in)	None	None	None	None
Cracks (excluding fracture planes): number, length (in)	None	1, 2" Deep	None	None
Other Comments	Bottom Piece left in hole, would have had to break up to remove, solid in hole	Concrete patch, Rounded coarse aggregate	Material at delamination missing	
General Quality of Concrete [3] (good, fair, bad)	Fair	Good	Fair	Good

[1] Preexisting Rupture (PRE), Induced during coring (IDC), Produced by shear from extracting the core (CEX), Generated during handling (HAN), Other cause (OTR)
[2] Orientation: traverse (Tr) or longitudinal (Lo); Corrosion: none (Co1), low (Co2), average (Co3), high (Co4)
[3] Good indicates no delaminations or visible deterioration. Fair indicates some visible deterioration including delaminations however concrete is in large sections. Bad indicates concrete shows a lot of deterioration and is in many pieces including several small pieces

Table B.2. Bridge A1479 Visual Core Evaluations, Cores B1 – B5

Core	B1	B2	B3	B4	B5
Diameter (in)	2.0	2.0	2.0	2.0	2.0
Length (in)	2.0-2.5	2.0-2.5	2.125-2.5	1.25-1.75	2.0-2.25
Surface (Asphalt: A, Concrete: C)	C	1.75-2.0 A	C	C	C
Number of Pieces	1	2	1	1	1
#1 Length (in) and failure mode [1]	2.0-2.5, CEX	1.75-2.0, PRE asphalt debonded	2.125-2.5, CEX	1.25-1.75, PRE	2.0-2.25, CEX
#2 Length (in) and failure mode	N/A	0.75, PRE	N/A	N/A	N/A
#3 Length (in) and failure mode	N/A	N/A	N/A	N/A	N/A
#4 Length (in) and failure mode	N/A	N/A	N/A	N/A	N/A
#5 Length (in) and failure mode	N/A	N/A	N/A	N/A	N/A
Rebar: diameter (in), length (in), orientation [2], corrosion [2]	None	None	None	None	None
Roughness (Smooth, Average, Very Rough)	Average	Average	Average	Average	Average
Voids (Number >0.25 in. diameter)	5	0	2	2	1
Coating of the Aggregate (good or bad)	Good	Good	Good	Good	Good
Volume of Paste (good or bad)	Good	Good	Good	Good	Good
Air Entrained (yes or no)	Yes	Yes	Yes	Yes	Yes
Flaking surface: thickness (in)	None	None	None	None	None
Discoloration: color, maximum length (in)	None	None	None	None	None
Delaminations: depths (in)	None	2.5	None	1.75	None
Segregation of Aggregate: depths (in)	None	None	None	None	None
Cracks (excluding fracture planes): number, length (in)	None	None	1, 2.25" deep, Induced by extraction	None	None
Other Comments		Mostly asphalt, asphalt was debonded from concrete sliver		Remaining core left in hole, solid in hole, would have broken up during removal	
General Quality of Concrete[3] (good, fair, bad)	Good	Bad	Good	Fair	Good

[1]Preexisting Rupture (PRE), Induced during coring (IDC), Produced by shear from extracting the core (CEX), Generated during handling (HAN), Other cause (OTR)
[2]Orientation: traverse (Tr) or longitudinal (Lo); Corrosion: none (Co1), low (Co2), average (Co3), high (Co4)
[3]Good indicates no delaminations or visible deterioration, Fair indicates some visible deterioration including delaminations however concrete is in large sections, Bad indicates concrete shows a lot of deterioration and is in many pieces including several small pieces

Core: A1 Visual Rating: Fair	Core: A2 Visual Rating: Good	Core: A3 Visual Rating: Fair

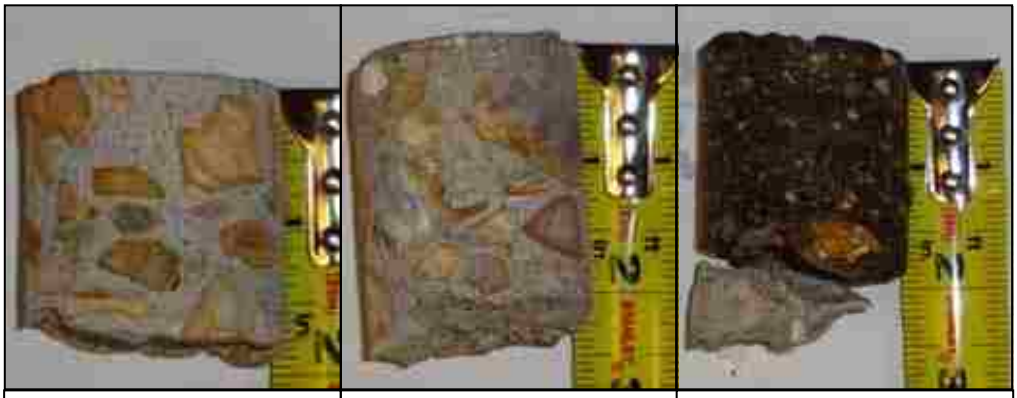

Core: A4 Visual Rating: Good	Core: B1 Visual Rating: Good	Core: B2 Visual Rating: Bad

Core: B3 Visual Rating: Good	Core: B4 Visual Rating: Fair	Core: B5 Visual Rating: Good

Figure B.1. Bridge A1479 Core Photographs

APPENDIX C.

BRIDGE A1297 INVESTIGATION DRAWINGS

C. BRIDGE A1297 INVESTIGATION DRAWINGS

1. INTRODUCTION

This appendix provides the bridge deck design, including the location of bents and girders, visual investigation results, GPR and PSPA results, core locations, and depth of material removal during the rehabilitation process results obtained by lidar. Each drawing includes a grid with five foot spacing. See Figure 3.1 and the corresponding discussion in Section 3.1 for descriptions of the drawings. The drawing is included in 95 foot segments. The first image of each segment is the bridge drawing with the visual investigation results. The second image of each segment is the bridge drawing with visual investigation results and the contour map of the GPR top transverse reinforcement reflection amplitudes. The third image of each segment is the contour map generated from the lidar survey measuring the depth of material removal during the rehabilitation process. All of the drawings included in this appendix are from a comprehensive PDF file which is included in the digital appendix.

2. CONTENTS

Page

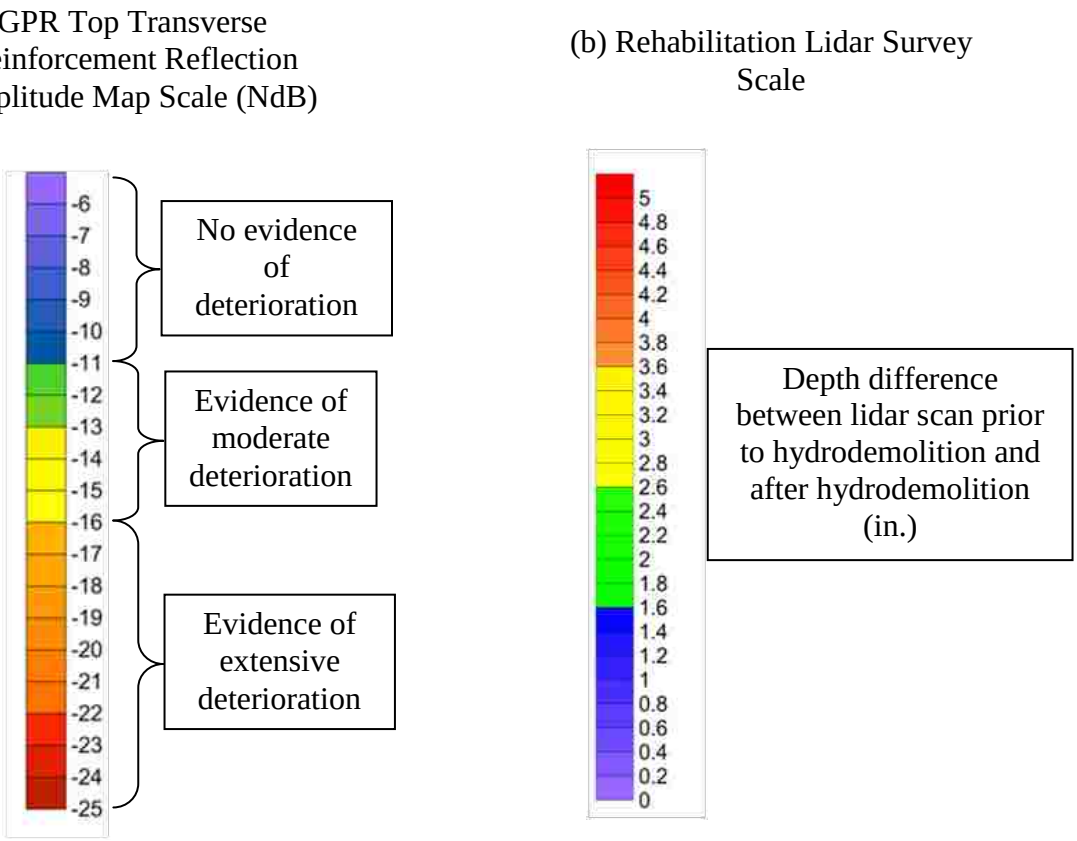

Figure C.1. Bridge A1297 GPR Map Scale (a) and Lidar Survey Scale (b)

North

Figure C.2. Bridge A1297 North for all Drawings in Appendix C

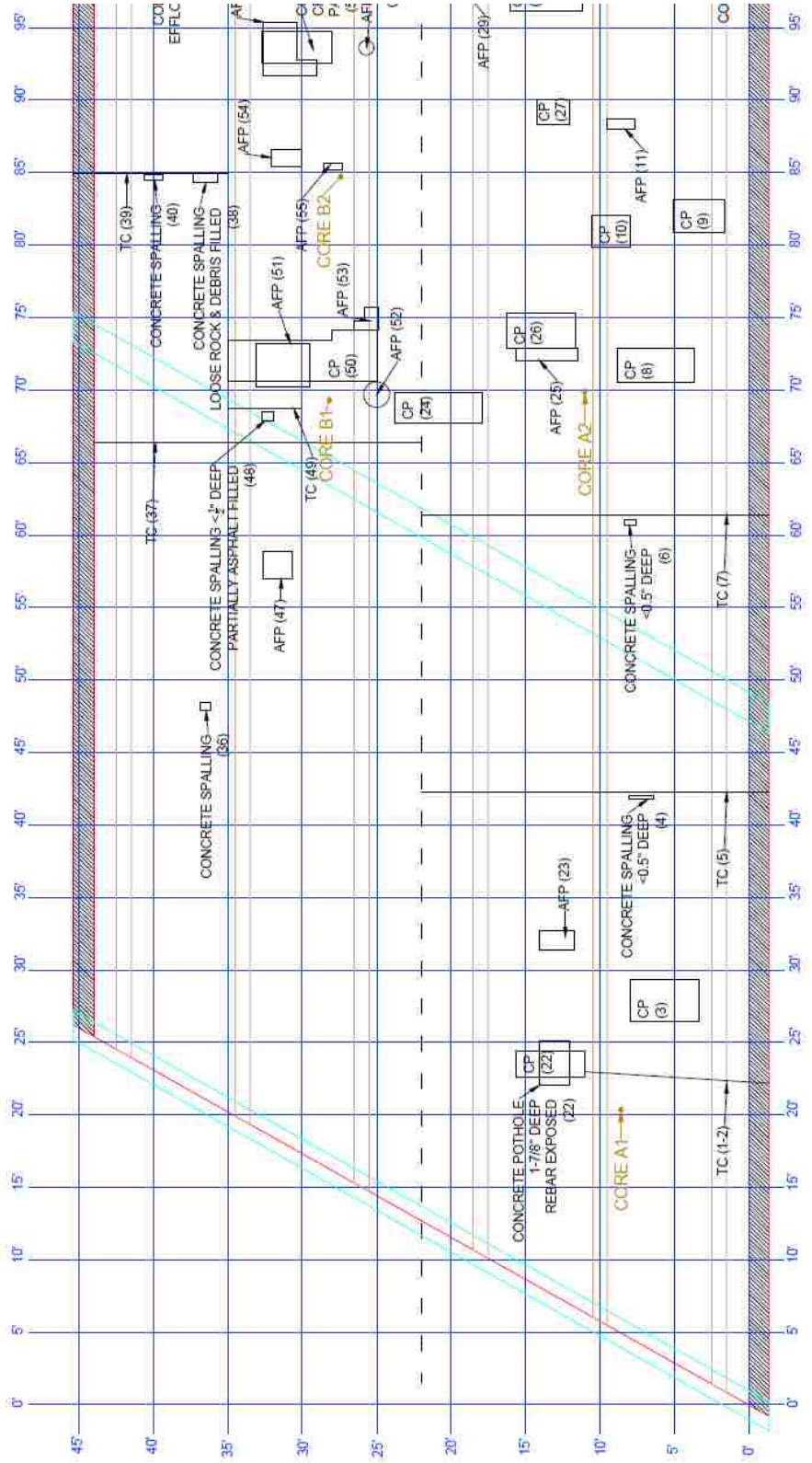

Figure C.3. Bridge A1297 Deck Investigation Drawing, Visual Inspection Results, Section 1 (0 ft. – 95 ft.)

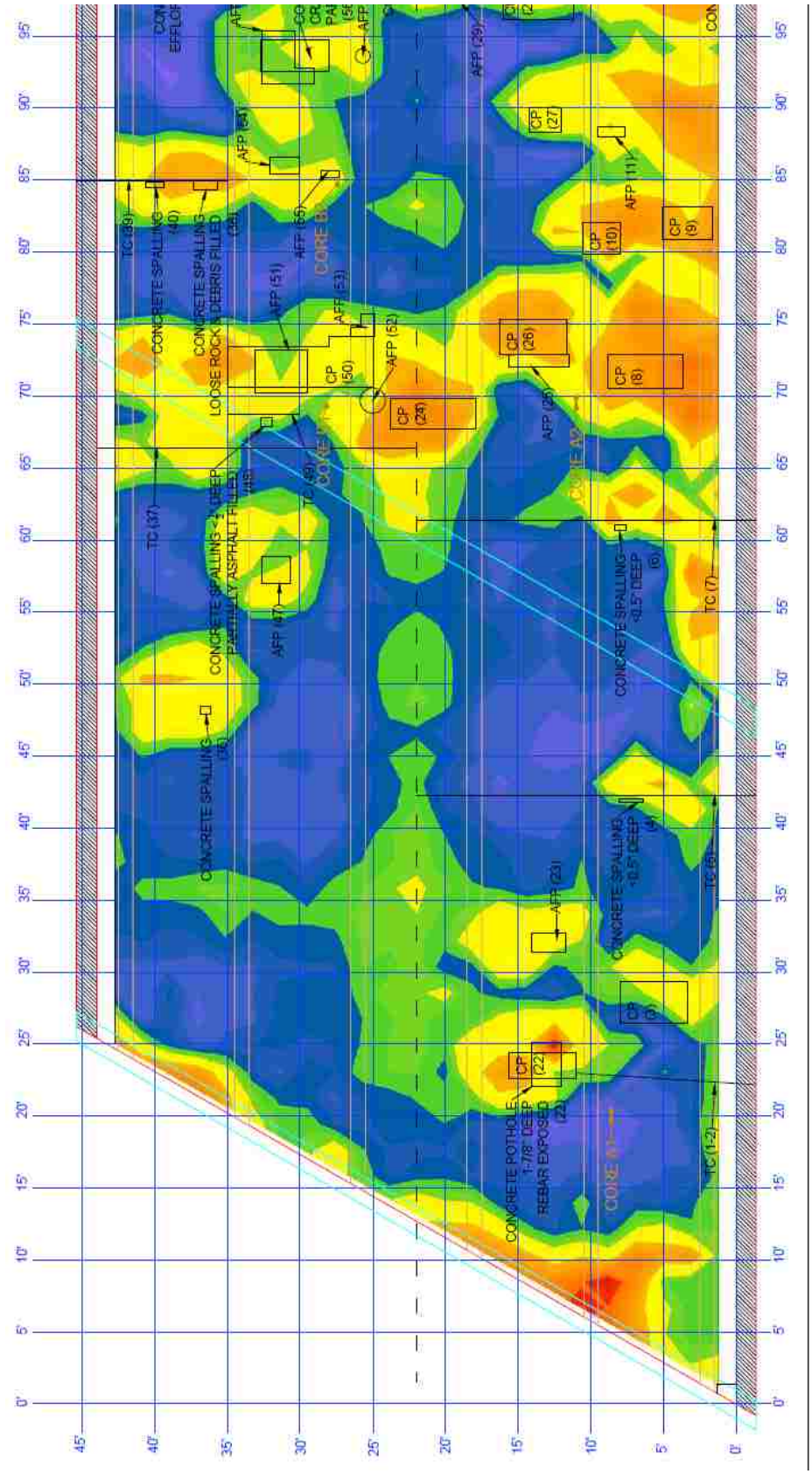

Figure C.4. Bridge A1297 Deck Investigation Drawing, GPR Results, Section 1 (0 ft. – 95 ft.)

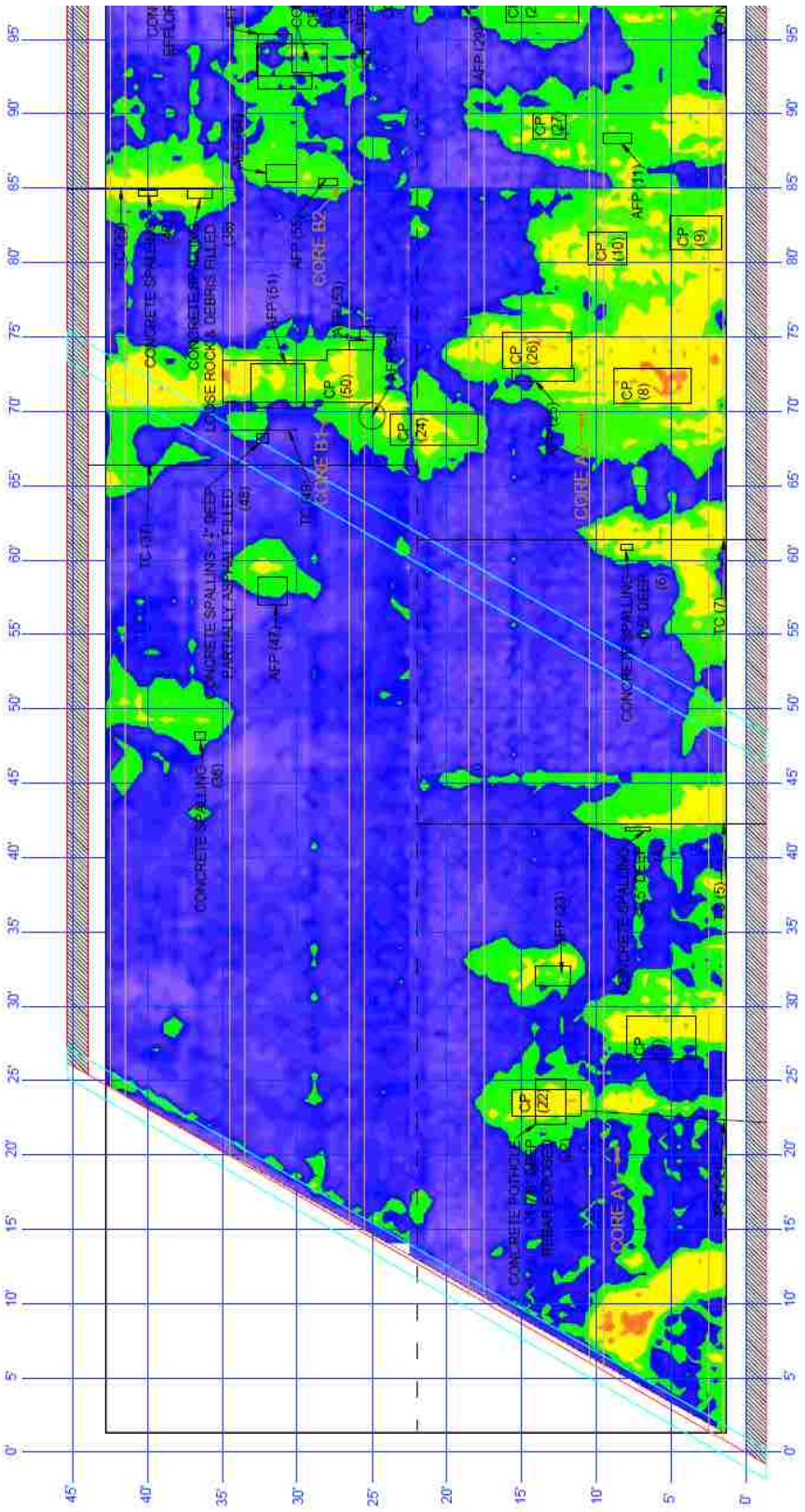

Figure C.5. Bridge A1297 Deck Investigation Drawing, Lidar Survey Results, Section 1 (0 ft. – 95 ft.)

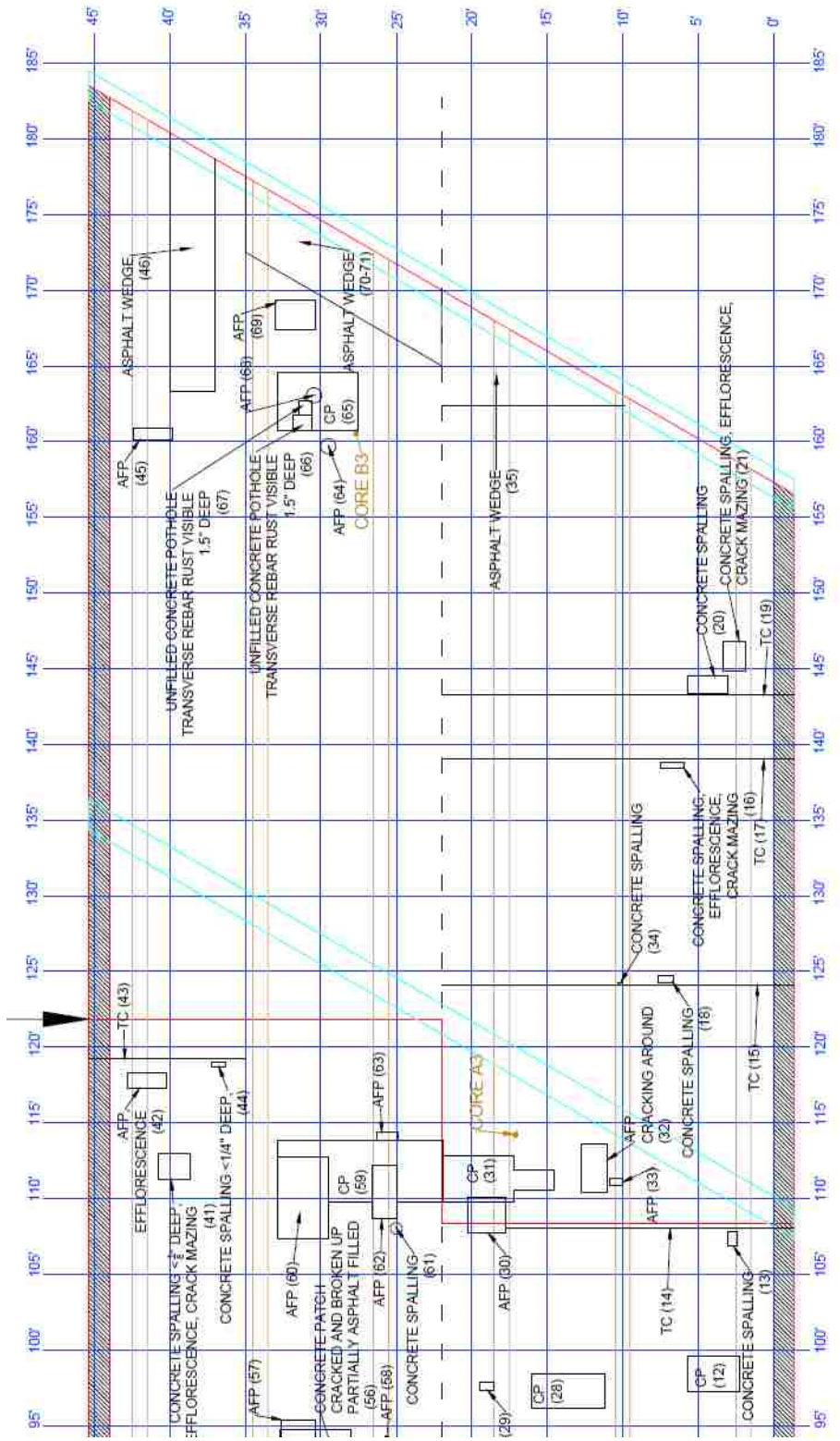

Figure C.6. Bridge A1297 Deck Investigation Drawing, Visual Inspection Results, Section 2 (95 ft. – 185 ft.)

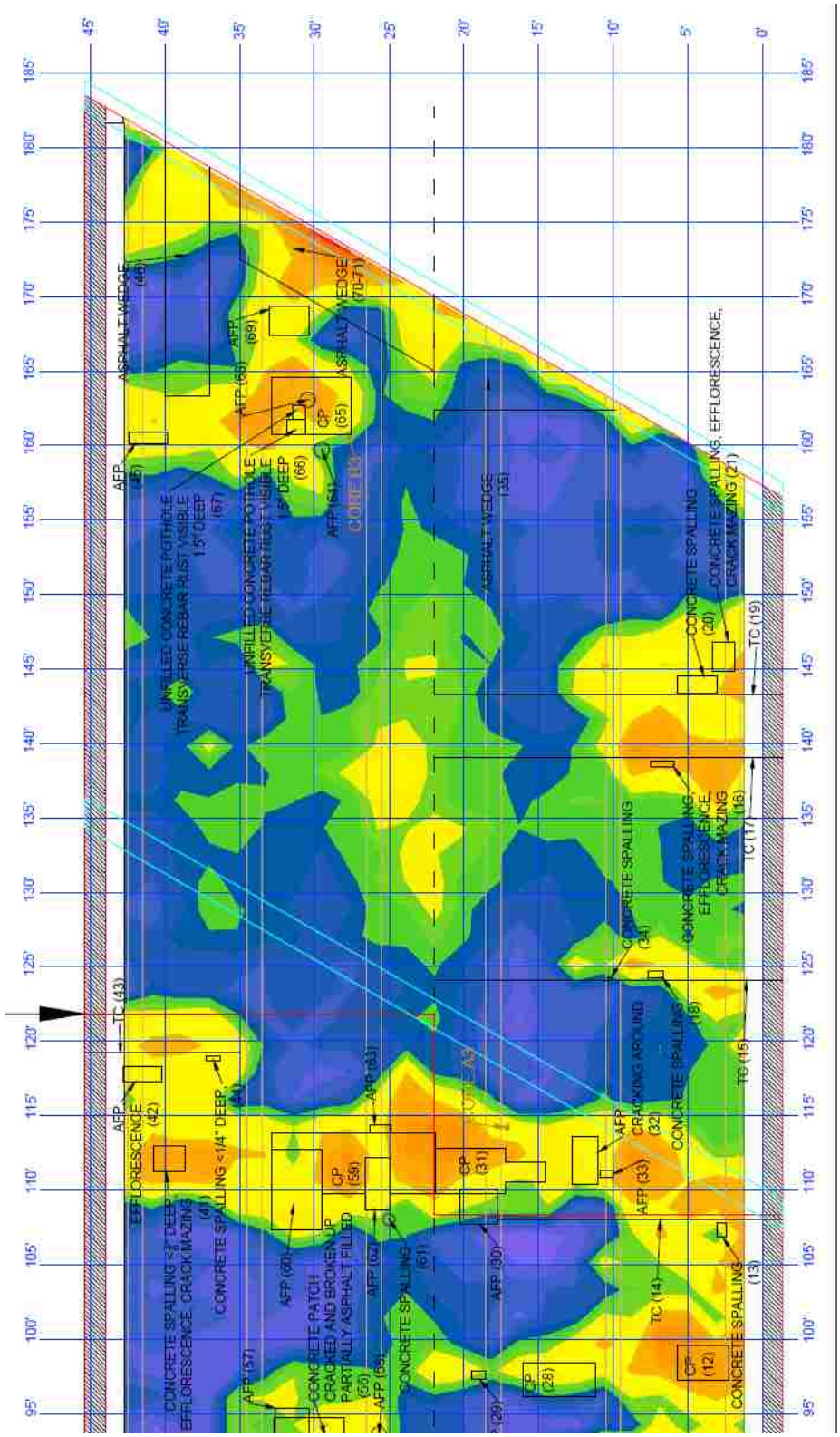

Figure C.7. Bridge A1297 Deck Investigation Drawing, GPR Results, Section 2 (95 ft. – 185 ft.)

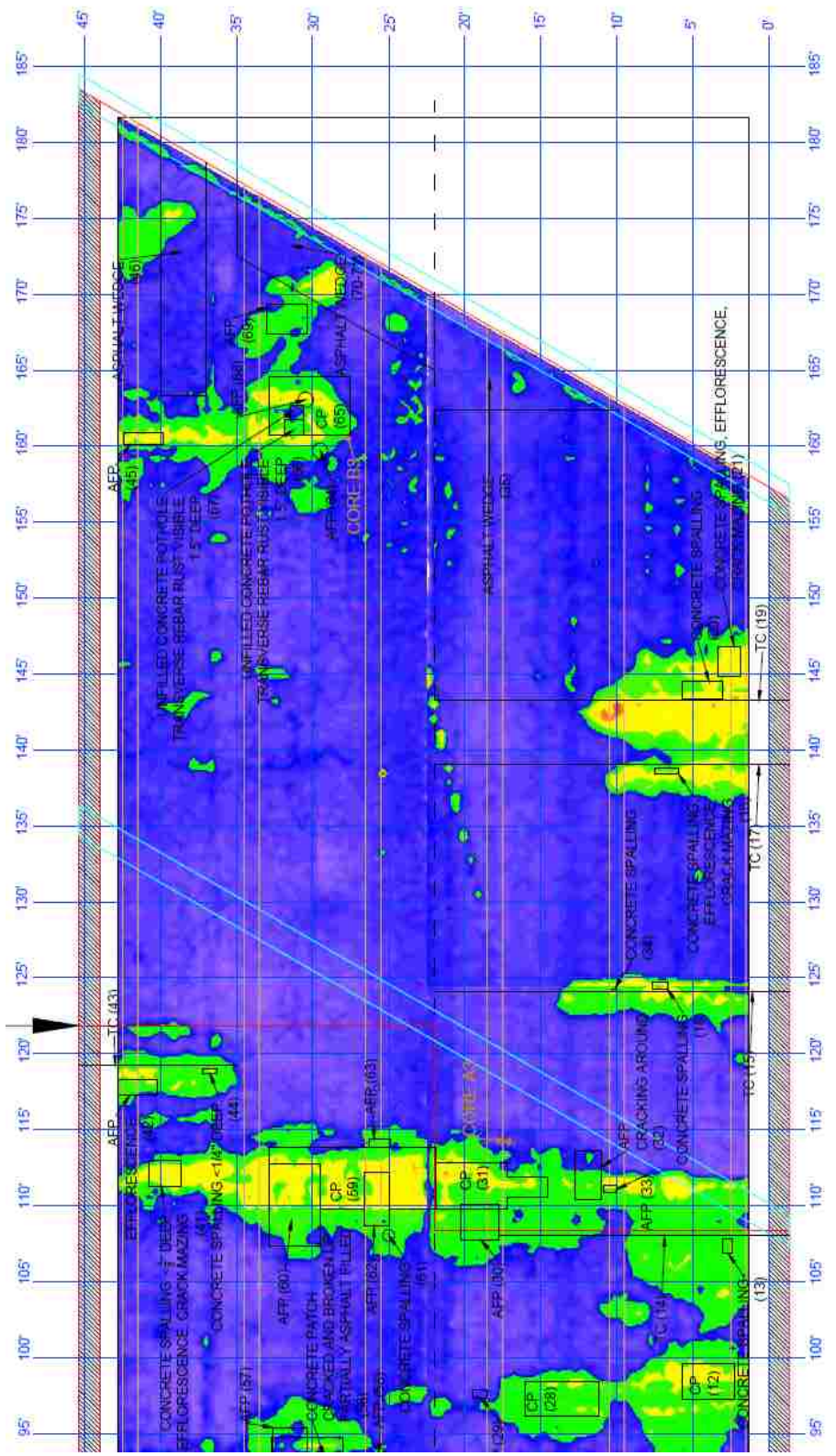

Figure C.8. Bridge A1297 Deck Investigation Drawing, Lidar Survey Results, Section 2 (95 ft. – 185 ft.)

APPENDIX D

BRIDGE A1297 VISUAL CORE EVALUATIONS

D. BRIDGE A1297 VISUAL CORE EVALAUTIONS

1. INTRODUCTION

This appendix provides the complete visual core evaluation results from Bridge A1297, along with photographs of each core.

2. CONTENTS

Page

Table D.1. Bridge A1297 Visual Core Evaluations

Core	A1	A2	A3	B1	B2	B3
Diameter (in)	2.0	2.0	2.0	2.0	2.0	2.0
Length (in)	2.5-3.0	2.75-3.375	3.125-3.75	~3.0	5.25-6.0	3.875-4.125
Surface (Asphalt: A, Concrete: C)	C	C	C	C	C	C
Number of Pieces	1	1	2	5	2	1
#1 Length (in) and failure mode [1]	2.5-3.0, CEX	2.75-3.375, CEX	1.875, PRE	1.5, PRE-Non rebar metal in core	0.25-1.0, PRE	3.875-4.125, CEX
#2 Length (in) and failure mode	N/A	N/A	1.25-1.75, CEX	0.25, PRE- Non rebar metal in core	4.25-4.75, CEX	N/A
#3 Length (in) and failure mode	N/A	N/A	N/A	0.25, PRE	N/A	N/A
#4 Length (in) and failure mode	N/A	N/A	N/A	0.25, PRE	N/A	N/A
#5 Length (in) and failure mode	N/A	N/A	N/A	0.25, CEX- Rebar marks visible on edge	N/A	N/A
Rebar: diameter (in), length (in), orientation [2], corrosion [2]	None	None	None	None	None	None
Roughness (Smooth, Average, Very Rough)	Smooth	Average	Average	Rough	Average	Average
Voids (Number >0.25 in. diameter)	1	2	0	0	5	1, 0.875" long 0.5" wide, 0.5" deep
Coating of the Aggregate (good or bad)	Good	Good	Good	Good	Good	Good
Volume of Paste (good or bad)	Good	Good	Good	Good	Good	Good
Air Entrained (yes or no)	Yes	Yes	Yes	Yes	Yes	Yes
Flaking surface: thickness (in)	None	None	None	None	None	None
Discoloration: color, maximum length (in)	None	None	None	Rust, 1.5 @ Bottom of piece 1 and 2	None	None
Delaminations: depths (in)	None	None	1.875	1.5, 1.75, 2.0	1.0	None
Segregation of Aggregate: depths (in)	None	None	None	None	None	None
Cracks (excluding fracture planes): number, type, length (in)	None	None	None	None	None	None
Other Comments						
General Quality of Concrete[3] (good, fair, bad)	Good	Good	Fair	Bad	Fair	Good

[1]Preexisting Rupture (PRE), Induced during coring (IDC), Produced by shear from extracting the core (CEX), Generated during handling (HAN), Other cause (OTR)
[2]Orientation: traverse (Tr) or longitudinal (Lo), Corrosion: none (Co1), low (Co2), average (Co3), high (Co4)
[3]Good indicates no delaminations or visible deterioration, Fair indicates some visible deterioration including delaminations however concrete is in large sections, Bad indicates concrete shows a lot of deterioration and is in many pieces including several small pieces

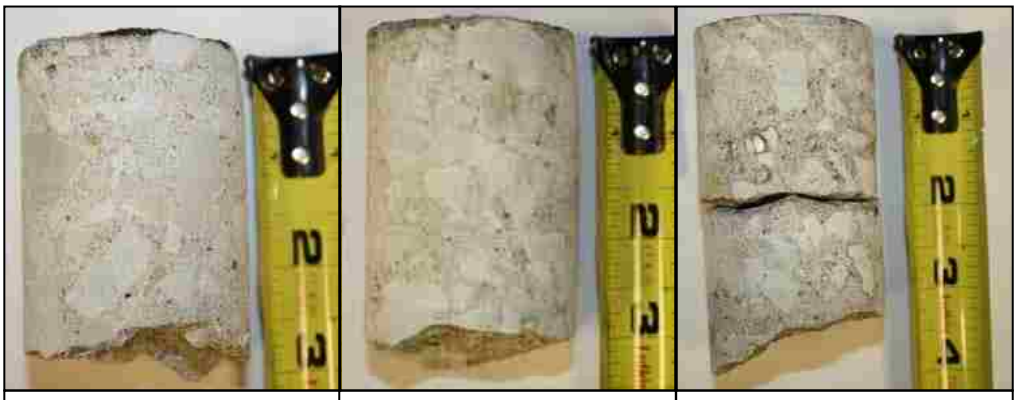

Core: A1 Visual Rating: Good	Core: A2 Visual Rating: Good	Core: A3 Visual Rating: Fair

Core: B1 Visual Rating: Bad	Core: B2 Visual Rating: Fair	Core: B3 Visual Rating: Good

Figure D.1. Bridge A1297 Core Photographs

APPENDIX E

VOLUME OF PERMEABLE PORE SPACE DATA

E. VOLUME OF PERMEABLE PORE SPACE DATA

1. INTRODUCTION

This appendix provides the all measured values which were used to determine the volume of permeable pore space of the extracted cores.

2. CONTENTS

Page

Table E.1. Volume of Permeable Pore Space Data

		ASTM C642-06 (Density, Absorption, and Voids in Hardened Concrete)												
		Piece Tested (If core in mult. pieces)	Initial mass (g)	A: Oven-Dry Mass (g)	B: Saturated Mass After Immersion (g)	C: Saturated Mass After Boiling (g)	D: Immersed Apparent Mass (g)	Absorption After Immersion (%)	Absorption After Immersion and Boiling (%)	Bulk Density, Dry (g/cm^3)	Bulk Density After Immersion (g/cm^3)	Bulk Density After Immersion and Boiling (g/cm3)	Apparent Density (g/cm3)	Volume of Permeable Pore Space (%)
Date/Time			2-28-13/ 4:15 PM	3-2-13/ 6:15 PM	3-4-13/ 8:30 PM									
A1297	A1		319.6	313.4	329.0	332.5	192.7	4.98	6.09	2.24	2.35	2.38	2.60	13.66
	A2		359.4	348.9	369.0	371.5	214.9	5.76	6.48	2.23	2.36	2.37	2.60	14.43
	A3	1,2	398.2	386.2	407.8	410.7	236.1	5.59	6.34	2.21	2.34	2.35	2.57	14.03
	B1	1	180.8	175.8	186.0	188.2	109.3	5.80	7.05	2.23	2.36	2.39	2.64	15.72
	B2	1,2	615.4	596.4	631.5	636	336	5.89	6.64	1.99	2.11	2.12	2.29	13.20
	B3		470.9	457.6	483.0	487.5	279	5.55	6.53	2.19	2.32	2.34	2.56	14.34
A1479	A1		97.9	95.5	100.4	101.2	58.9	5.13	5.97	2.26	2.37	2.39	2.61	13.48
	A2		205.2	189.2	222.7			17.71	Core Broke Apart After Immersion, No Further Testing on This Core					
	A3	1,2	180.2	174.2	185.4	186.5	106.2	6.43	7.06	2.17	2.31	2.32	2.56	15.32
	A4		150.9	148	155.6	157	87.8	5.14	6.08	2.14	2.25	2.27	2.46	13.01
	B1		199.2	193.7	204.2	205.4	119.6	5.42	6.04	2.26	2.38	2.39	2.61	13.64
	B2	Not Tested (Entire Core Asphalt)												
	B3		197.7	192.9	203.5	205.5	116.2	5.50	6.53	2.16	2.28	2.30	2.51	14.11
	B4		140.3	136.4	144.3	145.3	81.6	5.79	6.52	2.14	2.27	2.28	2.49	13.97
	B5		182.5	178.4	188.3	190.3	107.3	5.55	6.67	2.15	2.27	2.29	2.51	14.34

APPENDIX F

DIGITAL APPENDIX DESCRIPTION

F. DIGITAL APPENDIX DESCRIPTION

1. INTRODUCTION

This appendix provides details on the digital bridge investigation drawings that are located on the CD-ROM included with this thesis. As mentioned in Section 3.1, CAD drawings were generated showing structural bridge elements that were significant to the investigations discussed in this thesis. Visual inspection, GPR, core locations, and the rehabilitation lidar survey results were inserted into this drawing to create a comprehensive investigation drawing. These CAD drawings were then converted to a PDF file. When viewed using the software Adobe Reader, layers can be changed to be visible or hidden as shown in Figure F.1 below. One ft. and 5 ft. scales have been overlaid on each drawing. For optimal viewing of results, it is recommended to turn off the 1 foot scale layers, along with all reinforcement layers. The drawing files are large enough to allow the user to zoom in on small details. The GPR Map layer was positioned on top of the Lidar Hydrodemolition Map layer, so to see the lidar map, simply hide the GPR layer.

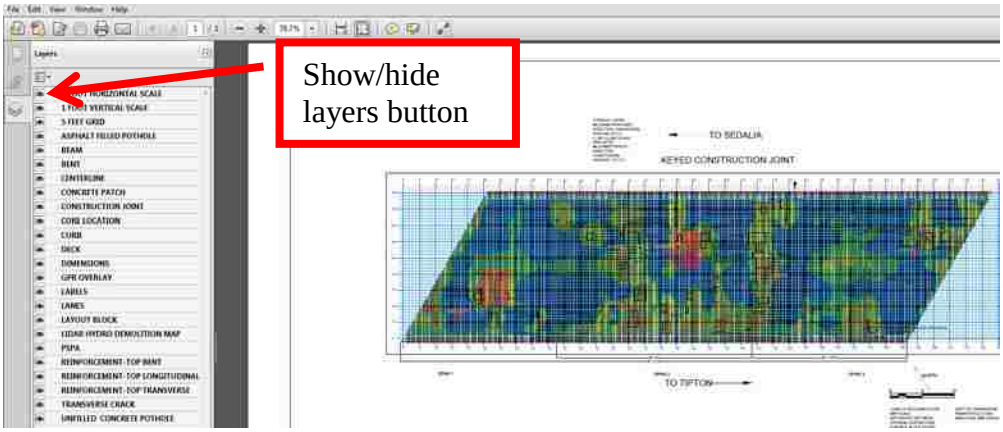

Figure F.1. Layers in Digital Drawing

2. CONTENTS

BRIDGE A1479 INVESTIGATION DRAWING.PDF

BRIDGE A1297 INVESTIGATION DRAWING.PDF

BIBLIOGRAPHY

[1] Missouri Department of Transportation (MoDOT), 2013. "Meet MoDOT." *Brochure,* Missouri Department of Transportation. Jefferson City, MO, September 2013.

[2] Portland Cement Association (PCA), 2013. "Corrosion of embedded metals." *Portland Cement Association,* <http://www.cement.org/tech/cct_dur_corrosion.asp> November 2013.

[3] Portland Cement Association (PCA), 2013. "Freeze-thaw resistance." *Portland Cement Association,* <http://www.cement.org/tech/cct_dur_freeze-thaw.asp> November 2013.

[4] Smith, J., Virmani, Y., 2000. "Materials and methods of corrosion control of reinforced and prestressed concrete structures in new construction." *Report,* Federal Highway Administration, FHWA-RD-00-081, November 2013.

[5] American Concrete Institute (ACI), 2013. "What is delamination?" *American Concrete Institute,* <http://www.concrete.org/Technical/CKC/troubleshooting/articles/053.htm> November 2013.

[6] Strategic Highway Research Program 2 (SHRP 2), 2013. "Deck delamination description." *Strategic Highway Research Program 2 NDToolbox,* <http://www.ndtoolbox.org/content/bridge/deck-delamination-description> November 2013.

[7] Missouri Department of Transportation (MoDOT), 2013. "Engineering polity guide." *Design Guide,* Section 751.10.1.5, Missouri Department of Transportation. Jefferson City, MO, October 2013.

[8] Vu, K., Stewart, M., (2000). "Structural reliability of concrete bridges including improved chloride-induced corrosion models." *Journal Article,* Structural Safety 22, pp. 313-333, October 2013.

[9] Thomas, M.D.A., Fournier, B., Folliard, K.J., (2013). "Alkali-aggregate reactivity (AAR) facts book." *Report,* Federal Highway Administration, FHWA-HIF-13-019, November 2013.

[10] Al-Khaja, W., (1997). "Influence of temperature, cement type and level of concrete consolidation on chloride ingress in conventional and high-strength concretes." *Journal Article,* Construction and Building Materials, Vol. 11, No. 1, pp. 9-13, November 2013.

[11] Ramey, G., Carden, A., (1998). "An assessment of concrete bridge deck evaporation rates and curing requirement categories for Alabama." *Report,* Auburn University, HRC 2-13746, November 2013.

[12] Zemajtic, J., (2013). "Curing concrete in construction." *Portland Cement Association,* <http://www.cement.org/tech/cct_curing.asp> November 2013.

[13] Kan, L., Shi, H., Sakulich, A., Li, Vi., (2010). "Self-healing characterization of engineered cementitious composite materials." *Journal Article,* ACI Materials Journal, Vol. 107, No. 6, pp. 617-624, November 2013.

[14] Sakulich, A., Bentz, D., (2011). "Increasing the service life of bridge decks by incorporating phase change materials to reduce freeze/thaw cycles." *Journal Article,* Journal of Materials in Civil Engineering, Vol. 24, No. 8, pp 1034-1042, November 2013.

[15] Gucunski, N., Romero, F., Kruschwitz, S., Feldmann, R., Parvardeh, H., (2011). "Comprehensive bridge deck deterioration mapping of nine bridges by nondestructive evaluation technologies." *Final Report,* Iowa Department of Transportation, Report No. SPR-NDEB(90)--8H-00, November 2013.

[16] Gucunski, N. et al., (2013). "Nondestructive testing to identify concrete bridge deck deterioration." *Report,* Strategic Highway Research Program 2, Report No. S2-R06A-RR-1, November 2013.

[17] Hema, J., Guthrie, W., Fonseca, F., (2004). "Concrete bridge deck condition assessment and improvement strategies." *Report,* Utah Department of Transportation, Report No. UT-04-16, November 2013.

[18] Hasan, H., Ramirez, J., Cleary, D., (1995). "Indiana evaluates epoxy-coated steel reinforcement." *Journal Article,* Better Roads, Vol. 65, No. 5, pp. 21-25, November 2013.

[19] Phares, B., Rolander, D., Graybeal, B., Washer, G., (2001). "Reliability of visual bridge inspection." *Journal Article,* Public Roads, Vol. 64, No. 5, November 2013.

[20] Missouri Department of Transportation (MoDOT), 2013. "Engineering polity guide." *Design Guide,* Section 753.2, Missouri Department of Transportation. Jefferson City, MO, October 2013.

[21] American Standard Test Method (ASTM) D 4580/ D 4580M, 2012. "Standard practice for measuring delaminations in concrete bridge decks by sounding." *Standard,* ASTM International, West Conshohocken, PA., November 2013.

[22] Strategic Highway Research Program 2 (SHRP 2), 2013. "Hammer sound/ chain drag description." *Strategic Highway Research Program 2 NDToolbox,* <http://www.ndtoolbox.org/content/bridge/cd-description > November 2013.

[23] Scott, M., et al. (2003). "A comparison of nondestructive evaluation methods for bridge deck assessment." *Journal Article,* NDT&E International, Vol. 36, pp. 245-255, November 2013.

[24] Gucunski, N., Antoljak, S, Maher, Ali., (2000). "Seismic methods in post construction condition monitoring of bridge decks." *Proceedings,* Use of Geophysical Methods in Construction, pp. 35-51, November 2013.

[25] Strategic Highway Research Program 2 (SHRP 2), 2013. "Ground penetrating radar description." *Strategic Highway Research Program 2 NDToolbox,* <http://www.ndtoolbox.org/content/bridge/gpr-description > November 2013.

[26] Maser, K., (2009). "Integration of ground penetrating radar and infrared thermography for bridge deck condition evaluation." *Proceedings,* Non-Destructive Testing in Civil Engineering 2009, Nantes, France, November 2013.

[27] Morrissey, J. (2013). "What is GPR?" *Previous Research,* <http://johnpmorrissey.com/gpr.html> November 2013.

[28] Strategic Highway Research Program 2 (SHRP 2), 2013. "Ground penetrating radar physical principle." *Strategic Highway Research Program 2 NDToolbox,* <http://www.ndtoolbox.org/content/bridge/gpr-physical-principle> November 2013.

[29] American Standard Test Method (ASTM) D 6087, 2008. "Standard test method for evaluating asphalt-covered concrete bridge decks using ground penetrating radar." *Standard,* ASTM International, West Conshohocken, PA., November 2013.

[30] Geophysical Survey Systems, Inc. (GSSI), (2013). "Bridge deck condition assessments with GSSI GPR." *Geophysical Survey Systems, Inc.,* < http://www.geophysical.com/bridgeinspection.htm#nogo> November 2013.

[31] Yehia, S., Abudayyeh, O., Abdel-Qader I., Zalt, A., (2008). "Ground-penetrating radar, chain drag, and ground truth." *Journal Article,* Transportation Research Record, No. 2044, pp. 39-50, October 2013.

[32] Strategic Highway Research Program 2 (SHRP 2), 2013. "Ground penetrating radar limitations." *Strategic Highway Research Program 2 NDToolbox,* <http://www.ndtoolbox.org/content/bridge/gpr-limitations> November 2013.

[33] Arndt, R.W., Jalinoos, F., Cui, J., Huston, D., (2010). "Periodic NDE in support of structural health monitoring of bridges." *Proceedings*, Fifth International IABMAS Conference, Philadelphia, USA, pp. 148, November 2013.

[34] Federal Highway Administration (FHWA), (2013). "RABIT™ Bridge Deck Assessment Tool." *Federal Highway Administration*, <http://www.fhwa.dot.gov/research/tfhrc/programs/infrastructure/structures/ltbp/ltbltbpresea/rabit/index.cfm> December 2013.

[35] American Standard Test Method (ASTM) C 42/C42M, 2013. "Standard test method for obtaining and testing drilled cores and sawed beams of concrete." *Standard*, ASTM International, West Conshohocken, PA., November 2013.

[36] American Standard Test Method (ASTM) C 856, 2011. "Standard practice for petrographic examination of hardened concrete." *Standard*, ASTM International, West Conshohocken, PA., November 2013.

[37] American Standard Test Method (ASTM) C 1152, 2004. "Standard test method for acid-soluble chloride in mortar and concrete." *Standard*, ASTM International, West Conshohocken, PA., November 2013.

[38] American Standard Test Method (ASTM) C 1218, 1999. "Standard test method for water-soluble chloride in mortar and concrete." *Standard*, ASTM International, West Conshohocken, PA., November 2013.

[39] Kepler, J., Darwin, D., Locke, C. Jr., (2000). "Evaluation of corrosion protection methods for reinforced concrete highway structures." *Report*, Structural Engineering and Engineering Materials, SM Report No. 58, November 2013.

[40] Missouri Department of Transportation (MoDOT), 2012. "Final bridge opened in safe and sound improvement program." *Press Release*, Missouri Department of Transportation. Jefferson City, MO, November 2013.

[41] Missouri Department of Transportation (MoDOT), 2011. "Safe and sound fact sheet." *Missouri Department of Transportation*, <http://www.modot.gov/safeandsound/Facts.htm> , Jefferson City, MO, November 2013.

[42] Wenzlick, J., (2005). "Deck replacement with precast reinforced segments." *Report*, Missouri Department of Transportation, Report No. OR06-003, November 2013.

[43] American Concrete Pavement Association, (2013). "How do I obtain "high early strength" concrete?" *American Concrete Pavement Association*, <http://www.pavement.com/concrete_pavement/technical/FATQ/Design/High_EarlE_Strength_Concrete.asp> , November 2013.

[44] American Concrete Institute (ACI), (2010). "Concrete removal using hydrodemolition." *Guide*, Field Guide to Concrete Repair Application Procedures, November 2013.

[45] Hydro-Technologies, Inc., (2013). "Home." *Hydro-Technologies, Inc.*, <http://www.hydro-technologies.com/> November 2013.

[46] Wenzlick, J., (2002). "Hydrodemolition and repair of bridge decks." *Report*, Missouri Department of Transportation, Report No. RTD02-002, November 2013.

[47] American Standard Test Method (ASTM) C 642, 2006. "Standard test method for density, absorption, and voids in hardened concrete." *Standard*, ASTM International, West Conshohocken, PA.

[48] American Standard Test Method (ASTM) C 1218/ C 1218M, 1999. "Standard test method for water-soluble chloride in mortar and concrete." *Standard*, ASTM International, West Conshohocken, PA.

[49] Missouri Department of Transportation (MoDOT), 2013. "Route 54 bridge deck work complete." *Press Release*, Missouri Department of Transportation. Jefferson City, MO, September 2013.

[50] Google Maps, (2013). "U.S. 54 Westbound Bridge over Osage River near city of Lake Ozark, MO." *Google Maps*, <https://maps.google.com/maps?q=Lake+Ozark,+MO&hl=en&ll=38.19151,-92.606973&spn=0.002757,0.005284&sll=38.68541,-93.037751&sspn=0.000685,0.001321&oq=lake+oz&t=h&hnear=Lake+Ozark,+Miller,+Missouri&z=18>, November 2013.

[51] Google Maps, (2013). "U.S. 50 Bridge over Railroad eight miles east of Sedalia, MO." *Google Maps*, <https://maps.google.com/maps?q=sedalia,+mo&hl=en&ll=38.68541,-93.037751&spn=0.000689,0.001321&sll=38.68149,-93.065529&sspn=0.175278,0.338173&t=h&hnear=Sedalia,+Pettis,+Missouri&z=20>, November 2013.

VITA

Brandon Tyler Goodwin was born in Quincy, Illinois. He graduated from Knox County High School in Edina, Missouri in May 2008 as valedictorian of his class. He then attended Missouri University of Science and Technology and obtained his Bachelor's of Science in Civil Engineering in May 2012 graduating Summa Cum Laude. While working towards his undergraduate degree, Brandon was a member of American Society of Civil Engineers (ASCE), Chi Epsilon, and Tau Beta Pi, having served as Treasurer for ASCE, along with Treasurer and Corresponding Secretary for Tau Beta Pi.

Brandon was employed as a Construction Inspection Intern for MoDOT, stationed in Macon, Missouri during the summers of 2009 and 2010. During the summer of 2012, he was a Civil Engineering Student Trainee for Southwestern Power Administration (U.S. Department of Energy), stationed in Tulsa, Oklahoma.

In August 2012, Brandon started as a graduate student at Missouri University of Science and Technology. In May 2014 he obtained his Master's of Science in Civil Engineering with an emphasis in structural engineering.